Al-Farabi Kazakh National University

UDC 524.3:537.876.22

YERNAZAROV TURSYNBEK IZMUKHANOVICH

The effects of nonlinear vacuum electrodynamics and general relativity for the passage of the front of electromagnetic waves through the magnetic field of the magnetar

8D05306 – Physics

Dissertation submitted in fulfillment of the requirements for the degree of Doctor of Philosophy (PhD)

Supervisors:
Toktarbay Saken
PhD, al-Farabi Kazakh National University.

Yerlan Aimuratov,
PhD, al-Farabi Kazakh National University.

Rahim Moradi,
PhD, associate professor,
ICRANet, Pescara, Italy

Republic of Kazakhstan
Almaty, 2024

CONTENTS

ABBREVIATIONS

NLED	Nonlinear electrodynamics
QED	Quantum electrodynamics
NS	Neutron stars
GRB	Gamma ray burst
EM	Electromagnetic

INTRODUCTION

General description of the research

This work is devoted to the study of the effects of nonlinear vacuum electrodynamics and general relativity on the passage of the front of electromagnetic waves through the magnetic field of the magnetar.

Relevance of the topic

It is obvious that according to modern theoretical models, vacuum electrodynamics is a nonlinear theory. This theory is studied in two sections: nonlinear optics, which studies nonlinear electrodynamic (NLED) processes occurring in material media, and NLED of vacuum, which studies similar processes occurring in a vacuum in the presence of strong electromagnetic fields.

Experiments on inelastic scattering of laser photons on gamma quanta, conducted at the Stanford linear accelerator, confirmed that vacuum electrodynamics has nonlinear properties. Many laboratory experiments were performed on Earth to observe the nonlinear effects of quantum electrodynamics [1,2]. In laboratory conditions, observation of the effects of nonlinear vacuum electrodynamics is possible only in experiments in which the relative measurement accuracy should be at the level of 10^{-19} – 10^{-20}. Only precision ring lasers and their application in precision optical measurements can provide such accuracy [3]. Although the accuracy of the instruments measuring NLED effects at present does not allow us to study the effects in the vacuum of NLED. Therefore, the nonlinear electrodynamics of vacuum is much less known. At the same time, under conditions of extremely high magnetic fields, unattainable in terrestrial laboratories, charged and magnetized astronomical objects are likely to provide a more detailed understanding of the nonlinear effects of electrodynamics [4,5]. Therefore, there is an increasing interest in astrophysical compact objects with high levels of electromagnetic field, in particular, in charged black holes and magnetars. The propagation of a weak electromagnetic wave in an external electromagnetic field is accompanied by several NLED effects, such as nonlinear electrodynamic bending of rays. Several works have been done to analytically and numerically study the angle of refraction of the EM beam passing through the magnet. In these works, the refraction angles of the beam are determined according to the boundary conditions and some models of nonlinear electrodynamics and are compared with the Shwarzschild case. At the same time, studies on data analysis of the data obtained by satellite telescopes also evaluated EM beam polarization, values of EM beam flux in real magnetars, and beam deflection angles. However, there are no quantitative studies of the refraction angle, beam deformation and flux densities of the EM beam on a non-equatorial surface in a combination of gravity and vacuum nonlinear electrodynamics that can be registered using high-precision detectors. Of course, the comparison of the results of these numerical studies with the data recorded by the detector in the near future has a great chance to gain a deeper understanding of the nonlinear electrodynamics of the vacuum. Therefore, the importance of research in this regard is considered very necessary now. will be relevant.

Connection of the dissertation topic with the plans of scientific works:

The dissertation work was completed by the plans of fundamental research work (R&D) of the Scientific Committee of the Ministry of Education and Science of the Republic of Kazakhstan "Grant financing of scientific research" on the topics: "Effects of nonlinear electrodynamics of vacuum and general relativity on magnetars" (2022-2024, code AP14869524 No. Agreement No. 253/30-22-24 dated October 18, 2022).

The goals of the research: The aim of the study is a numerical investigation of combined gravitational and nonlinear magnetic lensing of electromagnetic radiation on the dipole magnetic field of a magnetar.

To accomplish this aim, it is essential to address the **following objectives**:

1. Study the processes of beam deflection in the plane of the dipole axis and the plane perpendicular to it under the influence of gravitational and magnetic fields. Determine the dependences of the deflection angle on the impact distance and magnetic field intensity for different distances (15-100 km) and magnetic fields in the conditions of a strong magnetar ($B = 10^{13}$ G).
2. Study the deformation of the radiation front passing through the dipole magnetic field of the magnetar to identify patterns of change in its shape. Estimate the degree of deviation from the ideal circular shape and approach to an ellipse, and determine the key parameters influencing this deformation.
3. Conduct a study of changes in the distribution of the energy flux of the radiation front as it passes through the magnetic field of the magnetar. Determine the ratio of energy at the input and output of the front and identify the factors influencing the minimum and maximum of the energy flows.

The object of the research: dipole magnetic field of a magnetar, gamma-ray burst, magnetar.

The subject of the research: combined gravitational and magnetic lensing when an EM radiation front passes through a magnetar.

Research methods: The analytical portion of the research relies on the principles of general relativity and techniques from differential geometry, in addition to employing perturbation theory methods for obtaining approximate solutions. The numerical analysis mainly utilizes the Runge-Kutta and Adams methods, as well as spectral methods tailored to the characteristics of the equations being studied.

Scientific novelty: The uniqueness and innovation of the dissertation are demonstrated by the fact that;

– electromagnetic radiation passing through the combined gravitational and dipole magnetic field of the magnetar is deflected by a large angle in areas adjacent to the magnetar and by a small angle at a greater distance from it. When the dipole magnetic field strength on the surface of the magnetar approaches a critical value, the influence of nonlinear electrodynamics becomes significant;

– the combined gravitational and dipole magnetic field causes the electromagnetic radiation front to deform into an ellipse as it passes through the magnetar's magnetosphere. This phenomenon is not observed in an isolated gravitational field;

– as a result of the significant influence of the combined gravitational and dipole magnetic field on the flux density of gamma quanta passing through the magnetar's magnetosphere, a redistribution of this flux occurs.

Theoretical and practical significance of the dissertation. The results obtained in this dissertation will be highly valuable for studying the effects of nonlinear vacuum electrodynamics. Moreover, understanding the characteristics of focusing and intensity distribution of electromagnetic beams that pass through the magnetosphere of a magnetar will help confirm and explore vacuum NLED effects in distant astrophysical objects. The research conducted in this dissertation holds both theoretical and practical significance for expanding our knowledge in the fields of relativistic astrophysics, cosmology, and vacuum NLED physics.

Defence provisions:

1. The deflection of rays caused by both the gravitational and dipole magnetic fields is 86 degrees and 3.36 degrees, respectively, for an impact distance between 15 and 100 km, with a magnetic field strength of $B = 10^{13}$ G.
2. The deformation of the wavefront $\Delta = \frac{r_{max} - r_{min}}{r_{max}}$ (dimensionless quantity) of electromagnetic radiation caused by the gravitational and dipole magnetic fields of the magnetar is 0.07.
3. Due to the combined effects of gravitational and dipole magnetic lensing, the flux density of the electromagnetic beam from GRB091006360, measured 30 kilometers away from the magnetar (Swift J1822.3-1606), increases by 1.83 times compared to its initial value.

Reliability and validity of the results: The obtained results are confirmed by publications in leading scientific journals with an impact factor and journals recommended by the Committee of Education and Science of the Republic of Kazakhstan. Additionally, the presence of publications in the collection of materials from domestic and foreign international scientific conferences further supports the validity of the results. The sources for the research are the original scientific works listed in the bibliography.

Personal contribution of the author: Throughout the research process, including literature reviews, conducting relevant investigations to address research tasks, and obtaining satisfactory results, the author worked independently. However, the author consulted with supervisors to define tasks that align with the research topic and to analyze the results obtained.

Approbation of the dissertation.

The results of the work were presented and discussed at the following local and foreign international conferences:

- at the scientific seminars of the Theoretical and Nuclear Physics Department at Al-Farabi KazNU;
- at the International Scientific Conference of Students and Young Scientists "FARABI ALEMI", Almaty, April 6-8, 2023;
- at the International Scientific Online Conference «Sixteenth Marcel Grossmann Meeting» Rome, Italy, July 6-11, 2021;
- at the International Conference Abdildin readings (Actual problems of modern physics) Al Farabi Kazakh National University, Faculty of Physics and Technology, Almaty, Kazakhstan, April 12 - 15, 2023;

- at the conference of "New trends in theoretical physics", October 23-28, National University of Uzbekistan (NUUZ), Tashkent

- at the International Conference on Theoretical Physics and Astrophysics (ICTPA-2024), Institute of Fundamental and Applied Research, Tashkent, Uzbekistan, 13 - 18 May 2024.

Publications: According to materials presented in the dissertation 7 publications have been published in total: one article in journal indexed in: Web of Knowledge (Thomson Reuters, USA), Scopus (Elsevier, Netherlands); 4 articles in journals recommended by the Ministry of Science and Higher Education of the Republic of Kazakhstan; 2 publications in the collection of international scientific conferences.

Articles with a high impact factor in the Thomson Reuters database or publications included in the international scientific database Scopus:

1. Beissen, N., Abishev, M., Toktarbay, S., Yernazarov, T., Aimuratov, Y., Khassanov, M. Nonlinear electrodynamical lensing of electromagnetic waves on the dipole magnetic field of the magnetar //International Journal of Modern Physics D. – 2023. – Т. 32. – №. 16. – С. 2350106-142. (IF: 3.8, SCOPUS 80)

Articles in publications recommended by Committee for Quality Assurance in the Field of Science and Higher Education of Republic of Kazakhstan:

1. Beissen, N., Abishev, M., Toktarbay, S., Yernazarov, T., Utepova, D., Zhakipova, M. The Exploring nonlinear vacuum electrodynamics beyond Maxwell's Equations //International Journal of Mathematics and Physics. – 2023. – Т. 14. – №. 1. – С. 61-70.

2. Beissen, N. A., Utepova, D. S., Kossov, V. N., Toktarbay, S., Khassanov, M. K., Yernazarov, T., Seydalieva, M. The influence of deformation in compact objects on redshift and radar echo delay //Recent Contributions to Physics. – 2024. – Т. 88. – №. 1.

3. Beissen, N., Abishev, M., Toktarbay, S., Yernazarov, T., Khassanov, M., Utepova, D., Abduali, A. An overview of light ray deflection calculation by magnetars in nonlinear electrodynamics //Bulletin of the Karaganda University" Physics Series". – 2024. – Т. 11429. – №. 2. – С. 65-71.

4. Beissen, N. A., Utepova, D. S., Kossov, V. N., Toktarbay, S., Khassanov, M. K., Yernazarov, T., Imanbayeva, A. K. Comparing the efficiency of GPU and CPU in gravitational lensing simulation //International Journal of Mathematics and Physics. – 2024. – Т. 15. – №. 1. – С. 49-56.

5. Yernazarov T., Abishev M., Aimuratov Y. Correspondence of gamma radiation coming from GRBs and magnetars based on the effects of nonlinear vacuum electrodynamics //The Sixteenth Marcel Grossmann Meeting on Recent Developments in Theoretical and Experimental General Relativity, Astrophysics and Relativistic Field Theories: Proceedings of the MG16 Meeting on General Relativity Online; 5–10 July 2021. – 2023. – С. 4401-4409.

The structure and scope of the thesis: The dissertation includes an introduction, two chapters, and a reference list containing 116 sources. The main text covers 111 pages and features 27 figures.

1 DEFLECTION OF RAYS IN A SUPERSTRONG MAGNETIC FIELD IN NLED OF VACUUM

1.1 Methods for calculation of ray propagation in NLED.

Nonlinear electrodynamics (NLED) in intense fields is a captivating area of study in modern physics, investigating the complex interplay between quantum fields and electromagnetic forces. This concept is based on viewing the vacuum not as space but as a quantum field that can produce particles when exposed to strong electromagnetic fields. The historical journey towards comprehending NLED in a vacuum began with the establishment of the principles of quantum mechanics and quantum electrodynamics in the early twentieth century. The contributions of Max Born and Leopold Infeld in 1934, as well as Werner Heisenberg and Hans Euler in 1936, were crucial in shaping the evolution of nonlinear electrodynamics and field theory. The theory proposed by Born and Infeld presented an innovative outlook on electrodynamics, advocating a revision of Maxwell's equations to resolve infinite values and introduce a limit on the maximum strength of the electromagnetic field. These concepts significantly impacted field theory advancement and provided novel methodologies for investigating the interaction of powerful electromagnetic fields with vacuum. Heisenberg and Euler introduced a framework that facilitated the comprehension of quantum phenomena in the electromagnetic field, representing a significant advancement in studying the interaction of intense fields with the vacuum [1]. They formulated equations that described how a vacuum containing virtual particles could give rise to real particles under specific circumstances. This groundwork laid the foundation for further exploration of the phenomenon of particle creation from the vacuum.

Vacuum birefringence, which is another quantum effect, manifests itself in the presence of intense magnetic fields, causing the vacuum to exhibit birefringent properties towards low-energy photons. The PVLAS project [2], for example, sought to verify vacuum birefringence by employing the strong magnetic field of a permanent magnet in conjunction with optical laser photons. Similarly, there have been suggestions to employ ultra-powerful laser fields in combination with X-ray free electron laser photons to study this phenomenon. These investigations involve cutting-edge technologies such as ultra-powerful lasers, X-ray free electron lasers, and highly precise X-ray polarimetry, yet they concentrate on fields that are below the critical threshold.

Current technologies, including advanced lasers and particle accelerators [3,4,5] open up new avenues for experimentally exploring NLED in space. These experiments have the potential to address fundamental questions in quantum mechanics and general relativity, providing fresh perspectives on the nature of vacuum, particle creation, and vacuum energy. The implications of these investigations go beyond theoretical interest, hinting at possible ways to develop alternative energy sources, enhance our understanding of superconductivity, and drive advancements in quantum technology. Therefore, the study of NLED in a vacuum under intense fields remains a crucial and promising field of physics, promising novel discoveries and technological progress.

Stephen L. Adler's research [6], which focuses on photon splitting and dispersion in strong magnetic fields, offers a thorough examination of the profound effects of intense magnetic fields on photon characteristics, with a specific emphasis on the photon splitting process. Adler explores photon absorption and the rules governing polarization in a constant magnetic field. A key discovery of the study is the possibility of creating linearly polarized gamma rays through photon splitting. Furthermore, Adler investigates the influence of dispersion on photon absorption and splitting, providing detailed calculations of absorption coefficients. This research highlights the intricate nature of photon interactions under extreme magnetic field conditions, which is particularly relevant for understanding phenomena related to pulsars and other cosmic objects.

NLED splits into two primary areas: nonlinear optics, focusing on the complex electrodynamic behaviours within materials, and vacuum nonlinear electrodynamics, which investigates similar behaviours but in empty space under strong electromagnetic conditions [7]. Currently, nonlinear optics [8] and its effects are widely used in various theoretical and practical research in physics, leading to the development of devices that utilize these phenomena. However, the study of vacuum nonlinear electrodynamics is not as advanced. Typically, Maxwell's electrodynamics, which operates linearly in a vacuum, is recognized for its precise predictions across many topics and laid the foundation for special relativity, altering the traditional views of space and time established by Newtonian mechanics. Yet, certain fundamental physical principles suggest that Maxwell's electrodynamics is just an initial, simplified version of a more complex, nonlinear vacuum electrodynamics. This simplification holds true particularly in conditions of weak electromagnetic fields [9,10,11], especially when electromagnetic field strengths $\vec{B}$ and $\vec{E}$ are much less than the quantum electrodynamics threshold $B_q = m_0^2 c^3 / e\hbar = 4.41 \cdot 10^{13}$G. Werner Heisenberg and Hans Heinrich Euler were the pioneers behind the concept of NLED in a vacuum, building on Gustav Mie's fundamental electromagnetic principles [12,13]. With the advancement of high-power laser technology, several experiments have been conducted to test these theories, affirming that vacuum electrodynamics is indeed nonlinear [14-19]. Despite numerous experiments aiming to detect nonlinearity under strong magnetic fields, conclusive evidence has yet to be found.

An alternative approach for investigation involves examining cosmic-scale phenomena, where astronomical events might reveal more about NLED. Over the past decade, various NLED models, including rational, arcsin [20], arctangent [21], Mod-Max [22], among others [23, 24, 25], have been proposed, each offering unique insights for further exploration. Recent reviews have focused on the properties of nonlinear vacuum electrodynamics, light coupling phenomena, and observational data on galactic pulsars and their magnetic fields [26, 27, 28]. The identification of magnetars, with magnetic fields ranging between 10^{14} and 10^{15} Gauss, followed the 1979 discovery of a massive flare from SGR 0526-66 [29], leading to the term "magnetar" coined by Duncan and Thompson in subsequent research [30, 31, 32]. Additional studies have investigated the formation of virtual particles in the magnetosphere of axisymmetric pulsars [33] and the combination of nonlinear electrodynamics in

vacuum with gravitational effects [34], especially in the context of magnetars and black holes [35-37]. These investigations into the interaction between electromagnetic and gravitational forces offer new perspectives on astrophysical phenomena, contributing to theories of black holes and addressing electric field singularities at their centres [21].

Experimental advancements in the investigation of vacuum nonlinear electrodynamics have led to the exploration of light scalar and/or pseudoscalar particles that interact with two photons by studying the propagation of a laser beam ($\lambda = 514\ \mathrm{nm}$) in a transverse magnetic field [38]. The study set a constraint of $3.5 \times 10^{-23}\mathrm{rad}$ on the potential optical rotation of the beam's polarization for a distance of 2.2 km in a magnetic field of 3.25 T. The researchers inferred that the coupling $g_{\gamma\gamma} < 3.6 \times 10^{-11}\mathrm{GeV}^{-1}$ at a 95% confidence level, assuming $m_{\alpha} < 10\mathrm{meV}$. Similar limitations on the absence of ellipticity in the transmitted beam can be derived. Additionally, an investigation into photon regeneration in a magnetic field resulted in a restriction of $g_{\gamma\gamma} < 6.7 \times 10^{-11}\mathrm{GeV}^{-1}$ for the same mass range of particles. The authors extensively discuss the theoretical foundation for the quest for such particles, including the anomalous component of the triangle diagram, which enables particle generation by photons moving through a static magnetic field via the Primakoff effect. The study employed an Nd:YAG laser with a wavelength of 1064 nm, along with polarizers, a photoelastic modulator, and a photodiode for data acquisition. The calibration of the equipment using the Cotton-Mouton effect on oxygen and helium at low pressures to showcase the system's sensitivity is also addressed. The experimental setup involved the application of time-varying magnetic fields and a high-Q Fabry-Perot cavity. The authors elaborate on the experimental techniques and configuration, incorporating the use of Euler-Heisenberg electrodynamics, where $\beta_1 = 4, \beta_2 = \frac{\alpha}{45\pi}$, and α represents the fine structure constant. They also present proposed experimental methods and setups, including Nd:YAG lasers with a wavelength of 1064 nm, polarizers, photoelastic modulators, and photodiodes for data collection. A significant part of the review discusses the calibration of the apparatus using the Cotton-Mouton effect on oxygen and helium at low pressures to demonstrate the sensitivity of the system. Data were gathered by rotating two magnets at frequencies ranging from 2.4 to 3 Hz for 210 hours, confirming a notable enhancement in measuring magnetic birefringence in vacuum and establishing new boundaries for millicharged particles.

In the realm of astrophysics, neutron stars, particularly magnetars [32, 39, 40, 41], which are neutron stars with extremely strong magnetic fields, may exhibit magnetic fields that approach or even surpass the critical threshold. The exploration of nonlinear electrodynamics in vacuum regions surrounding astrophysical bodies with intense magnetic fields, such as pulsars and magnetars, is becoming increasingly prominent. This field of study delves into phenomena like the generation of multiple harmonics by rotating pulsars [42,43], and the influence of a pulsar's swift rotation on the delay of X-ray emissions near its surface. Magnetars, a specific category of neutron stars characterized by their remarkably powerful magnetic fields, play a pivotal role in these investigations. These celestial objects, which emit X-ray and gamma-ray radiation, were initially categorized as Soft Gamma Repeaters (SGR) and Anomalous

X-Ray Pulsars (AXP) [44, 40, 31, 39]. The detection of a colossal flare from SGR 0526-66 in 1979 [29] played a crucial role in the recognition of magnetars, which exhibit magnetic fields ranging from 10^{14} to 10^{15} Gauss [30-32].

In a different study, the authors investigate the impact of vacuum birefringence in the presence of strong magnetic fields [37]. They analyze how photons interact with virtual electron-positron pairs within a magnetic field-contained vacuum, focusing primarily on how strong magnetic fields affect the polarization and dispersion characteristics of the vacuum. To study this phenomenon, a modified effective Lagrangian is utilized, which considers contributions from both the EM field and loop corrections arising from electron-positron pairs. This methodology allows for the computation of alterations in the refractive index of the vacuum when subjected to a strong magnetic field. Notably, these variations can result in the observable occurrence of vacuum birefringence [45], which is experimentally detectable. The research also investigates the influence of quantum corrections on the electrodynamical features of the vacuum. The authors explore how the magnetic field impacts vacuum polarization and propose using this effect to investigate the fundamental aspects of quantum electrodynamics. They conduct a theoretical examination of the feasibility of detecting this phenomenon, making the study relevant for theoretical physicists and experimental researchers alike. In essence, this paper significantly enhances our comprehension of intricate quantum electrodynamical processes under extreme magnetic field conditions and introduces new avenues for exploring the quantum characteristics of the vacuum.

In a different investigation, the emphasis lies on the creation of pairs and the alignment of the vacuum by particles of any spin possessing electric dipole moments [46]. The research provides precise solutions to wave equations for particles of any spin with both electric and magnetic dipole moments in a steady and uniform electromagnetic field. The author also computes the likelihood of pair production of particles by an external electromagnetic field using these precise solutions. The research examines the imaginary component of the effective Lagrangian for electromagnetic fields and determines nonlinear adjustments to the Maxwell Lagrangian, considering the alignment of the vacuum by particles of any spin.

Another research work explores the phenomenon of particle pair generation from the vacuum through the use of high-intensity lasers [47]. The researchers concentrate on the dynamic Schwinger effect, which is linked to the non-perturbative nature of quantum electrodynamics. They investigate the circumstances under which vacuum particle pairs can be produced and eliminated in intense electric fields produced by intersecting laser beams. The study particularly examines the impact of the duration and intensity of laser pulses on the processes of pair creation. Furthermore, the research delves into how the density of the plasma and its electromagnetic characteristics can be employed to experimentally confirm the Schwinger effect.

The paper by Novello investigates the behavior of light in the realm of nonlinear electrodynamics within the framework of modified quantum electrodynamical vacuums [48]. The central focus of the research is to examine the impact of nonlinear adjustments to Maxwell's equations on the geometry of spacetime and, consequently, the paths taken by photons. The authors illustrate that the equation governing the propagation of light can be characterized in relation to alterations in the effective

geometry of the underlying spacetime structure. In order to arrive at these findings, the authors introduce a general representation of this effective geometry and delve into the novel implications stemming from this approach. They employ a modified Lagrangian that is dependent solely on two invariants of the electromagnetic field. This enables them to depict the transmission of electromagnetic waves as if the metric configuration of the backdrop had transitioned from Minkowski to an alternative effective metric, contingent on the behavior of the background electromagnetic field.

The research discussed in this paper focuses on the propagation of light within the framework of nonlinear electrodynamics [49]. Particularly in the presence of strong magnetic fields, it is crucial to investigate how nonlinear effects influence the characteristics of light transmission. The study commences by outlining the fundamental theoretical concepts related to light propagation in nonlinear media. The author elucidates on the modified Maxwell equations that consider the impact of intense magnetic fields on the dynamics of electricity. These equations not only describe conventional light properties like speed and direction of propagation but also more intricate phenomena such as double reflection. It is noted that the distribution of light varies based on its polarization, leading to diverse paths of light propagation with varying polarizations [50,51], in nonlinear mediums. This results in birefringence, where light passing through such a medium split into two rays with distinct properties. To validate their theoretical findings, the authors employed numerical techniques to analyze different conditions and parameters of nonlinear electrodynamic environments, demonstrating how alterations in these parameters affect the properties of light propagation. Through these computations, one can assess the influence of nonlinear electrodynamic processes on light and anticipate novel phenomena that may arise under extreme propagation conditions. Consequently, this study integrates theoretical advancements with numerical simulations to comprehensively examine the consequences of nonlinear electrodynamics on light transmission. This investigation contributes to a better comprehension of the physical mechanisms in intense magnetic fields and holds relevance for diverse fields in physics and astrophysics.

The research conducted by Eduardo Battaner and colleagues focuses on investigating the impact of magnetic fields on the transmission of cosmic rays [52]. The central concept is that specific magnetic field configurations, generated by diverse astrophysical entities, have the ability to function as magnetic lenses, akin to gravitational lenses, albeit with several notable distinctions. The authors examine a basic setup involving a consistent azimuthal magnetic field within a disk-shaped entity and illustrate how such a lens can alter the path of cosmic rays in a predictable geometric manner. It is demonstrated that the lens is effective within a particular segment of the cosmic ray spectrum and can exhibit either converging or diverging behavior, contingent upon the orientation of the magnetic field and the charge of the cosmic ray. The authors explore how the depiction of a monochromatic point source can manifest as one, two, or four points based on the relative positioning of the source, observer, and center of the lens. In cases of perfect alignment and a lens situated in the orthogonal plane, the image transforms into a ring. Additionally, the study reveals that the presence of a lens may introduce subtle fluctuations and asymmetries in the abundance of matter and antimatter in the emissions from remote sources. This study

introduces the notion of a cosmic magnetic lens, which could offer insights into potential patterns observed in the cosmic ray flux across various energy levels.

In a different study, the vacuum is explored as a nonlinear optical medium within the context of the standard model of particle physics, examining phenomena expected to occur at low energies. This includes effects foreseen by quantum electrodynamics for photons with energies below the electron's rest mass. The document emphasizes that despite the theory's long history, experimental validations of these anticipated effects were lacking until recently [14]. Nevertheless, advancements in field sources and technical capabilities suggest that investigating vacuum nonlinear optics will soon be feasible for researchers. The manuscript delves into foundational theories, such as the general formalism and the effective Lagrangian of QED, as well as the tools and techniques involved, like light sources and electrostatic fields. It also addresses phenomenology and associated experiments, covering topics such as three- and four-wave mixing, magnetic birefringence in vacuum, and the experimental methodologies employed. The authors detail the experimental setup, which incorporates Nd:YAG lasers, polarizers, photoelastic modulators, and photodiodes for data acquisition, along with calibration procedures utilizing the Cotton-Mouton effect. The paper extensively examines the experimental approaches and outcomes, which include data gathering via rotating magnets and enhancements in the measurement of magnetic birefringence in vacuum. These developments bring us closer to theoretical projections and establish new thresholds for millicharged particles.

An important experiment that demonstrated vacuum birefringence involved measuring optical linear polarization from the isolated neutron star RX J1856.5-3754 using the Very Large Telescope (VLT) [53, 54]. The data obtained supported the existence of vacuum birefringence, a phenomenon predicted by quantum electrodynamics (QED) in the presence of strong magnetic fields around the star. The "Magnificent Seven" (M7) are a group of radio-quiet isolated neutron stars identified by their thermal surface radiation in soft X-rays. Due to the high magnetic fields (around 10^{13} Gauss) assumed to surround these stars, it is expected that the radiation emitted from them would exhibit significant polarization, regardless of the mechanism responsible for the thermal radiation. However, the detection of a high degree of polarization can only be achieved if QED polarization effects are present in the magnetized vacuum surrounding the star. Thus, observing strongly linearly polarized signals would serve as the first observational evidence of QED effects in regions with strong magnetic fields. The experimental setup involved an Nd:YAG laser with a wavelength of 1064 nm, polarizers, a photoelastic modulator, and a photodiode for data acquisition. The calibration of the equipment was performed using the Cotton-Mouton effect on oxygen and helium at low pressures to showcase the system's sensitivity. Data collection was carried out by rotating two magnets at frequencies ranging from $2.4\text{to}3$ Hz over a period of 210 hours, demonstrating significant advancements in measuring magnetic birefringence in vacuum and establishing new constraints for millicharged particles. The experimental configuration incorporated time-varying magnetic fields and a high-Q Fabry-Perot cavity. The authors detailed the experimental techniques and setup, including the application of Euler-Heisenberg electrodynamics, where $\beta_1 = 4$, $\beta_2 = \alpha/(45\pi)$, and α represents the fine structure

constant. The observed optical rotation of the beam's polarization aligns with the presence of vacuum birefringence as anticipated by QED. This research represents a significant progression in understanding the interaction between light and magnetic fields in the cosmic vacuum, offering new avenues for investigating quantum electrodynamics in extreme conditions.

Various models have been proposed and investigated to depict the nonlinear behavior of vacuum electrodynamics [21-24]. These models correspond to different phenomena observed in astrophysics and cosmology. Some of these models examine the refraction or birefringence of an electromagnetic beam within a vacuum under a strong field [20,55]. By employing analytical solutions of the nonlinear field equation, it becomes feasible to derive the wave equation and ascertain the refractive indices for two polarization modes: parallel and perpendicular [20]. Consequently, in the presence of birefringence in vacuum ($\gamma \neq 0$), the refractive index for the parallel case is given by:

$$n_{\parallel} = \sqrt{1 + \frac{\gamma B_0^2 \sqrt{1-(\beta B_0^2)^2}}{2C + \sqrt{1-(\beta B_0^2)^2}}}. \tag{1.1}$$

Hence, the refractive index is contingent on the phase velocity in parallel polarization. On the other hand, the refractive index for the perpendicular case is:

$$n_{\perp} = \sqrt{\varepsilon\mu} = 1. \tag{1.2}$$

Here, $c = 1$, and ε, μ represent the electric and magnetic permeability of vacuum, respectively. Through this approach, both analytical and numerical values of the refractive indices have been computed for scenarios involving a strong magnetic field and a weak electric field, as well as weak magnetic and electric fields, by utilizing the effective Lagrangian derived from the sum of the Lagrangians of the first and second contour macroscopic field [37]. In a separate study, analytically calculated refractive index values were obtained for the effective nonlinear Lagrangian, which combines approximations of the Born-Infeld and Heisenberg-Euler Lagrangians [56].

$$n_{\perp} = \sqrt{1 + \mathbf{B}^2\beta^2},\ n_{\parallel} = \sqrt{1 + \frac{\mathbf{B}^2}{\gamma^2}}. \tag{1.3}$$

Here is **B** the induction of external magnetic field. The results obtained are compared with the observatory results. In the same way, refractive indices values can be obtained depending on the types of Lagrangians of NLED [11].

The following study offers a comprehensive analysis of the influence of nonlinear vacuum electrodynamics on the polarization of light [57]. The research delves into a category of Plebanski theories that elucidate nonlinear phenomena in a vacuum. Particular emphasis is placed on investigating the rotation of the polarization

plane in different spacetimes within the realm of general relativity and electromagnetic fields. The authors present an elaborate theoretical exploration that includes formulating equations to examine phenomena like birefringence and polarization dispersion in a vacuum. This research significantly enhances our comprehension of how light interacts with intense magnetic and electric fields.

In a subsequent scholarly publication, researchers delve into the concept of photon time delay within a magnetized vacuum, taking into account radiative corrections within a single loop approximation process [58]. The primary focus of the investigation lies in the transmission of photons within the magnetosphere of a neutron star, conceptualized as a magnetized vacuum. The study introduces a modified photon dispersion equation incorporating the self-energy of the magnetized photon within the transparency region. The resolution of the dispersion equation is articulated through analytical functions. The study reveals that as the magnetic field strength increases, the phase velocity of photons diminishes, causing the dispersion curve to progressively diverge from the light cone. A notable aspect of the research is the exploration of how photon time delay varies with magnetic field intensity and distance, employing a magnetic dipole configuration. A significant discovery is that photons of higher energy encounter lengthier time delays, challenging conventional understandings of photon delay in the interstellar medium. The methodology entails solving the dispersion equation with radiative corrections stemming from the self-energy of the magnetized photon, employing hypergeometric functions for computations. The analysis is carried out within the framework of a magnetic dipole model for the magnetosphere, considering different scenarios based on magnetic field strength and distance from the source. The paper also delves into the potential implications and practical applications of the findings, particularly in comprehending photon behavior under the extreme magnetic field conditions of neutron stars. This study makes a substantial contribution to the realms of astrophysics and quantum electrodynamics, offering a fresh perspective on phenomena within neutron star magnetospheres.

The research conducted by A. S. Habibina and H. S. Ramadhan is centered on exploring the geodesic paths of electrically charged black holes using polynomial Maxwell Lagrangian models associated with NLED [45]. Various models proposed by Kruglov, Ayón-Beato-García, and others are investigated in this study. The focus is particularly on analyzing the stable trajectories of photons around extremal black holes, in contrast to ReissnerNordström black holes. Additionally, the study examines how NLED affects the bending of light rays by black holes, unveiling adjustments to the angle of slight deflection.

The research focuses on investigating how high-intensity electromagnetic waves interact with particles within a powerful magnetic field setting. When the wave's amplitude surpasses the magnetic field's strength, particles can gain energy through multiple resonant interactions, quickly reaching the radiation reaction threshold [28]. This results in substantial wave scattering. These phenomena play a crucial role in the theoretical frameworks of Fast Radio Bursts (FRB) and magnetars, as particles accelerated by the waves emit gamma rays that may initiate electron-positron cascades. Instead of dissipating entirely, the waves can provoke X-ray bursts.

The research conducted by Chul Min Kim and Sang Pyo Kim focuses on investigating quantum electrodynamical phenomena like Schwinger pair creation and vacuum birefringence in the presence of extremely powerful magnetic fields surrounding highly magnetized neutron stars, based on the Goldreich-Julian pulsar model [59, 60]. The study delves into the realm of strong-field physics, encompassing Schwinger pair creation, vacuum birefringence, and the wrench effect, which is anticipated to be observed through X-ray polarimetry in forthcoming space missions. The research extensively examines quantum electrodynamics loop corrections, resulting in nonlinear electrodynamics where the vacuum exhibits field-dependent dielectric and magnetic properties, particularly in terms of the magnetoelectric response. In scenarios with intense electric fields, the vacuum undergoes decay due to the spontaneous generation of electron-positron pairs [61]. To investigate the impact of vacuum birefringence on photons within the electromagnetic fields of neutron stars, this study employs the Heisenberg-Euler-Schwinger (HES) effective action, which incorporates quantum electrodynamics loop corrections and characterizes nonlinear electrodynamics. The researchers derive a novel analytical expression for the HES action, encompassing both supercritical and subcritical magnetic fields. The key equation utilized in the research describes Schwinger pair creation [62] and the decay rate of the vacuum in a constant electromagnetic field, as dictated by the HES action.

$$R\left(r,\theta_n;\frac{B_0}{B_c}\right)=\frac{\pi e^{-\frac{\pi}{b_3}}a_3b_3m^4}{8\pi^2b_3}\coth\left(\frac{\pi}{b_3}\right), \tag{1.4}$$

where a_3 and b_3 are dimensionless parameters that are directly related to the magnetic and electric fields, B_0 represents the magnetic field strength at the surface of the neutron star, and B_c denotes the critical magnetic field value. The researchers analyze the occurrence of Schwinger pair production in the presence of extremely strong magnetic fields and induced subcritical electric fields [63], resulting in the significant generation of electron-positron pairs within an astrophysical scale volume in Compton units near the neutron star's north and south poles. The study also explores vacuum birefringence effects on low-energy photons within intense electromagnetic fields, which could lead to detectable polarization effects that are measurable using X-ray polarization techniques. These findings have the potential to provide insights into the electromagnetic field configurations of neutron stars and charged or magnetized black holes.

Transitioning from an overview of modern approaches to investigating the impacts of nonlinear electrodynamics in vacuum and gravity to an in-depth examination of techniques for computing ray deflection angles and the occurrence of double refraction within the framework of NLED in vacuum and gravity near dense objects showcases the progression of our comprehension of the interplay between quantum and gravitational effects. This section on methodologies signifies a crucial advancement towards a more thorough examination and simulation of how light and other particles behave in the extreme environments typical of compact celestial bodies. The discussed computational techniques not only push the limits of our theoretical

knowledge but also furnish valuable instruments for deciphering observed astronomical occurrences, thereby enriching our insight into the fundamental laws of the universe.

The study conducted by Viktor I. Denisov et al. explores the nonlinear bending of X-ray and gamma-ray beams in the magnetic fields of pulsars and magnetars [64 − 66]. The research delves into the impact of strong magnetic fields on the paths of electromagnetic waves, particularly within the realm of vacuum nonlinear electrodynamics. The authors introduce a theoretical framework to address the phenomena that may occur in the extreme magnetic fields surrounding pulsars and magnetars. By employing modified Maxwell equations, they describe how electromagnetic waves propagate in these unique environments. The investigation focuses on the influence of magnetic fields on the refraction and curvature of beam trajectories, with a specific emphasis on the bending angles in the presence of intense magnetic fields. The findings reveal that in the powerful magnetic fields of magnetars, the degree of electrodynamical bending can be notably significant, potentially observable in X-rays and gamma rays. This discovery marks a significant advancement in comprehending the effects of magnetic fields on the transmission of electromagnetic waves, with important implications for astrophysics and the exploration of pulsars and magnetars. The authors also consider potential astronomical observations and experiments to validate their theoretical projections and ponder the repercussions of these phenomena on the broader comprehension of vacuum nonlinear electrodynamics.

The additional work conducted by Jin Young Kim and Taekoon Lee delves into the phenomenon of light bending resulting from alterations in the quantum electrodynamical vacuum induced by non-electric factors, like the magnetic field of a neutron star [61,67,68]. The scholars examine how the magnetic field of a neutron star can induce a refractive index gradient due to nonlinear electrodynamical effects, and they compute the deflection angle experienced by light in close proximity to a magnetized neutron star. Furthermore, they investigate how thermal radiation can also cause light deflection, assuming the neutron star behaves as an isothermal black body, and they estimate the deflection angles, comparing them with the gravitational deflection angle. The variation in the speed of light within a QED vacuum [69,12] affected by electric or magnetic fields, leading to an alteration in the light cone's configuration, is discussed. The effective EulerHeisenberg Lagrangian is employed to elucidate the interaction in a low-intensity field. The authors derive the equation governing the trajectory of light traversing the modified QED vacuum, utilizing the concepts of refractive index and Snell's law to elucidate the light's path in an uneven medium.

$$\frac{1}{n}\frac{d\vec{u}}{ds} = (u \times \nabla n) \times u, \tag{1.5}$$

where u represents the unit vector aligned with the direction of the light ray, s stands for the distance parameter along the light trajectory, and $n = c/v$ denotes the refractive index. The study investigates the deflection of light due to a magnetic dipole, taking into account the dipole's orientation concerning the incident ray. The researchers

calculate the horizontal (δ_h) and vertical (δ_v) deflection angles by integrating the trajectory equation. The analysis includes the deflection of light caused by black body radiation emitted from a neutron star, utilizing the general formula proposed by Dittrich and Gies[70] to ascertain the changes in velocity and refractive indices for soft photons traversing through modified QED vacuums. The findings indicate that the deflection induced by the magnetic dipole field prevails over the deflection caused by radiation for impact parametres $b < 10^3 r_0$, yet both deflection angles are notably smaller than the gravitational deflection.

In the study conducted by V.I. Denisov et al.[66,71,72], the influence of vacuum nonlinear electrodynamics on the emission and slowing down of the rotation of rapidly rotating pulsars is examined using a theoretical framework rooted in quantum electrodynamics within the postMaxwellian approximation. By employing NLED equations, the researchers investigate the electromagnetic fields surrounding pulsars that exhibit intense magnetic fields capable of displaying quantum electrodynamical phenomena. The authors develop mathematical expressions for the brightness of pulsar emissions, taking into account adjustments resulting from nonlinear quantum electrodynamics effects. The primary methodological strategy involves the utilization of linearized equations to address minor nonlinear modifications to Maxwell's electromagnetic equations. This approach facilitates the computation of corrections to the electromagnetic emissions from pulsars and the evaluation of their influence on the overall rotational dynamics of the pulsars. The theoretical investigation hinges on solving equations governing the electromagnetic field within the post-Maxwellian approximation, which incorporates corrections associated with vacuum nonlinear electrodynamics. The study evaluates how these corrections affect the deceleration of pulsar rotation, consequently altering their radiative characteristics. A crucial aspect of the analysis involves determining the energy flow density (Poynting vector) and emission brightness by utilizing equations pertaining to polarized vectors and polarization tensors that consider the effects of vacuum nonlinearity. These computations aid in understanding the role of nonlinear effects in the broader context of pulsar emissions. An essential component of the methodology is the use of an approximation to quantify emission brightness, which encompasses adjustments originating from vacuum nonlinear electrodynamics. These adjustments are elucidated through parameters of post-Maxwellian electrodynamics and enable an examination of the impact of nonlinear effects on pulsar emissions in the presence of strong magnetic fields.

The research conducted by Abishev et al. investigates the nonlinear impacts of vacuum electrodynamics within the magnetic quadrupole field of a pulsar, with a specific emphasis on the behavior of electromagnetic waves in this particular setting [73]. The study is carried out using the parameterized post-Maxwellian vacuum electrodynamics framework and employs the eikonal approximation. The primary objective is to analyze the propagation of electromagnetic pulses within the intense magnetic field of a pulsar, transmitted through two normal modes characterized by orthogonal polarizations. One of the pivotal equations highlighted in the paper pertains to the polarized elements of the magnetic field in the quadrupole approximation, which, under the Maxwellian approximation, can be represented as:

$$B_r = -\frac{BR_s^4}{4r^2}(1 + 3\cos^2\theta)\cos\phi_1 - \frac{3\sin 2\theta\cos\phi\sin\phi_1\cos\phi_2}{2r^5} +$$

$$+\frac{3\sin^2\theta\cos 2\phi\sin\phi_1\sin\phi_2}{2r^5}. \quad (1.6)$$

where R_s represents the radius of the neutron star, B is a constant with the dimensions of magnetic induction, and ϕ_1 and ϕ_2 denote angles that define the particular geometry of the quadrupole magnetic field. The researchers subsequently convert this setup into a rectangular Cartesian coordinate system and derive equations for the elements of the magnetic induction vector within the quadrupole field:

$$B_x = \frac{5B_0R_s^4}{6r^7}[x(r^2 - 5z^2)f_1 + 2z(5x^2 - r^2)f_2 + x(5z^2 - 3r^2 + 10y^2)f_3], \quad (1.7)$$

where B_0, f_1, f_2, and f_3 represent parameters that determine both the strength and direction of the quadrupole field. The authors also examine the impact of magnetic dipole and quadrupole fields [74] on the transmission of electromagnetic waves, which can lead to variations in the time taken for waves to travel between the source and receiver due to the nonlinear electromagnetic influence of these fields. The authors also explore how these fields affect the polarization characteristics of electromagnetic pulses, including the linear polarization of the initial segment of the pulse and the elliptical polarization of the subsequent portion. This research highlights the importance of accounting for the nonlinear effects of vacuum electrodynamics when studying the propagation of electromagnetic waves in the intense magnetic fields of pulsars and magnetars, offering new insights into these celestial bodies.

Romero and colleagues' research explores the photon time delay in a magnetized vacuum, taking into account radiative corrections within the framework of a single-loop process [58]. The primary objective of the study is to examine how photons propagate in the magnetosphere of a neutron star, which is conceptualized as a magnetized vacuum. The study introduces a modified photon dispersion equation that incorporates the self-energy of the magnetized photon within the transparency region. The solution to this dispersion equation is presented through analytical functions. The researchers observed that as the magnetic field strength increases, the phase velocity of photons decreases, causing the dispersion curve to deviate further from the light cone. A notable aspect of the investigation is the analysis of how photon time delay varies with the magnetic field strength and distance, employing a magnetic dipole configuration. A key discovery is that photons of higher energy encounter longer time delays, challenging conventional assumptions about photon delay in the interstellar medium. The methodology involves solving the dispersion equation with radiative corrections derived from the self-energy of the magnetized photon, utilizing hypergeometric functions [75,76,77] for computations. The analysis is carried out within the framework of a magnetic dipole model for the magnetosphere, considering

different scenarios based on the magnetic field strength and distance from the source. The article also explores the potential implications and practical applications of the findings, particularly in enhancing our comprehension of photon behavior in the extreme magnetic fields of neutron stars. This study makes a significant contribution to the realms of astrophysics and quantum electrodynamics, offering fresh insights into the processes occurring within neutron star magnetospheres.

The paper authored by Jin Young Kim delves into a detailed examination of how the Coulomb charge impacts the path of a light beam within the framework of Born-Infeld electrodynamics, a nonlinear theory of electromagnetism aimed at resolving the divergences arising from the selfinteraction of charged particles and establishing a theoretical framework consistent with quantum mechanics principles[78]. The research primarily focuses on mathematically modeling and analytically determining the deflection angle of light beams as they pass close to Coulomb charges. In contrast to the linear propagation of light in classical electrodynamics and the weak gravitational lensing[79] in general relativity [80, 81, 82, 83], in Born-Infeld nonlinear electrodynamics, light undergoes deflection due to its interaction with the electromagnetic fields produced by Coulomb charges. The primary methodology employed in the study involves solving the Born-Infeld field equations through approximate integration techniques and numerical analysis. Kim makes specific assumptions and sets boundary conditions that mirror the real-world scenario of light interacting with a charge, and employs perturbation theory methods to calculate adjustments to the light's trajectory induced by the electromagnetic field. The author details the process of deriving and scrutinizing solutions, with a particular emphasis on the physical interpretations of the derived quantities and their reliance on the charge and light parameters. By comparing the outcomes with analogous effects in other theories, distinctive characteristics of the interaction between light and electromagnetic fields within Born-Infeld electrodynamics are identified. A significant portion of the study revolves around forecasting experimental outcomes and the feasibility of observing the described effects in astrophysical environments, such as in proximity to compact stellar objects[84,85,86] where intense electromagnetic fields can lead to noticeable light deflection. Consequently, the paper makes a noteworthy contribution to advancing the comprehension of intricate interactions between light and electromagnetic fields in nonlinear mediums, pushing the boundaries of contemporary physics and opening up new avenues for theoretical and experimental investigations in this domain.

The following research conducted by Kim et al. delves into the phenomenon of vacuum birefringence resulting from the interaction of the vacuum with supercritical magnetic fields and subcritical electric fields [87]. The investigation is centered on elucidating the birefringence effect, taking into account the impact of a mild electric field in conjunction with an immensely strong magnetic field. The authors introduce a comprehensive analytical representation for the one-loop effective Lagrangian in the presence of combined magnetic and electric fields, building upon the specific formula for the one-loop effective Lagrangian under arbitrarily intense magnetic fields. This formulation is subsequently employed to deduce the polarization and magnetization of the vacuum, enabling the determination of the dielectric permittivity and magnetic

permeability for weak probing fields. Ultimately, the researchers ascertain the refractive indices and corresponding polarization vectors for scenarios involving parallel magnetic and electric fields. The proposed model anticipates that an electric field aligned with the magnetic field diminishes birefringence and alters the orientation of the polarization vectors.

In a different fascinating study outlined in [88,89,90], diverse approaches for determining the deflection angle of light rays are examined, particularly when they traverse the equatorial plane of a magnetic dipole. The paper presents essential equations that elucidate the procedure for computing the deflection angle of light rays in the framework of generalized Born-Infeld electrodynamics and employing the GBT[91]. Effective refractive indices:

$$n_{\perp} \approx 1 + \frac{2B^2}{\beta^2},\ n_{\parallel} \approx 1 + \frac{2B^2}{\gamma^2}. \tag{1.8}$$

The following equations illustrate the relationship between the refractive index and the properties of the magnetic field generated by the magnetic dipole. Here, B represents the magnetic field, whereas β and γ are the parameters linked to this field. The formula for the deflection angle of light is also provided.

$$\Delta\theta_{\perp} = -\frac{15\pi B^2}{16\beta^2 b^6}. \tag{1.9}$$

In this formula, $\Delta\theta_{\perp}$ denotes the light's deflection angle, B stands for the magnetic field's strength, β is a factor related to Born-Infeld electrodynamics, and b represents the impact parameter. The minus sign signifies that the deflection happens towards the magnetic dipole. By employing the Gauss-Bonnet theorem for computing the deflection angle:

$$\Delta\theta = \iint_D K dS, \tag{1.10}$$

here, K represents the Gaussian curvature, dS stands for an area element on the surface, and the integration is performed over the domain D, which covers the vicinity of the magnetic dipole. This equation enables the determination of the angle of deflection of the light by utilizing spatial geometry. These expressions illustrate the connection between the electromagnetic and geometric characteristics of the magnetic field and how they impact the bending of light beams. It is worth mentioning that the methods and formulas employed in the analysis are tailored to specific scenarios: the equatorial plane and a single light ray, while not accounting for birefringence.

In a different study, techniques for computing the deflection angle of light as it travels through the magnetic field created by a magnetic dipole are elaborated within the framework of generalized Born-Infeld NLED and the general theory of relativity[92, 34, 93, 94]. The analysis commences with the fundamentals of geometric

optics, where the trajectory equation of light, derived from Snell's law, is adjusted to accommodate the variation in the refractive index within the magnetic field. This methodology enables the precise computation of the angle of slight deflection of light, assuming the light beam traverses the equatorial plane of the magnetic dipole. Additionally, the paper presents a functional action for generalized Born-Infeld electrodynamics, encompassing both classical and quantum amendments to electrodynamics, enabling the incorporation of effects linked to intense magnetic fields. This functional action results in modified equations of motion that depict the propagation of light in such scenarios. A crucial aspect of the analysis involves the utilization of geodesic equations for determining the deflection angle of light, considering general relativistic implications. These equations facilitate the evaluation of light deflection under the influence of gravitational and magnetic fields surrounding celestial bodies like magnetars, illustrating how the deflection angle relies on the mass and magnetic moment parameters of the entity. To sum up, the paper deliberates on the potential application of these theoretical findings in astrophysics, specifically in estimating the deflection angle of light within the potent magnetic fields of magnetars. This approach underscores the importance of a holistic examination of classical and quantum effects in electrodynamics and the general theory of relativity to gain profound insights into astrophysical phenomena.

Another research on birefringence and light polarization in dense objects [51, 95, 96, 97, 98] has delved into the bending angles and temporal delays of polarized light during light deflection [71, 88, 99-105]. Both theoretical and computational assessments of the light bending angles have been presented [92]. Nonetheless, these investigations primarily concentrate on the equatorial plane of the magnetosphere. By utilizing the trajectory equation of geometrical optics, the bending angles of rays traversing magnetic and electric fields were characterized and contrasted with those in the gravitational field [104,105]. Furthermore, by employing the effective geodesic equation for a single photon, the values of the impact parameter corresponding to the bending angle for various ratios of the impact parameter to the magnetar radius were analytically determined and juxtaposed concerning gravitational and magnetic fields [71,92,101]. It is acknowledged that exploring different NLED models beyond those examined in the current study is crucial. Models like rational, arcsin, arctan, Born-Infeld type, and others possess unique features and implications that necessitate further investigation. Nevertheless, it is crucial to stress that this exploration goes beyond the scope of this paper. Given the significance of experimental or observational validation of nonlinear electrodynamic effects, studies proposing alternative approaches and uncovering novel effects are pivotal. While analytical computations of the bending angles of electromagnetic radiation traversing magnetar fields and their temporal delays in the equatorial plane have been conducted [92,100,103] computations for regions outside the equatorial plane remain uncharted.

1.2Deflection of rays in a uniform magnetic field in a NLED vacuum.

In the NLED of Born-Infeld, the nonlinearity of the equations "activates" in areas of strong fields and suppresses the unbounded growth of the field. Indeed,

consider a point particle. Since the problem possesses spherical symmetry, in this case, the equations of Born-Infeld NLED take the form:

$$L_{BI} = -\frac{1}{4\pi a^2}\left[\sqrt{1 + a^2\left(\vec{B}^2 - \vec{E}^2\right) - a^4\left(\vec{B}^2\vec{E}^2\right)^2} - 1\right] \tag{1.11}$$

where a – constant having a dimension inverse to the dimension of magnetic field induction.

$$\frac{1}{r^2}\frac{d}{dr}[r^2 D_r] = 4\pi q\delta(\vec{r}),\ \mathrm{rot}\,\vec{E} = 0. \tag{1.12}$$

From the equation of this system, it follows that $D_r = q/r^2$. The material equation in the static spherically symmetric case takes the form: $D_r = E_r/\sqrt{1 - a^2E_r^2}$. Solving this equation for E_r, we obtain: $E_r = D_r/\sqrt{1 + a^2D_r^2}$.

Substituting the explicit expression for D_r into the right side, we have: $E_r = q/\sqrt{r^4 + a^2q^2}$. Investigating this expression, for $r >> a|q|$ it takes the Coulomb form $E_r = q/r^2$, remaining finite as $r \to 0$: $E_r = q/(|q|a)$. Therefore, the energy of the electrostatic field of a point charged particle in the nonlinear electrodynamics of Born-Infeld is also a finite quantity. Then, the nonlinear electrodynamics of the vacuum, which is a consequence of quantum electrodynamics (the Heisenberg-Euler electrodynamics), its Lagrangian, field equations, and dynamic characteristics are considered.

The equations of the electromagnetic field in the nonlinear electrodynamics of Heisenberg-Euler without sources are analogous to the equations of macroscopic electrodynamics of continuous media:

$$L_{EH} = -\frac{1}{8\pi}\left[\vec{B}^2 - \vec{E}^2\right] + \frac{\alpha}{360\pi^2B_q^2}\left\{\left(\vec{B}^2 - \vec{E}^2\right)^2 + 7(\vec{B}\vec{E})^2\right\}, \tag{1.13}$$

$$\mathrm{rot}\,\mathbf{H} = \frac{1}{c}\frac{\partial \mathbf{D}}{\partial t}, \mathrm{div}\,\mathbf{D} = 0, \mathbf{D} = 4\pi\frac{\partial L}{\partial \mathbf{E}}, \tag{1.14}$$

$$\mathrm{rot}\,\mathbf{E} = -\frac{1}{c}\frac{\partial \mathbf{B}}{\partial t}, \mathrm{div}\,\mathbf{B} = 0, \mathbf{H} = -4\pi\frac{\partial L}{\partial \mathbf{B}}. \tag{1.15}$$

Using expression (16), it is not difficult to obtain the expansions of the **D** and **H** vectors in terms of powers of B/B_q and E/B_q with post-Maxwellian accuracy of the first order:

$$\mathbf{D} = \mathbf{E} + \frac{\alpha}{45\pi B_q^2}\{2(\mathbf{E}^2 - \mathbf{B}^2)\mathbf{E} + 7(\mathbf{BE})\mathbf{B}\}, \tag{1.16}$$

$$\mathbf{H} = \mathbf{B} + \frac{\alpha}{45\pi B_q^2}\{2(\mathbf{E}^2 - \mathbf{B}^2)\mathbf{B} - 7(\mathbf{BE})\mathbf{E}\}. \qquad (1.17)$$

The system of electromagnetic field equations in the nonlinear electrodynamics of Heisenberg-Euler has an exact solution in the form of a plane elliptically polarized wave.

$$\mathbf{E} = \mathbf{E}_1 \cos(\Omega t - \mathbf{Kr}) + \mathbf{E}_2 \sin(\Omega t - \mathbf{Kr}),$$

$$(\mathbf{E}_1\mathbf{E}_2) = 0,\ \mathbf{B} = \frac{c}{\Omega}[\mathbf{KE}], \frac{\Omega^2}{c^2} = \mathbf{K}^2,\ (\mathbf{KE}_1) = (\mathbf{KE}_2) = 0. \qquad (1.18)$$

The invariants of this wave are equal to zero. Finally, parameterized post-Maxwellian electrodynamics of the vacuum is considered as a generalization of nonlinear models in the case of weak fields.

There are other models of nonlinear electrodynamics. Current experiments cannot resolve the question of which theory is most adequate to nature. To select the nonlinear electrodynamics most adequate to nature, it is necessary to calculate nonlinear effects in various theories and compare their predictions with the results of corresponding experiments. To facilitate such calculations in the approximation of a weak electromagnetic field, we propose using a parameterized post-Maxwellian formalism, which, in a certain sense, is analogous to the parameterized post-Newtonian formalism in the theory of gravity, applied to calculate various gravitational effects in the weak field of the Solar System.

The fundamental premise of such formalism is considered to be that the Lagrangian of nonlinear electrodynamics in vacuum is an analytical function of the invariants $J_1 = \left(\vec{E}^2 - \vec{B}^2\right)/B_q^2$ и $J_2 = (\vec{E}\vec{B})^2/B_q^4$, at least in the vicinity of their zero values. Therefore, in the case of a weak electromagnetic field $J_1 << 1, J_2 << 1$, this Lagrangian can be expanded in a series by the whole powers of these invariants:

$$\mathcal{L} = \frac{B_q^2}{8\pi}\sum_{n=0}^{\infty}\sum_{m=0}^{\infty} L_{nm} J_1^n J_2^m. \qquad (1.19)$$

Since as $J_1 \to 0, J_2 \to 0$ the theory with Lagrangian (1.13) must transition into Maxwell's electrodynamics, then $L_{00} = 0, L_{10} = 1$. With this approach, each nonlinear electrodynamics corresponds to a well-defined set of post-Maxwellian parameters L_{nm}. From the perspective of experiments conducted in a weak electromagnetic field, one nonlinear electrodynamics will differ from another only in the values of these parameters.

Thus, the post-Maxwellian formalism, abstracting from the details of any particular nonlinear electrodynamics, its equations, hypotheses, and postulates, in other words, everything that constitutes its complete theoretical framework, takes only the final result: the Lagrangian expansion, which, according to the given theory, is valid in

the approximation of a weak electromagnetic field. Further analysis of theories and determining how their predictions match experimental results is of a general nature and formally boils down to answering two questions: what values of post-Maxwellian parameters does the studied theory have and what are these parameters according to the results of corresponding experiments. Therefore, one of the tasks facing this formalism is to identify those nonlinear electrodynamics that are consistent with experiments conducted in a weak electromagnetic field.

However, from our point of view, the opportunity provided by this formalism for systematic calculation of nonlinear electrodynamical effects, regardless of any nonlinear theory, holds equal importance: the task of theory and experiment in this case should not only be the search for a particular effect that disproves a certain nonlinear electrodynamics, but also systematic calculation and conducting experiments with the aim of testing the hypothesis of the Lagrangian's analyticity near $J_1 = 0, J_2 = 0$ and subsequently determining with the required accuracy the values of all post-Maxwellian parameters.

As a result of implementing this program, a generalized post-Maxwellian theory of the electromagnetic field capable of describing all experiments in a weak electromagnetic field may be constructed. It is quite clear that this theory will not be able to answer many questions about the properties of nonlinear electromagnetic interaction and its primary purpose will be to describe one of the limiting cases of precise nonlinear electrodynamics - the approximation of a weak electromagnetic field. After successful implementation of this program, any nonlinear electrodynamics claiming to adequately describe reality must transition into this post-Maxwellian theory in the limit of a weak electromagnetic field.

Since it is quite evident that, given the current level of development in experimental techniques, such a program can only be implemented for a few of the first coefficients of expansion (1.19), let us write down the expression, limiting ourselves to the accuracy necessary for our purposes.

$$\mathcal{L} = \frac{1}{8\pi}\left[\vec{E}^2 - \vec{B}^2\right] + \xi\left[\eta_1\left(\vec{E}^2 - \vec{B}^2\right)^2 + 4\eta_2(\vec{B}\vec{E})^2\right] +$$

$$+\xi^2\left[\eta_3\left(\vec{E}^2 - \vec{B}^2\right)^3 + \eta_4\left(\vec{E}^2 - \vec{B}^2\right)(\vec{B}\vec{E})^2\right] +$$

$$+\xi^3\left[\eta_5\left(\vec{E}^2 - \vec{B}^2\right)^4 + \eta_6\left(\vec{E}^2 - \vec{B}^2\right)^2(\vec{B}\vec{E})^2 + \eta_7(\vec{B}\vec{E})^4\right], \qquad (1.20)$$

where $\xi = 1/B_q^2$, a $\eta_1, \eta_2, \eta_3, \eta_4, \eta_5, \eta_6, \eta_7$ - dimensionless post-Maxwellian parameters.

In the Born-Infeld theory, these parameters take the form:

$$\eta_1 = \frac{a^2 B_q^2}{32\pi},\ \eta_2 = \frac{a^2 B_q^2}{32\pi},\ \eta_3 = -\frac{a^4 B_q^4}{64\pi},$$

$$\eta_4 = -\frac{a^4 B_q^4}{16\pi},\ \eta_5 = \frac{5a^6 B_q^6}{512\pi}, \tag{1.21}$$

$$\eta_6 = \frac{3a^6 B_q^6}{64\pi},\ \eta_7 = -\frac{a^6 B_q^6}{32\pi}.$$

In NLED, only Heisenberg-Euler-Schwinger parameters are reliably known as

$$\eta_1 = \frac{\alpha}{360\pi^2},\ \eta_2 = \frac{7\alpha}{90\pi^2}, \tag{1.22}$$

and the rest can be found if you use the higher approximations of the theory of quantum electrodynamic excitations.

The equations of the electromagnetic field in nonlinear electrodynamics are analogous to the equations of macroscopic electrodynamics:

$$\mathrm{rot}\,\vec{H} = \frac{1}{c}\frac{\partial \vec{D}}{\partial t},\ \mathrm{div}\,\vec{D} = 0, \mathrm{rot}\,\vec{E} = -\frac{1}{c}\frac{\partial \vec{B}}{\partial t},\ \mathrm{div}\,\vec{B} = 0, \tag{1.23}$$

different from them in terms of vectors $\vec{D}$ and $\vec{H}$ Using the expression (1.20), it is easy to obtain the expansion of these vectors in powers of ξ up to and including ξ^3:

$$\vec{D} = 4\pi\frac{\partial \mathcal{L}}{\partial \vec{E}} = \vec{E} + 4\pi\{\xi\left[4\eta_1\left(\vec{E}^2 - \vec{B}^2\right)\vec{E} + 8\eta_2\left(\vec{B}\vec{E}\right)\vec{B}\right] +$$

$$+\xi^2\left[6\eta_3\left(\vec{E}^2 - -\vec{B}^2\right)^2\vec{E} + 2\eta_4(\vec{B}\vec{E})^2\vec{E} + 2\eta_4\left(\vec{E}^2 - \vec{B}^2\right)(\vec{B}\vec{E})\vec{B}\right] +$$

$$+\xi^3\left[8\eta_5\left(\vec{E}^2 - \vec{B}^2\right)^3\vec{E} + 4\eta_6\left(\vec{E}^2 - \vec{B}^2\right)(\vec{B}\vec{E})^2\vec{E} +\right.$$

$$\left.+2\eta_6\left(\vec{E}^2 - \vec{B}^2\right)^2(\vec{B}\vec{E})\vec{B} + 4\eta_7(\vec{B}\vec{E})^3\vec{B}\right]\}, \tag{1.24}$$

$$\vec{H} = -4\pi\frac{\partial \mathcal{L}}{\partial \vec{B}} = \vec{B} + 4\pi\{\xi\left[4\eta_1\left(\vec{E}^2 - \vec{B}^2\right)\vec{B} - 8\eta_2\left(\vec{B}\vec{E}\right)\vec{E}\right] +$$

$$+\xi^2\left[6\eta_3\left(\vec{E}^2 - \vec{B}^2\right)^2\vec{B} + 2\eta_4(\vec{B}\vec{E})^2\vec{B} - 2\eta_4\left(\vec{E}^2 - \vec{B}^2\right)(\vec{B}\vec{E})\vec{E}\right] +$$

$$+\xi^3\left[8\eta_5\left(\vec{E}^2 - \vec{B}^2\right)^3\vec{B} + 4\eta_6\left(\vec{E}^2 - \vec{B}^2\right)(\vec{B}\vec{E})^2\vec{B} -\right.$$

$$\left.-2\eta_6\left(\vec{E}^2 - \vec{B}^2\right)^2(\vec{B}\vec{E})\vec{E} - 4\eta_7(\vec{B}\vec{E})^3\vec{E}\right]\}, \tag{1.25}$$

$$\vec{D} = 4\pi\frac{\partial \mathcal{L}}{\partial \vec{E}} = \vec{E} + 4\pi\{\xi\left[4\eta_1\left(\vec{E}^2 - \vec{B}^2\right)\vec{E} + 8\eta_2\left(\vec{B}\vec{E}\right)\vec{B}\right] +$$

$$\xi^2\left[6\eta_3\left(\vec{E}^2 - -\vec{B}^2\right)^2\vec{E} + 2\eta_4(\vec{B}\vec{E})^2\vec{E} + 2\eta_4\left(\vec{E}^2 - \vec{B}^2\right)(\vec{B}\vec{E})\vec{B}\right] +$$

$$+\xi^3\left[8\eta_5\left(\vec{E}^2 - \vec{B}^2\right)^3\vec{E} + 4\eta_6\left(\vec{E}^2 - \vec{B}^2\right)(\vec{B}\vec{E})^2\vec{E} +\right.$$

$$\left.+2\eta_6\left(\vec{E}^2 - \vec{B}^2\right)^2(\vec{B}\vec{E})\vec{B} + 4\eta_7(\vec{B}\vec{E})^3\vec{B}\right]\}, \qquad (1.26)$$

$$\vec{H} = -4\pi\frac{\partial \mathcal{L}}{\partial \vec{B}} = \vec{B} + 4\pi\{\xi\left[4\eta_1\left(\vec{E}^2 - \vec{B}^2\right)\vec{B} - 8\eta_2\left(\vec{B}\vec{E}\right)\vec{E}\right] +$$

$$+\xi^2\left[6\eta_3\left(\vec{E}^2 - \vec{B}^2\right)^2\vec{B} + 2\eta_4(\vec{B}\vec{E})^2\vec{B} - 2\eta_4\left(\vec{E}^2 - \vec{B}^2\right)(\vec{B}\vec{E})\vec{E}\right] +$$

$$+\xi^3\left[8\eta_5\left(\vec{E}^2 - \vec{B}^2\right)^3\vec{B} + 4\eta_6\left(\vec{E}^2 - \vec{B}^2\right)(\vec{B}\vec{E})^2\vec{B} -\right.$$

$$\left.-2\eta_6\left(\vec{E}^2 - \vec{B}^2\right)^2(\vec{B}\vec{E})\vec{E} - 4\eta_7(\vec{B}\vec{E})^3\vec{E}\right]\}. \qquad (1.27)$$

Based on the analysis, the eikonal equation for a weak electromagnetic wave propagating in an external electromagnetic field according to the laws of post-Maxwellian electrodynamics is derived.

The vector $\vec{B}$ and $\vec{E}$ in the approximation of geometrical optics can be written as:

$$\vec{B} = \vec{B}_0 + \vec{b}\exp\left[-i\left(\omega t - \vec{k}\vec{r}\right)\right],\ \vec{E} = \vec{E}_0 + \vec{e}\exp\left[-i\left(\omega t - \vec{k}\vec{r}\right)\right], \qquad (1.28)$$

where ω - frequency, $\vec{k}$ - wave vector and we will consider vector $\vec{b}$ and $\vec{e}$ as the weakly varying functions t and $\vec{r}$ compared to the function of exp $[i(\omega t - \vec{k}\vec{r})]$.

By restricting our analysis to the linear approximation of the vectors $\vec{b}$ and $\vec{e}$, and utilizing expressions (1.26, 1.27, 1.28), we simplify the first equation in (1.23) to the following form:

$$[\vec{k}\vec{b}] + \frac{\omega}{c}\vec{e} + 4\pi\{\xi\{4\eta_1\left(\vec{E}_0^2 - \vec{B}_0^2\right)\left[\vec{k}\vec{b}\right] + 8\eta_1 Q_1\left[\vec{k}\vec{B}_0\right] -$$

$$-8\eta_2 Q_2\left[\vec{k}\vec{E}_0\right] + \frac{8\omega}{c}\eta_1 Q_1\vec{E}_0 + \frac{4\omega}{c}\eta_1\left(\vec{E}_0^2 - \vec{B}_0^2\right)\vec{e} +$$

$$+\frac{8\omega}{c}\eta_2 Q_2\vec{B}_0\} + \xi^2\left\{6\eta_3\left(\vec{E}_0^2 - \vec{B}_0^2\right)^2[\vec{k}\vec{b}] + 2\eta_4\left(\vec{B}_0\vec{E}_0\right)^2[\vec{k}\vec{b}] +\right.$$

$$+24\eta_3 Q_1\left(\vec{E}_0^2-\vec{B}_0^2\right)\left[\vec{k}\vec{B}_0\right]+4\eta_4 Q_2\left(\vec{B}_0\vec{E}_0\right)\left[\vec{k}\vec{B}_0\right]-$$

$$-4\eta_4 Q_1\left(\vec{B}_0\vec{E}_0\right)\left[\vec{k}\vec{E}_0\right]-2\eta_4 Q_2\left(\vec{E}_0^2-\vec{B}_0^2\right)\left[\vec{k}\vec{E}_0\right]+$$

$$+\frac{6\omega}{c}\eta_3\left(\vec{E}_0^2-\vec{B}_0^2\right)^2\vec{e}+\frac{24\omega}{c}\eta_3 Q_1\left(\vec{E}_0^2-\vec{B}_0^2\right)\vec{E}_0+$$

$$+\frac{2\omega}{c}\eta_4\left(\vec{B}_0\vec{E}_0\right)^2\vec{e}+\frac{4\omega}{c}\eta_4 Q_2\left(\vec{B}_0\vec{E}_0\right)\vec{E}_0+\frac{4\omega}{c}\eta_4 Q_1\left(\vec{B}_0\vec{E}_0\right)\vec{B}_0+$$

$$+\frac{2\omega}{c}\eta_4 Q_2\left(\vec{E}_0^2-\vec{B}_0^2\right)\vec{B}_0\Big\}+$$

$$+\xi^3\Big[8\eta_5\left(\vec{E}_0^2-\vec{B}_0^2\right)^3[\vec{k}\vec{b}]+48\eta_5 Q_1\left(\vec{E}_0^2-\vec{B}_0^2\right)^2\left[\vec{k}\vec{B}_0\right]+$$

$$+4\eta_6\left(\vec{E}_0^2-\vec{B}_0^2\right)\left(\vec{B}_0\vec{E}_0\right)^2\left[\vec{k}\vec{b}\right]+8\eta_6 Q_1\left(\vec{B}_0\vec{E}_0\right)^2\left[\vec{k}\vec{B}_0\right]+$$

$$+8\eta_6 Q_2\left(\vec{E}_0^2-\vec{B}_0^2\right)\left(\vec{B}_0\vec{E}_0\right)\left[\vec{k}\vec{B}_0\right]-$$

$$-8\eta_6 Q_1\left(\vec{E}_0^2-\vec{B}_0^2\right)\left(\vec{B}_0\vec{E}_0\right)\left[\vec{k}\vec{E}_0\right]-$$

$$-2\eta_6 Q_2\left(\vec{E}_0^2-\vec{B}_0^2\right)^2\left[\vec{k}\vec{E}_0\right]-12\eta_7 Q_2\left(\vec{B}_0\vec{E}_0\right)^2\left[\vec{k}\vec{E}_0\right]+$$

$$+\frac{8\omega}{c}\eta_5\left(\vec{E}_0^2-\vec{B}_0^2\right)^3\vec{e}+\frac{48\omega}{c}\eta_5 Q_1\left(\vec{E}_0^2-\vec{B}_0^2\right)^2\vec{E}_0+$$

$$+\frac{4\omega}{c}\eta_6\left(\vec{E}_0^2-\vec{B}_0^2\right)\left(\vec{B}_0\vec{E}_0\right)^2\vec{e}+\frac{8\omega}{c}\eta_6 Q_1\left(\vec{B}_0\vec{E}_0\right)^2\vec{E}_0+$$

$$+\frac{8\omega}{c}\eta_6 Q_2\left(\vec{E}_0^2-\vec{B}_0^2\right)\left(\vec{B}_0\vec{E}_0\right)\vec{E}_0+$$

$$+\frac{8\omega}{c}\eta_6 Q_1\left(\vec{E}_0^2-\vec{B}_0^2\right)\left(\vec{B}_0\vec{E}_0\right)\vec{B}_0+$$

$$+\frac{2\omega}{c}\eta_6 Q_2\left(\vec{E}_0^2-\vec{B}_0^2\right)^2\vec{B}_0. \qquad (1.29)$$

where the notations have been introduced:

$$Q_1=\left(\vec{e}\vec{E}_0\right)-\left(\vec{b}\vec{B}_0\right),\ Q_2=\left(\vec{b}\vec{E}_0\right)+\left(\vec{B}_0\vec{e}\right) \qquad (1.30)$$

Substituting the relation (1.28) into the third equation system (19), we will have: $\vec{b} = c[\vec{k}\vec{e}]/\omega$. Using this equality, we eliminate the vector $\vec{b}$ from expression (1.29). As a result, we arrive at a homogeneous system of three linear algebraic equations with respect to the three components of the vector $\vec{e}$, which can be conveniently written in tensor form:

$$\Pi^{\alpha\beta} e_\beta = 0 \tag{1.31}$$

where

$$\Pi^{\alpha\beta} = A_0 \left\{ k^\alpha k^\beta + \left(\frac{\omega^2}{c^2} - \vec{k}^2 \right) \delta^{\alpha\beta} \right\} + A_1 \left\{ N_B^\alpha N_B^\beta + \frac{\omega}{c} \left[E_0^\alpha N_B^\beta + \right. \right.$$

$$\left. + N_B^\alpha E_0^\beta \right] + \frac{\omega^2}{c^2} E_0^\alpha E_0^\beta \Big\} + A_2 \left\{ N_E^\alpha N_E^\beta - \frac{\omega}{c} \left[B_0^\alpha N_E^\beta + N_E^\alpha B_0^\beta \right] + \frac{\omega^2}{c^2} B_0^\alpha B_0^\beta \right\} +$$

$$+ A_3 \left\{ \frac{\omega}{c} \left[B_0^\alpha N_B^\beta + N_B^\alpha B_0^\beta \right] - \left[N_E^\alpha N_B^\beta + N_B^\alpha N_E^\beta \right] - \right.$$

$$\left. - \frac{\omega}{c} \left[E_0^\alpha N_E^\beta + N_E^\alpha E_0^\beta \right] + \frac{\omega^2}{c^2} \left[B_0^\alpha E_0^\beta + E_0^\alpha B_0^\beta \right] \right\} \tag{1.32}$$

and for brevity, the following notations have been introduced:

$$A_0 = 1 + 4\pi \left\{ 4\eta_1 \xi \left(\vec{E}_0^2 - \vec{B}_0^2 \right) + 6\eta_3 \xi^2 \left(\vec{E}_0^2 - \vec{B}_0^2 \right)^2 + \right.$$

$$\left. + 2\eta_4 \xi^2 \left(\vec{B}_0 \vec{E}_0 \right)^2 + + 8\eta_5 \xi^3 \left(\vec{E}_0^2 - \vec{B}_0^2 \right)^3 + 4\eta_6 \xi^3 \left(\vec{B}_0 \vec{E}_0 \right)^2 \left(\vec{E}_0^2 - \vec{B}_0^2 \right) \right\}, \tag{1.33}$$

$$A_1 = 4\pi \left\{ 8\eta_1 \xi + 24\eta_3 \xi^2 \left(\vec{E}_0^2 - \vec{B}_0^2 \right) + 48\eta_5 \xi^3 \left(\vec{E}_0^2 - \vec{B}_0^2 \right)^2 + 8\eta_6 \xi^3 \left(\vec{B}_0 \vec{E}_0 \right)^2 \right\}, \tag{1.34}$$

$$A_2 = 4\pi \left\{ 8\eta_2 \xi + 2\eta_4 \xi^2 \left(\vec{E}_0^2 - \vec{B}_0^2 \right) + 2\eta_6 \xi^3 \left(\vec{E}_0^2 - \vec{B}_0^2 \right)^2 + 12\eta_7 \xi^3 \left(\vec{B}_0 \vec{E}_0 \right)^2 \right\}, \tag{1.35}$$

$$A_3 = 4\pi \left\{ 4\eta_4 \xi^2 \left(\vec{B}_0 \vec{E}_0 \right) + 8\eta_6 \xi^3 \left(\vec{E}_0^2 - \vec{B}_0^2 \right) \left(\vec{B}_0 \vec{E}_0 \right) \right\}, \tag{1.36}$$

$$\vec{N}_E = \left[\vec{k}\vec{E}_0 \right], \vec{N}_B = \left[\vec{k}\vec{B}_0 \right], \tag{1.38}$$

$\delta^{\alpha\beta}$ - the Kronecker symbol, which in Cartesian coordinates of Euclidean space is a metric tensor.

For the existence of nontrivial solutions to the system of equations (1.31), it is necessary to require that

$$\det\|\Pi^{\alpha\beta}\| = 0 \tag{1.39}$$

The most straightforward method to compute the determinant of tensor (1.32) involves leveraging formulas from tensor algebra concerning the powers of a second-rank tensor and its determinant. The determinant of a second-rank tensor in three-dimensional Euclidean space can be expressed as:

$$2\Pi_{(3)} - 3\Pi_{(1)}\Pi_{(2)} + \Pi_{(1)}^3 = 0, \tag{1.40}$$

where

$$\Pi_{(N)} = \Pi_{\alpha_1\beta_1}\delta_{\beta_1\alpha_2}\Pi_{\alpha_2\beta_2}\delta_{\beta_2\alpha_3}\dots\Pi_{\alpha_N\beta_N}\delta_{\beta_N\alpha_1}. \tag{1.41}$$

Utilizing expression (1.32) and forming powers of the tensor $\Pi^{\alpha\beta}$, and after canceling out $\omega^2 A_0/c^2$, we arrive at the following dispersion equation:

$$\frac{\omega^4}{c^4}\left\{A_4\left[\vec{B}_0\vec{E}_0\right]^2 + A_2A_0\vec{B}_0^2 + A_1A_0\vec{E}_0^2 + A_0^2 + 2A_0A_3\left(\vec{B}_0\vec{E}_0\right)\right\} -$$

$$-\frac{2\omega^3}{c^3}\left(\vec{k}\left[\vec{E}_0\vec{B}_0\right]\right)\left\{A_4\vec{B}_0^2 + A_4\vec{E}_0^2 + A_1A_0 + A_2A_0\right\} +$$

$$+\frac{\omega^2}{c^2}\left\{A_4\left[\vec{k}\,\vec{B}_0\right]^2\vec{B}_0^2 - A_2A_0\vec{B}_0^2\vec{k}^2 - A_4\left(\vec{k}\vec{E}_0\right)^2\vec{B}_0^2 -\right.$$

$$-A_1A_0\vec{E}_0^2\vec{k}^2 + A_4\vec{E}_0^2\left[\vec{k}\vec{E}_0\right]^2 - A_4\vec{E}_0^2\left(\vec{k}\vec{B}_0\right)^2 +$$

$$+2A_4\vec{k}^2\left(\vec{B}_0\vec{E}_0\right)^2 - 2A_0^2\vec{k}^2 - 4A_0A_3\vec{k}^2\left(\vec{B}_0\vec{E}_0\right) +$$

$$+A_2A_0\left[\vec{k}\quad\vec{E}_0\right]^2 + 4A_4\left(\vec{k}\left[\vec{E}_0\quad\vec{B}_0\right]\right)^2 + A_1A_0\left[\vec{k}\quad\vec{B}_0\right]^2 -$$

$$\left.-A_1A_0\left(\vec{k}\quad\vec{E}_0\right)^2 - A_2A_0\left(\vec{k}\quad\vec{B}_0\right)^2\right\} - \frac{2\omega}{c}\left(\vec{k}\left[\vec{E}_0\quad\vec{B}_0\right]\right)\times$$

$$\times\left\{A_4\left[\vec{k}\quad\vec{B}_0\right]^2 - A_1A_0\vec{k}^2 - A_2A_0\vec{k}^2 + A_4\left[\vec{k}\quad\vec{E}_0\right]^2 -\right.$$

$$\left.-\frac{2\omega}{c}\left(\vec{k}\left[\vec{E}_0\quad\vec{B}_0\right]\right)\left\{A_4\left[\vec{k}\quad\vec{B}_0\right]^2 - A_1A_0\vec{k}^2 - A_2A_0\vec{k}^2 + A_4\left[\vec{k}\quad\vec{E}_0\right]^2 -\right.\right.$$

$$-A_4\left(\vec{k}\vec{B}_0\right)^2 - A_4\left(\vec{k}\vec{E}_0\right)^2\Big\} - A_4\vec{k}^4\left(\vec{B}_0\vec{E}_0\right)^2 + A_0^2\vec{k}^4 + 2A_0A_3\vec{k}^4\left(\vec{B}_0\vec{E}_0\right) -$$

$$-A_2A_0\vec{k}^2\left[\vec{k} \quad \vec{E}_0\right]^2 - A_1A_0\vec{k}^2\left[\vec{k} \quad \vec{B}_0\right]^2 + A_1A_0\vec{k}^2\left(\vec{k}\,\vec{E}_0\right)^2 +$$

$$+A_2A_0\vec{k}^2\left(\vec{k} \quad \vec{B}_0\right)^2 + A_4\left[\vec{k} \quad \vec{E}_0\right]^2\left[\vec{k} \quad \vec{B}_0\right]^2 -$$

$$-A_4\left[\vec{k} \quad \vec{E}_0\right]^2\left(\vec{k} \quad \vec{E}_0\right)^2 -$$

$$-A_4\left[\vec{k} \quad \vec{B}_0\right]^2\left(\vec{k} \quad \vec{B}_0\right)^2 + A_4\left(\vec{k}\,\vec{B}_0\right)^2\left(\vec{k}\,\vec{E}_0\right)^2 = 0, \qquad (1.42)$$

where $A_4 = A_1A_2 - A_3^2$.

The solution $\omega = \omega(\vec{k})$ for this equation is to be sought in the form of an expansion in powers of ξ, similarly to the expansion of the Lagrangian (1.20) being considered.

$$\omega = ck[1 + \pi\xi F + \pi^2\xi^2 U + \pi^3\xi^3 W], \qquad (1.43)$$

where F, U и W - unknown functions.

Now, let's substitute this expansion into the dispersion equation (1.42). Since the Lagrangian (1.20) is specified with accuracy up to terms proportional to ξ^3, inclusive, we will also omit unreliable terms $\sim \xi^4$ when conducting the calculations. As a result, we obtain an expression containing 128 terms and having the form of an expansion in powers of ξ, which we will not write out due to its complexity.

In this expression, terms proportional to the zeroth and first powers of ξ are absent. Terms proportional to ξ^2, contain only one unknown function F, and terms proportional to ξ^3 contain functions F and U, and do not contain the function W. It should be noted that among all the parameters $\eta_1, \eta_2, \eta_3, \eta_4, \eta_5, \eta_6$ and η_7, only parameters $\eta_1, \eta_2, \eta_3, \eta_4$ are included in this expression, the rest were incorporated as coefficients into higher powers of ξ and therefore were discarded.

By setting the coefficients of this expansion in powers of ξ to zero, we obtain two equations with respect to the two unknown functions F and U. In the lowest approximation, we have:

$$\left\{Fk^2 - 16\eta_1\left[2k\left(\vec{k}\left[\vec{E}_0 \quad \vec{B}_0\right]\right) - \left[\vec{k} \quad \vec{B}_0\right]^2 - \left[\vec{k} \quad \vec{E}_0\right]^2\right]\right\} \times$$

$$\times\left\{Fk^2 - 16\eta_2\left[2k\left(\vec{k}\left[\vec{E}_0 \quad \vec{B}_0\right]\right) - \left[\vec{k} \quad \vec{B}_0\right]^2 - \left[\vec{k} \quad \vec{E}_0\right]^2\right]\right\} = 0. \qquad (1.44)$$

Upon resolving equation (26), we derive two solutions:

$$F_1 = \frac{16\eta_1}{k^2}\left\{2k\left(\vec{k}\left[\vec{E}_0 \quad \vec{B}_0\right]\right) - \left[\vec{k} \quad \vec{B}_0\right]^2 - \left[\vec{k} \quad \vec{E}_0\right]^2\right\}, \qquad (1.45)$$

$$F_2 = \frac{16\eta_2}{k^2}\left\{2k\left(\vec{k}\left[\vec{E}_0 \quad \vec{B}_0\right]\right) - \left[\vec{k} \quad \vec{B}_0\right]^2 - \left[\vec{k} \quad \vec{E}_0\right]^2\right\}. \qquad (1.46)$$

Therefore, according to the nonlinear electrodynamics of the vacuum in a constant and uniform electromagnetic field, the propagation of two types of "weak" plane electromagnetic waves with frequencies is possible.

$$\omega_1 = ck\left\{1 + \frac{16\pi\eta_1\xi}{k^2}\left[2k\left(\vec{k}\left[\vec{E}_0 \quad \vec{B}_0\right]\right) - \left[\vec{k} \quad \vec{B}_0\right]^2 - \left[\vec{k} \quad \vec{E}_0\right]^2\right]\right\}, \qquad (1.47)$$

$$\omega_2 = ck\left\{1 + \frac{16\pi\eta_2\xi}{k^2}\left[2k\left(\vec{k}\left[\overrightarrow{E_0} \quad \vec{B}_0\right]\right) - \left[\vec{k} \quad \vec{B}_0\right]^2 - \left[\vec{k} \quad \vec{E}_0\right]^2\right]\right\}, \qquad (1.48)$$

which, in the general case, differ by terms proportional to ξ.

Starting to analyze the obtained relations (1.47, 1.48), we note first of all that for $\eta_2 = \eta_1$ the expressions for ω_1 and ω_2 coincide up to terms proportional to ξ^2. In this case, only one type of electromagnetic waves can propagate in each direction. This means that nonlinear electrodynamics, the post-Maxwellian parameters of which satisfy the relation $\eta_2 = \eta_1$, is in a sense a distinguished theory among other nonlinear electrodynamics.

An example of such a theory, in particular, is Born-Infeld electrodynamics, the post-Maxwellian parameters of which satisfy the indicated relationship. If we had used the exact expression for the Lagrangian, rather than its post-Maxwellian expansion, it would have led to the exact dispersion equation

$$\omega_1 = \omega_2 = ck\left\{1 + \frac{a^2}{2k^2}\left[2k\left(\vec{k}\left[\vec{E}_0 \quad \vec{B}_0\right]\right) - \left[\vec{k} \quad \vec{B}_0\right]^2 - \left[\vec{k} \quad \vec{E}_0\right]^2\right]\right\}, \qquad (1.49)$$

which shows that in Born-Infeld electrodynamics, in the presence of constant and uniform electromagnetic fields, only one type of electromagnetic waves can propagate in each direction.

And finally, for nonlinear theories in which the post-Maxwellian parameters η_1 and η_2 are equal to zero, the frequencies ω_1 and ω_2 differ from the Maxwellian value ck by terms proportional to ξ^2. Considering that at the maximum achievable fields in laboratory conditions $E_0 \sim B_0 \sim 10^6$, the following estimates are valid:

$$\xi^2 B_0^4 \sim \xi^2 E_0^4 \sim \xi^2\left(\vec{B}_0\vec{E}_0\right)^2 \sim 10^{-31}, \qquad (1.50)$$

it can be stated that nonlinear electrodynamic effects in such theories are unlikely to be observed experimentally in the near future.

1.3Deflection of rays in a dipole magnetic field in a NLED vacuum.

In the following study, the authors focus on analyzing the effects of beam bending and studying changes in phase and group velocities under the influence of external fields. Particular attention is paid to the interaction of weak electromagnetic waves with a neutron star's strong dipole magnetic and gravitational fields. As a basis for describing the space-time metric, researchers use the Schwarzschild solution, which allows for a deeper understanding of the processes that occur when electromagnetic waves pass through such intense fields in the context of astrophysics:

$$g_{00} = 1 - \frac{r_g}{r},$$

$$g_{rr} = -\frac{r}{r - r_g},$$

$$g_{\theta\theta} = -r^2,$$

$$g_{\varphi\varphi} = -r^2 \sin^2\theta, \tag{1.51}$$

where r_g – is the gravitational radius of the neutron star. In this and other works, calculations of the main nonlinear electrodynamic and gravitational effects are carried out with quadratic accuracy in the parameter r_g/r and linear accuracy in the parameter $\eta_{1,2}\xi\mathbf{B}^2$. To do this, the eikonal equation is derived for an electromagnetic wave propagating in a magnetic dipole field. In the linear approximation, the solution to the electromagnetic field equations describing the dipole magnetic field of a neutron star has the form:

$$F_{31}^{(0)} = -\frac{|\mathbf{m}|}{r^2}\sin^2\theta,$$

$$F_{32}^{(0)} = \frac{2|\mathbf{m}|}{r}\sin\theta\cos\theta, \tag{1.52}$$

where $\mathbf{m}$ represents the magnetic dipole moment.

Next, an equation was obtained that is satisfied by the eikonal of a weak high-frequency electromagneti.c wave propagating in the gravitational (1.51) and magnetic (1.52) fields of a neutron star. The electromagnetic field tensor, included in the electromagnetic field equations, in this case, was presented as the sum of the dipole magnetic field $F_{ik}^{(0)}$ of the star (1.52) and the field of a weak electromagnetic wave

$$f_{ik}: F_{ik} = F_{ik}^{(0)} + f_{ik.}. \tag{1.53}$$

Using a linear approximation using a weak electromagnetic wave f_{ik}, the electromagnetic field equations are obtained:

$$\frac{1}{\sqrt{-g}}\frac{\partial}{\partial x^n}\{\sqrt{-g}Q_{(1)}^{mn}\} = 0,$$

$$\frac{\partial f_{mn}}{\partial x^k} + \frac{\partial f_{nk}}{\partial x^m} + \frac{\partial f_{km}}{\partial x^n} = 0, \tag{1.54}$$

where

$$Q_{(1)}^{mn} = \left[1 + \xi(\eta_1 - 2\eta_2)J_2^{(0)}\right] f^{mn} + 4\xi\eta_2 \left[f^{ml}F_{lk}^{(0)}F_{(0)}^{kn} +\right.$$

$$\left.+F_{(0)}^{ml}f_{lk}F_{(0)}^{kn} + F_{(0)}^{ml}F_{lk}^{(0)}f^{kn}\right] + \left[2\xi(\eta_1 - 2\eta_2)f_{ik}F_{(0)}^{ki}\right]F_{(0)}^{mn}. \tag{1.55}$$

Since this work examines the effect of the gravitational and magnetic fields of a star on the rays of a weak electromagnetic wave, we found an equation that should satisfy the eikonal in the case under consideration. For this, the tensor f_{nm} of a weak electromagnetic wave is represented as:

$$f_{nm} = A_{nm}(\mathbf{r}, t)e^{iS(\mathbf{r},t)}. \tag{1.56}$$

where, as usual, the amplitude $A_{nm}(\mathbf{r}, t)$ is a slowly varying function of coordinates and time, and the eikonal $S(\mathbf{r}, t)$ is a rapidly varying function. As a result, the derivatives of S turn out to be extremely large values, so that the condition is satisfied:

$$\left|\frac{A_{nm}(\mathbf{r}, t)\,\partial S}{\partial x^l}\right| \gg \left|\frac{\partial A_{nm}(\mathbf{r}, t)}{\partial x^l}\right|. \tag{1.57}$$

Substituting expression (1.56) into equations (1.54), it is taken into account that for points located outside the star, the following relations are satisfied in order of magnitude:

$$\frac{\partial F_{nm}^{(0)}}{\partial r} \sim \frac{F_{nm}^{(0)}}{R}, \quad \left|\frac{\partial g_{nm}^{(0)}}{\partial r}\right| \ll \left|\frac{g_{nm}^{(0)}}{R}\right|, \quad \frac{\partial S}{\partial r} \sim \frac{S}{\lambda}, \tag{1.58}$$

where R is the radius of the star, λ is the wavelength.

Since for high-frequency electromagnetic radiation $R/\lambda >> 1$, then when differentiating $Q_{(1)}^{nm}$ in equations (1.54) only derivatives of the eikonal S are left, as a result, the equations of system (1.54) take the form of a homogeneous system of linear algebraic equations:

$$\left[1+\xi(\eta_1-2\eta_2)J_2^{(0)}\right]f^{\mu n}\frac{\partial S}{\partial x^n}+$$

$$+4\xi\eta_2\left[f^{\mu l}F_{lk}^{(0)}F_{(0)}^{kn}+F^{\mu l}f_{lk}F_{(0)}^{kn}+F_{(0)}^{\mu l}F_{lk}^{(0)}f^{kn}\right]\frac{\partial S}{\partial x^n}+$$

$$+\left[2\xi(\eta_1-2\eta_2)f_{ik}F_{(0)}^{ki}\right]F_{(0)}^{\mu n}\frac{\partial S}{\partial x^n}=0, \tag{1.59}$$

$$f_{\alpha\beta}\frac{\partial S}{\partial x^0}+f_{\beta 0}\frac{\partial S}{\partial x^\alpha}+f_{0\alpha}\frac{\partial S}{\partial x^\beta}=0. \tag{1.60}$$

Multiplying the first equation of system (1.60) by $\partial S/\partial x^0$ and eliminating the components $f_{\alpha\beta}$ from it using the second equation, we obtain a system of equations of the form:

$$\Pi^{\mu\beta}f_{0\beta}=0. \tag{1.61}$$

The eikonal equation, as is known, is a consequence of the condition that the determinant of the matrix consisting of the components of the energy-momentum tensor is equal to zero. Applying the rules of tensor algebra to express the result in a form independent of the choice of coordinates, and simplifying it by discarding a factor that does not affect the result, we obtained the eikonal equation.

$$G_{(1)}^{ik}G_{(2)}^{nm}\left(\frac{\partial S}{\partial x^i}\right)\left(\frac{\partial S}{\partial x^k}\right)\left(\frac{\partial S}{\partial x^n}\right)\left(\frac{\partial S}{\partial x^m}\right)=0, \tag{1.62}$$

$$G_{(1,2)}^{ik}=g^{ik}+\eta_{1,2}F^{ip}F_p^{\cdot k}. \tag{1.63}$$

By using tensor algebra to obtain the result in a form invariant to the choice of the coordinate system and subsequent simplification by eliminating unimportant factors, the authors derive the eikonal equation:

$$G_{(1)}^{ik}\left(\frac{\partial S}{\partial x^i}\right)\left(\frac{\partial S}{\partial x^k}\right)=0, G_{(2}^{ik}\left(\frac{\partial S}{\partial x^i}\right)\left(\frac{\partial S}{\partial x^k}\right)=0. \tag{1.64}$$

By placing the origin of coordinates at the center of the neutron star and directing the z-axis along the vector of the dipole magnetic moment m, in the plane of the magnetic equator, where $\theta=\pi/2$, the polar coordinates r and φ are introduced.

$$\left(1+\frac{r_g}{r}+\frac{r_g^2}{r^2}\right)\left(\frac{\partial S}{\partial x^0}\right)^2-\left(1-\frac{r_g}{r}\right)\left(\frac{\partial S}{\partial r}\right)^2-\frac{1}{r^2}\left(\frac{\partial S}{\partial \varphi}\right)^2+$$

$$+\frac{4\eta_{1,2}\xi\mathbf{m}^2}{r^6}\left[\left(\frac{\partial S}{\partial r}\right)^2+\frac{1}{r^2}\left(\frac{\partial S}{\partial \varphi}\right)^2\right]=0. \tag{1.65}$$

Solution with the variable separation method:

$$S=-\mathcal{E}_0 t+\alpha\varphi\pm\int^r d\,dr\sqrt{f(r)}, \tag{1.66}$$

where the plus sign corresponds to the propagation of an electromagnetic wave from a neutron star, and the minus sign to the star, $\mathcal{E}_0$ and α are arbitrary constants and the following notation is introduced:

$$f(r)=\frac{\mathcal{E}_0^2}{c^2}\left[1+\frac{2r_g}{r}+\frac{3r_g^2}{r^2}+\frac{4\xi\eta_{1,2}\mathbf{m}^2}{r^6}\right]-\frac{\alpha^2}{r^2}\left[1+\frac{r_g}{r}+\frac{r_g^2}{r^2}\right]. \tag{1.67}$$

Further, a certain ray of an electromagnetic wave with frequency ω_0, originating at spatial infinity and having an impact distance $b_{1,2}$, is considered. As the ray circumnavigates the neutron star in a clockwise direction, the integration constants $\mathcal{E}_0$ and α, included in the expression, are written as:

$$\mathcal{E}_0=\omega_0,\ \alpha=-\frac{\omega_0 b_{1,2}}{c}. \tag{1.68}$$

Differentiating expression (1.67) concerning α and equating the result to some constant φ_0, the following equation is obtained:

$$\varphi=\varphi_0\mp\frac{\omega_0 b_{1,2}}{c}\int^r\frac{dr}{r^2\sqrt{f(r)}}\frac{dr}{r^2\sqrt{f(r)}}\left[1+\frac{r_g}{r}+\frac{r_g^2}{r^2}\right]. \tag{1.69}$$

In this context, two electromagnetic waves are considered, one of which is polarized in the plane of the magnetic equator of the neutron star, and the other is perpendicular to this plane, propagating along rays that have identical aiming parameters at $R_0\to\infty$: $b_1=b_2=b$. Within the adopted accuracy, they found the bending angles of these rays:

$$\delta\varphi_{1,2}=-\frac{2r_g}{b}-\frac{15\pi r_g^2}{16b^2}-\frac{15\pi\eta_{1,2}\xi\mathbf{m}^2}{4b^6}. \tag{1.70}$$

The first two terms in this expression account for the gravitational bending of the ray, while the last one represents the nonlinear electrodynamical bending. The minus sign in expression (1.70) indicates that the gravitational and magnetic fields of the neutron star in the plane of the magnetic equator act on electromagnetic waves as a

converging lens. The angle $\delta\varphi$ between the asymptotes of these two rays, when $R_1 = \infty$, will be equal to:

$$\delta\varphi = \delta\varphi_1 - \delta\varphi_2 = \frac{15\pi(\eta_2 - \eta_1)\xi\mathbf{m}^2}{4b^6}. \quad (1.71)$$

Nonlinear models of vacuum electrodynamics, where the post-Maxwellian parameters η_1 and η_2 differ, predict that the phase v_{ph} and group v_{gr} velocities of electromagnetic signals in an external field will depend on their polarization. Accordingly, electromagnetic waves polarized along the vector $\vec{B}_0$, propagate at the speeds:

$$v_{ph} = c\left\{1 - \frac{2\eta_1\xi}{k}\left[\vec{k}\vec{B}_0\right]\right\},\ v_{gr} = c\left\{\frac{\vec{k}}{k}(1 - 2\eta_1\xi B_0^2) + \frac{4\eta_1\xi}{k}\left(\vec{k}\vec{B}_0\right)\vec{B}_0\right\}. \quad (1.72)$$

For the electromagnetic waves polarized in the perpendicular plane:

$$v_{ph} = c\left\{1 - \frac{2\eta_2\xi}{k}\left[\vec{k}\vec{B}_0\right]\right\},\ v_{gr} = c\left\{\frac{\vec{k}}{k}(1 - 2\eta_2\xi B_0^2) + \frac{4\eta_2\xi}{k}\left(\vec{k}\vec{B}_0\right)\vec{B}_0\right\}. \quad (1.73)$$

Thus, with $\eta_1 \neq \eta_2$, a signal of one polarization in the magnetic field of the neutron star should outpace a signal of another polarization.

The derived formulas allow for an analysis of the nonlinear electrodynamical effect of birefringence in an external field. The essence of the birefringence effect in a vacuum external electromagnetic field lies in the dependence of the propagation speed of electromagnetic signals in this field on their polarization. Therefore, if two signals with two different polarizations are emitted at the same moment from a single source and then pass through the field of a neutron star, they will not arrive at the detector simultaneously. Consequently, measuring the delay time of an electromagnetic pulse with one standard polarization compared to an electromagnetic pulse with another standard polarization will allow for a more detailed verification of the predictions of nonlinear electrodynamics of the vacuum. Since the magnetospheres of pulsars and magnetars may contain matter that absorbs electromagnetic waves, hereafter, under electromagnetic waves, we understand gamma-ray pulses, for which the magnetosphere is transparent by definition.

In studying an electromagnetic wave moving in the plane of the magnetic equator of the star, where $\theta = \pi/2$, it is found that the eikonal equation for this wave, arising from the equations of nonlinear electrodynamics by Heisenberg-Euler, varies depending on its polarization.

For the electromagnetic wave polarized perpendicular to the plane $\theta = \pi/2$, the eikonal S_1 satisfies the equation

$$\left(1+\frac{r_g}{r}+\frac{r_g^2}{r^2}\right)\left(\frac{\partial S_1}{\partial x^0}\right)^2-\left(1-\frac{r_g}{r}\right)\left(\frac{\partial S_1}{\partial r}\right)^2-\frac{1}{r^2}\left(\frac{\partial S_1}{\partial \varphi}\right)^2+$$

$$+\frac{7\alpha|\mathbf{m}|^2}{45\pi B_q^2 r^6}\left\{\left(\frac{\partial S_1}{\partial r}\right)^2+\frac{1}{r^2}\left(\frac{\partial S_1}{\partial \varphi}\right)^2\right\}=0, \tag{1.74}$$

Whereas for the electromagnetic wave polarized in the plane of the magnetic equator, the eikonal S_2 is satisfied by the equation:

$$\left(1+\frac{r_g}{r}+\frac{r_g^2}{r^2}\right)\left(\frac{\partial S_2}{\partial x^0}\right)^2-\left(1-\frac{r_g}{r}\right)\left(\frac{\partial S_2}{\partial r}\right)^2-\frac{1}{r^2}\left(\frac{\partial S_2}{\partial \varphi}\right)^2+$$

$$+\frac{4\alpha|\mathbf{m}|^2}{45\pi B_q^2 r^6}\left\{\left(\frac{\partial S_2}{\partial r}\right)^2+\frac{1}{r^2}\left(\frac{\partial S_2}{\partial \varphi}\right)^2\right\}=0. \tag{1.75}$$

Upon analyzing the first equation and employing standard formalism, the authors effortlessly derive the ray equation for an electromagnetic wave with the first type of polarization. By determining the distance to the nearest approach point of the ray as b_1, within the context of polar coordinates r and φ the following relationship is established:

$$\varphi=\varphi_0\mp b_1\int^r\frac{dr}{r^2\sqrt{F(r)}}\frac{dr}{r^2\sqrt{F(r)}}\left[1+\frac{r_g}{r}+\frac{r_g^2}{r^2}\right], \tag{1.76}$$

where

$$F(r)=1+\frac{2r_g}{r}+\frac{3r_g^2}{r^2}+\frac{7\alpha|\mathbf{m}|^2}{45\pi B_q^2 r^6}-\frac{b_1^2}{r^2}\left[1+\frac{r_g}{r}+\frac{r_g^2}{r^2}\right]. \tag{1.77}$$

Employing the ray equation in its original formulation, denoted as (1.76), proves impractical for the intended purposes. Consequently, the researchers turn to Darwin's method to transform the mentioned expression (1.76) into a format that better suits their goals.

$$r=\frac{b_1}{V_1+W_1\sin\Psi_1(\varphi)}, \tag{1.78}$$

where

$$V_1=\frac{r_g}{2b_1},\ W_1=1+\frac{7\alpha|\mathbf{m}|^2}{90\pi B_q^2 b_1^6}+\frac{5r_g^2}{8b_1^2}, \tag{1.79}$$

$$\Psi_1(\varphi) = \varphi + \varphi_1 + \frac{r_g}{2b_1}\cos(\varphi + \varphi_1) - \frac{r_g^2}{32b_1^2}\{30(\varphi + \varphi_1) + \sin 2(\varphi + \varphi_1)\} -$$

$$-\frac{7\alpha|\mathbf{m}|^2}{2880\pi B_q^2 b_1^6}\{60(\varphi + \varphi_1) + \sin 4(\varphi + \varphi_1) - 16\sin 2(\varphi + \varphi_1)\}. \qquad (1.80)$$

The angle φ_1 and the impact distance b_1 are identified as parameters, the variation of which allows exploring the entire family of rays. Specifically, when the source of electromagnetic waves is positioned at a point with radial distance $r = R_0$, and azimuthal angle $\varphi = \pi$, then

$$\varphi_1 = -\xi_1 + \frac{r_g}{2b_1}\cos\,\xi_1 + \frac{3r_g^2}{32b_1^2}\{10(\pi - \xi_1) + \sin\,2\xi_1\} +$$

$$+\frac{7\alpha|\mathbf{m}|^2}{2880\pi B_q^2 b_1^6}[60(\pi - \xi_1) - \sin 4\xi_1 + 16\sin 2\xi_1], \qquad (1.81)$$

where to simplify the notation, the following designation is introduced as

$$\xi_1 = \arcsin\left\{\frac{b_1}{R_0}\left[1 - \frac{7\alpha|\mathbf{m}|^2}{90\pi B_q^2 b_1^6} - \frac{5r_g^2}{8b_1^2}\right] - \frac{r_g}{2b_1}\right\}. \qquad (1.82)$$

Utilizing the specified formulas, the authors easily calculated the angle of gravitational and nonlinear electrodynamical bending of a specific ray:

$$\delta\varphi_1 = -\frac{2r_g}{b_1} - \frac{7\alpha|\mathbf{m}|^2}{48B_q^2 b_1^6} - \frac{15\pi r_g^2}{16b_1^2}. \qquad (1.83)$$

The negative sign in this expression indicates that the gravitational and magnetic fields of the neutron star in the plane of the magnetic equator act on electromagnetic waves like a converging lens.

Similarly, the authors developed equations for the rays of electromagnetic waves of the second type of polarization. In this context, denoting the impact parameter of such rays as b, the following is obtained:

$$r = \frac{b}{V + \mathrm{W}\sin\Psi(\varphi)}, \qquad (1.84)$$

where

$$V = \frac{r_g}{2b},\ W = 1 + \frac{2\alpha|\mathbf{m}|^2}{45\pi B_q^2 b^6} + \frac{5r_g^2}{8b^2}, \tag{1.85}$$

$$\Psi(\varphi) = \varphi + \varphi_0 + \frac{r_g}{2b}\cos(\varphi + \varphi_0) - \frac{r_g^2}{32b^2} \times$$

$$\times \{30(\varphi + \varphi_0) + \sin 2(\varphi + \varphi_0)\} - -\frac{\alpha|\mathbf{m}|^2}{720\pi B_q^2 b^6} \times$$

$$\times \{60(\varphi + \varphi_0) + \sin 4(\varphi + \varphi_0) - 16\sin 2(\varphi + \varphi_0)\}. \tag{1.86}$$

For a ray passing through the point $r = R_0, \varphi = \pi$, the angle φ_0 is given by:

$$\varphi_0 = -\xi_0 + \frac{r_g}{2b}\cos\xi_0 + \frac{3r_g^2}{32b^2}\{10(\pi - \xi_0) + \sin 2\xi_0\} +$$

$$+ \frac{\alpha|\mathbf{m}|^2}{720\pi B_q^2 b^6}[60(\pi - \xi_0) - \sin 4\xi_0 + 16\sin 2\xi_0], \tag{1.87}$$

Where the notation is introduced

$$\xi_0 = \arcsin\left\{\frac{b}{R_0}\left[1 - \frac{2\alpha|\mathbf{m}|^2}{45\pi B_q^2 b^6} - \frac{5r_g^2}{8b^2}\right] - \frac{r_g}{2b}\right\}. \tag{1.88}$$

The bending angle of the electromagnetic ray with this polarization turns out to be less than the bending angle given by equation (1.83):

$$\delta\varphi = -\frac{2r_g}{b} - \frac{\alpha|\mathbf{m}|^2}{12B_q^2 b^6} - \frac{15\pi r_g^2}{16b^2}. \tag{1.89}$$

Finally, the authors provide a comprehensive analysis of how strong gravitational and dipole magnetic fields of neutron stars affect the trajectories and speeds of electromagnetic waves, focusing on polarization differences. The research demonstrates significant ray-bending effects and changes in wave speeds caused by the combined action of gravitational forces and nonlinear electrodynamics. The use of metrics based on the Schwarzschild solution ensures an accurate description of gravitational impacts, while the analysis of the dipole magnetic field's influence opens avenues for understanding nonlinear electrodynamical effects. The authors discovered that the differences in wave speeds with varying polarization in the presence of strong magnetic fields offer new perspectives for astrophysical observations, which could enhance our understanding of the structure of neutron stars' magnetospheres. This study also emphasizes the importance of birefringence effects and the delay in arrival times of pulses with different polarization, which could form the basis for experimental

verification of nonlinear electrodynamics theories. The results of this research not only reveal complex interactions between electromagnetic waves and extreme fields in space but also enrich our understanding of the fundamental principles of quantum electrodynamics and gravity theory.

The subsequent paper examines the effect of ultra-strong magnetic fields on the bending of light, especially in the context of magnetars - neutron stars, the magnetic fields on the surface of which exceed the critical value for quantum electrodynamics (QED)[97]. The authors emphasize that the traditional approach using the Euler-Heisenberg action assumes an asymptotic representation and is limited in its applicability to weak fields [10], which makes it unsuitable for analyzing conditions of super strong fields. Thus, to gain a deep understanding of the nonlinear electromagnetic effects exhibited at fields above the critical QED threshold, it is critical to develop a theoretical framework adequate for the high-field limit. The research aims to analyze the bending of light beams in the context of extreme magnetic fields such as those observed in magnetars. The authors of the study begin to analyze light bending under conditions where electromagnetic field strength exceeds a critical QED threshold. They emphasize the need for a complete action expression and take part in recent research based on Schwinger's integral approach, which has explored an analysis series representation of the one-row effective action of QED. In the case of electric or magnetic fields exceeding this critical limit, light propagation through such extremely strong electromagnetic fields differs from the state of the light cone established, resulting in a speed different from *c*. To solve this problem, they used a well-defined equation for the average light velocity of such extreme electric and magnetic fields, originally proposed by Cho et al. [106].

The discussion further shifts to the phenomenon of light bending as it traverses close to astronomical bodies endowed with electric or magnetic fields surpassing the critical threshold. Theoretically, a charged black hole serves as a plausible source of an ultra-strong electric field. On the other hand, for an ultra-strong magnetic field source, magnetars are considered, with their surface magnetic field strength estimated to be in the vicinity of 10^{11} T. Neutron stars are bound by a physical magnetic field limit ranging between 10^{12} T and 10^{14} T [107]. Exceeding this boundary would lead to internal fluid mixing and the subsequent dissipation of the magnetic field, underscoring that no celestial bodies could sustain fields beyond this upper limit.

Given that quantum corrections in ultra-strong magnetic fields are expressed through the index of refraction, light's behavior in such conditions can be analogously modeled within the framework of geometric optics, treating it as propagation through a classical medium. This approach allows for the trajectory of light to be formulated using Snell’s law, as detailed in references [108]. It was assumed that the direction of light photons goes from minus infinity to plus infinity along the Oh axis. At the same time, the direction of the dipole's magnetic field is assumed to be along the z-axis. Using these initial conditions and transforming the above equation (5), we obtain the following light trajectory equation:

$$\frac{d^2x}{ds^2} = 0,\ \frac{d^2y}{ds^2} = \eta_2,\ \frac{d^2z}{ds^2} = \eta_3. \tag{1.90}$$

The magnetic field at a point located at a distance r along the equatorial line of a magnetic dipole is described by

$$\mathrm{B} = B_0 \frac{r_0^3}{r^3}(-\hat{z}), \tag{1.91}$$

where B_0 represents the magnetic field strength at the neutron star's surface.

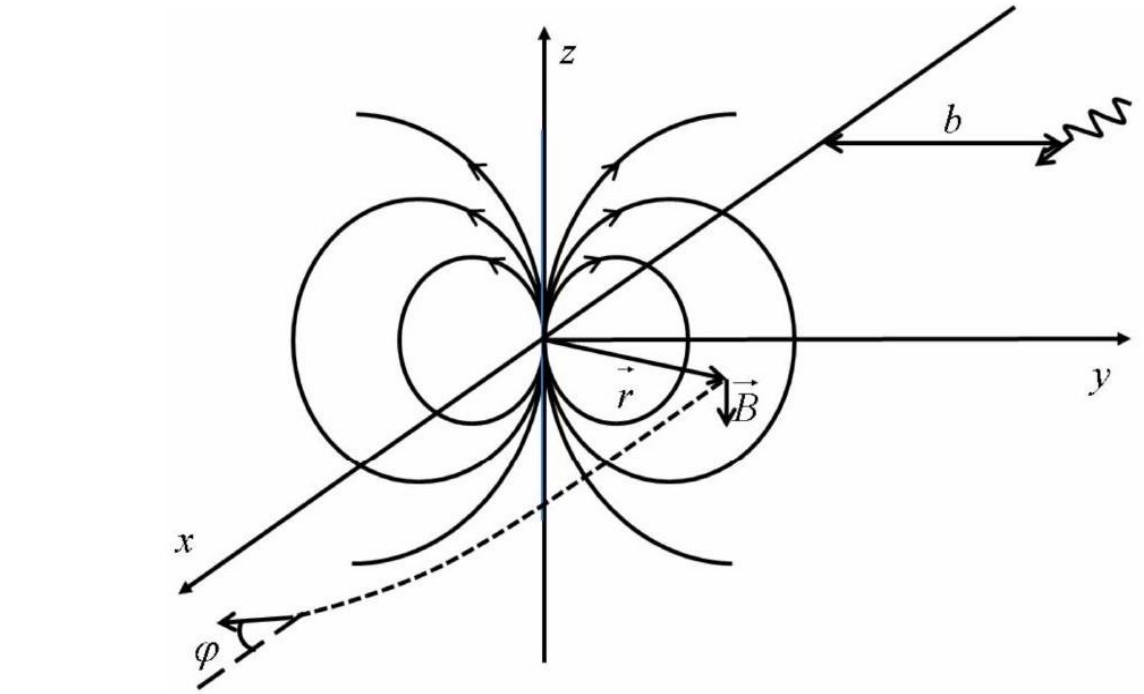

Figure 1.1 – Diagram illustrating the curvature of light around a magnetic dipole when the photon trajectory lies along the dipole's equatorial plane.

Putting all constants in the refractive index equation and taking into account the linear dependence of the refractive index value on the magnitude of the magnetic field, the following equation was obtained by approximation:

$$\bar{n}_{\mathrm{m}} \simeq 1 + \frac{\alpha}{6\pi}(c_1 - c_2 + 1) + \frac{\alpha}{12\pi}\frac{B_0}{B_{\mathrm{c}}}\left(\frac{r_0}{r}\right)^3. \tag{1.92}$$

The equation that determines the deflection angle of light in a strong magnetic field is written as follows:

$$|y'(\infty)| = \tan\varphi_{\mathrm{m}} \simeq \varphi_{\mathrm{m}}, \tag{1.93}$$

$$\varphi_{\mathrm{m}} = \frac{\alpha}{3\pi}\frac{B_0}{B_{\mathrm{c}}}\frac{r_0^3}{b^3}. \tag{1.94}$$

Overall, the type of equation that determines the angle of deflection of light in an ultra-strong magnetic field was analytically calculated using the expression of the refractive index. At the same time, the author considere it useful to obtain a different approximated form of the Euler-Heisenberg Lagrangian for a strong magnetic field.

In the following paper [78], when the magnetic field on the surface of a neutron star is $B_0 < B_c$, the light deviation angle is calculated analytically and numerically using the method of the GBT. Here, the generalized BI Lagrangian is used and only the weak-field approximation is introduced. Based on the assumption that the direction of the magnetic dipole coincides with the z-axis, the magnetic moment of the dipole is denoted as by $\mathbf{m} = \mu\hat{z}$. The magnetic field at the equator is expressed by:

$$\overline{\mathbf{B}} = -\frac{\mu\hat{z}}{r^3}, \tag{1.95}$$

where $r = \sqrt{x^2 + y^2}$ represents the radius in plane perpendicular to the dipole axis. As well as, two key indices of refraction, $n_\perp$ and $n_\parallel$, are introduced to describe light traveling in directions perpendicular and parallel to the dipole axis, respectively. These indices depend on distance and magnetic moment, which indicates a change in the properties of the medium under the influence of a magnetic field.

$$\iint_D \mathcal{K} dS + \sum_{a=1}^{N} \iint_{\partial D_a} k_g dl + \sum_{a=1}^{N} \theta_a = 2\pi\chi(D). \tag{1.96}$$

In this analysis, the region D is characterized by a Gaussian curvature $\mathcal{K}$, which is mapped through a curved surface S capable of free orientation and possessing an infinitesimal area element dS. The boundaries of this area are designated as ∂D_a, and their number varies from 1 to N. When analyzing the path, denoted as dl, the geodesic curvature k_g is taken into account, taking the positive direction. In addition, θ_a denotes the shock angle, and $\chi(D)$ is the Euler characteristic for a given region. In this context it is equal to 1, indicating that D is located in a region without singular points. The study mentioned in the source [109] shows that in conditions of a static spherically symmetric space-time with asymptotic flatness, the equation denoted as (8) can be represented in a certain form.

$$\Delta\theta_\perp = -\iint_D^m \mathcal{K} dS. \tag{1.97}$$

According to the documentation in [83], the formula for the Gaussian optical curvature $\mathcal{K}$ is articulated using the coordinates and the index of refraction in the following manner:

$$\mathcal{K} = -\frac{n(r)n''(r)r - \left(n'(r)\right)^2 r + n(r)n'(r)}{n^4(r)r}. \tag{1.98}$$

By introducing some substitutions, they determined the deflection angle of light for a dipole magnetic field. In the framework of generalized Born-Infeld electrodynamics, the equation delineating the angle of deflection, denoted as $\Delta\theta_\perp$, is formulated as

$$\Delta\theta_\perp = -\frac{15\pi}{16}\frac{\mu^2}{\beta^2 b^6}\,, \tag{1.99}$$

as presented in expression (1.99). Here, b represents the impact parameter, with the negative sign signifying that the deflection is directed towards the magnetic dipole. This specific formula quantifies the deflection angle of light within the context of GBI NED, predicated on the β^2 parameter scale. This parameter itself integrates two additional variables, as established in Equation (1.156). Notably, with β_0 approaching infinity, expression (1.99) condenses to the deflection angle found in EH NED, which is expressed as

$$\Delta\theta_\perp = \frac{\pi}{3}\frac{\alpha^2}{m_e^4}\frac{\mu^2}{b^6}, \tag{1.100}$$

here, with the mode parallel to it being

$$\Delta\theta_\parallel = \frac{7}{4}\Delta\theta_\perp. \tag{1.101}$$

Such outcomes are in exact concurrence with the deflection angles calculated from the Euler-Heisenberg Lagrangian, as referenced in [61, 97].

This study examines how light is deflected around neutron stars when their magnetic fields are below a critical level $B_0 < B_c$ utilizing the Gauss-Bonnet Theorem and generalized Born-Infeld Lagrangian within a weak-field framework. It investigates the effect of the magnetic field, oriented along the z-axis, on the trajectory of light, particularly across the equator. The research introduces refraction indices for light paths that are perpendicular and parallel to the direction of the magnetic field, highlighting the influence of the magnetic dipole moment. Through comprehensive analysis, the paper derives an equation for calculating the angle of light deflection, consistent with findings from the Euler-Heisenberg Lagrangian, thereby enhancing theoretical insights into the interaction between light and potent magnetic fields.

Nonlinear post-Maxwell electrodynamics, emerging from quantum electrodynamics, offers profound insights into electromagnetic phenomena within gravitational fields. Through a methodical approach, the subsequent study delves into its Lagrangian formulation and field equations, coupled with Einstein's gravitational equations, to unravel the complex dynamics around pulsars, particularly focusing on

polarization splitting within their magnetic fields [68]. The authors consider the pulsar's gravitational influence to be perfectly spherical, expanding the metric in harmonic Fock coordinates by a series in the small parameter α/r, where α equates to $\gamma M/c^2$ (with γ denoting the gravitational constant and M the pulsar's mass), ensuring the precision meets their analytical needs.

$$g_{00} = 1 - \frac{2\alpha}{r},\ g_{rr} = -1 - \frac{2\alpha}{r},\ g_{\theta\theta} = r^2 g_{rr},\ g_{\phi\phi} = g_{\theta\theta}\sin^2\theta\,. \qquad (1.102)$$

They propose that at $t = 0$, a potent radiation burst is emitted from a point $\mathbf{r} = \mathbf{r}_0$ within the pulsar's magnetosphere. This burst, upon interaction with the pulsar's magnetic field, undergoes birefringence, resulting in its division into two distinct impulses characterized by orthogonal polarizations and disparate velocities. For analytical convenience, the authors adopt a spherical coordinate system. By tracing a tangent to the initially emitted beam at $\mathbf{r} = \mathbf{r}_0$, they orient the coordinate system's axis such that this tangent and the pulsar's center reside within a singular plane, with θ set at $\pi/2$, and the azimuthal coordinate ϕ of the radiation's origin at $\phi = 0$. Without restricting the generality of their approach, they position the pulsar's magnetic dipole moment vector m towards a point specified by spherical coordinates θ_0 and ϕ_0. This leads to the derivation of the Cartesian components of $\mathbf{m}$ in the specified coordinate system.

$$m_x = |\mathbf{m}|\sin\theta_0\cos\phi_0\,,\ m_y = |\mathbf{m}|\sin\theta_0\sin\phi_0\,,\ m_z = |\mathbf{m}|\cos\theta_0\,. \qquad (1.103)$$

Following established celestial mechanics conventions, they substitute the radial coordinate r with $u = 1/r$. This allows for a detailed representation of the non-zero components of the pulsar's dipole electromagnetic field tensor in the $u, \theta, \phi,$ coordinate system, tailored to the scope of their research.

$$F_{u\theta} = -F_{\theta u} = |\mathbf{m}|\sin\theta_0\sin(\phi - \phi_0)\,, \qquad (1.104)$$

$$F_{\phi\theta} = -F_{\theta\phi} = 2|\mathbf{m}|u\sin\theta[\sin\theta_0\sin\theta\cos(\phi - \phi_0) + \cos\theta\cos\theta_0]\,. \qquad (1.105)$$

The authors highlight that within electrodynamics, the eikonal method is prevalently employed for solving a wide array of problems. This method is particularly valued for its utility in analyzing the movement of electromagnetic impulses via their beams. Through its application to nonlinear electrodynamics, findings [33,37] have underscored that electromagnetic wave propagation through external electromagnetic and gravitational fields in this domain can be equated to the movement of normal modes along isotropic geodesics within an effective space-time. In this context, the effective space-time is characterized by a metric tensor denoted as $G_{\nu\mu}^{eff(1,2)}$, structured as per the field equations (2.1) - (2.3).

$$G_{\nu\mu}^{\text{eff}\,(1,2)} = g_{\nu\mu} - 4\eta_{(1,2)}\xi F_{\nu\beta}g^{\beta\sigma}F_{\sigma\mu}. \qquad (1.106)$$

They argue that to effectively examine how electromagnetic pulses propagate through the magnetic (2.5) and gravitational (2.4) fields surrounding a pulsar, it's more efficient to forego the direct application of equations (2.1) - (2.2). Instead, they suggest leveraging an analysis of isotropic geodesics within a spacetime defined by the metric tensor (6). Proceeding with this methodology, they incorporate the expressions from (2.4) and (2.5) into equation (2.6), enabling them to delineate the components of the effective spacetime metric tensor, $G_{\nu\mu}^{\text{eff}\ (1,2)}$, as $G_{\nu\mu}^{(1,2)}$, in a clear and explicit manner.

$$G_{00}^{(1,2)} = 1 - 2\alpha u, \tag{1.107}$$

$$G_{uu}^{(1,2)} = -\frac{1+2\alpha u}{u^4} - 4\mathbf{m}^2\xi\eta_{1,2}u^2 \times$$

$$\times \{\sin^2\theta_0 \sin^2(\phi-\phi_0) + [\sin\theta_0\cos\theta\cos(\phi-\phi_0) - \sin\theta\cos\theta_0]^2\}, \tag{1.108}$$

$$G_{u\theta}^{(1,2)} = 8\mathbf{m}^2\xi\eta_{1,2}u^3\,[\sin\theta_0\sin\theta\cos(\phi-\phi_0) + \cos\theta\cos\theta_0] \times$$

$$\times [\sin\theta_0\cos\theta\cos(\phi-\phi_0) - \sin\theta\cos\theta_0], \tag{1.109}$$

$$G_{u\phi}^{(1,2)} = -8\mathbf{m}^2\xi\eta_{1,2}u^3[\sin\theta_0\sin\theta\cos(\phi-\phi_0) + \cos\theta\cos\theta_0] \times$$

$$\sin\theta\sin\theta_0\sin(\phi-\phi_0), \tag{1.110}$$

$$G_{\theta\theta}^{(1,2)} = -\frac{(1+2\alpha u)}{u^2} - 4\mathbf{m}^2\xi\eta_{1,2}u^4 \times$$

$$\times \{\sin^2\theta_0\sin^2(\phi-\phi_0) + 4[\sin\theta_0\sin\theta\cos(\phi-\phi_0) + \cos\theta\cos\theta_0]^2\}, \tag{1.111}$$

$$G_{\theta\phi}^{(1,2)} = -4\mathbf{m}^2\xi\eta_{1,2}u^4\,[\sin\theta_0\cos\theta\cos(\phi-\phi_0) -$$

$$-\sin\theta\cos\theta_0\,]\sin\theta\sin\theta_0\sin(\phi-\phi_0), \tag{1.112}$$

$$G_{\phi\phi}^{(1,2)} = -\left\{\frac{(1+2\alpha u)}{u^2} + 4\mathbf{m}^2\xi\eta_{1,2}u^4\{[\sin\ \theta_0\cos\ \theta\cos\,(\phi-\phi_0) -\right.$$

$$\left.-\sin\theta\cos\theta_0]^2 + 4[\sin\theta_0\sin\theta\cos(\phi-\phi_0) + \cos\theta\cos\theta_0]^2\}\right\}\sin^2\theta\,. \tag{1.113}$$

The authors have formulated equations that describe isotropic geodesics within an effective space-time, characterized by the metric tensor detailed in equation (2.7). In their approach, differentiation is executed not in relation to the affine parameter σ but with respect to the azimuthal angle ϕ. This modification in the method of differentiation is a key aspect of their analytical framework.

$$\frac{d^2x^0}{d\phi^2} + \left\{\Gamma^0_{\beta\mu} - \frac{dx^0}{d\phi}\Gamma^3_{\beta\mu}\right\}\frac{dx^\beta}{d\phi}\frac{dx^\mu}{d\phi} = 0, \tag{1.114}$$

$$\frac{d^2u}{d\phi^2} + \left\{\Gamma^1_{\beta\mu} - \frac{du}{d\phi}\Gamma^3_{\beta\mu}\right\}\frac{dx^\beta}{d\phi}\frac{dx^\mu}{d\phi} = 0. \tag{1.115}$$

The authors note that the Christoffel symbols, denoted as $\Gamma^\nu_{\beta\mu}$, are defined within the context of the effective space-time governed by the metric tensor outlined in equation (2.7). This definition is crucial for understanding the behavior of isotropic geodesics in their model, where differentiation is uniquely carried out with respect to the azimuthal angle ϕ, rather than the conventional affine parameter σ. As well as, the authors introduce a first integral to the system of equations detailed as (2.8), presented in the form of equation (2.9):

$$G^{(1,2)}_{\beta\mu}\frac{dx^\beta}{d\phi}\frac{dx^\mu}{d\phi} = 0. \tag{1.116}$$

They note that although equations (2.8) and (2.9) are inherently non-linear, the presence of small parameters αu and $\mathbf{m}^2\xi\eta_{1,2}u^6$ in their specific scenario allows for a solution through the method of successive approximations, leveraging these small parameters. The authors highlight the significance of accounting for different bending angles in the beams of the first and second normal modes due to nonlinear-electrodynamic effects, even when considering meridian and equatorial planes, as referenced in [27-29]. This discrepancy necessitates distinct boundary conditions for each mode to ensure that both impulses can be detected by the same apparatus on a spacecraft near Earth [38]. For the initial conditions, they specify that the beam of the first normal mode should emanate from $u = u_0 = 1/r_0, \theta = \pi/2, \phi = 0$, with the coordinate u at the pericenter set to a predetermined value $u_p = 1/r_p > u_0$. Here, r_0 represents the distance from the center of the pulsar to the high-energy radiation source, and r_p denotes the distance from the pulsar to the beam's pericenter. Additionally, they impose $r_p > R_n$, with R_n being the neutron star's radius. Furthermore, they establish an additional condition based on the problem's setup: for a beam initiated from the point $\phi = 0, u = u_0, \theta = \pi/2$, and making contact with the plane $\theta = \pi/2$, it must hold that $d\theta/d\phi = 0$ for the beam of the first normal mode at $\phi = 0$. This requirement is crucial for ensuring the correct trajectory and behavior of the beam under the specified conditions.

In their analysis, the authors proceed by considering the initial approximation where small parameters are ignored. Under the specified boundary conditions, the trajectory of the beam in this approximation would manifest as a straight line within the plane $\theta = \pi/2$, initiating from the point $u = u_0, \phi = 0$ and reaching $u = u_p$ at its pericenter. Consequently, this leads to the realization that, in this approximation, the derivative $d\theta/d\phi = 0$ maintains a value of zero across all points on the chosen beam, simplifying the system of equations (2.8, 2.9) to the following form:

$$\frac{d^2x^0}{d\phi^2} = -\frac{2}{u}\left(\frac{du}{d\phi}\right)\left(\frac{dx^0}{d\phi}\right),$$

$$\frac{d^2u}{d\phi^2} = -u,$$

$$u^4\left(\frac{dx^0}{d\phi}\right)^2 - u^2 - \left(\frac{du}{d\phi}\right)^2 = 0. \qquad (1.117)$$

Solving this set of equations with the given boundary conditions yields:

$$u(\phi) = u_p \sin(\phi + \psi),$$

$$x^0(\phi) = ct = \frac{\cos\psi}{u_p \sin\psi} - \frac{\cos(\phi + \psi)}{u(\phi)},$$

$$\theta(\phi) = \frac{\pi}{2}, \qquad (1.118)$$

here ψ is determined by the relation $\sin\psi = u_0/u_p$. Given the context of the magnetosphere where $r_0 < 100R_n$, the angle ψ satisfies $0 < \psi < \pi$. Further refining their solution, the authors incorporate the small parameters into their analysis for the beam of the first normal mode, presenting the equation in a form typical for such problems:

$$u(\phi) = u_p \sin(\phi + \psi) + \alpha u_p^2 \Phi_1(\phi) + \mathbf{m}^2 \xi \eta_1 u_p^7 \Phi_2(\phi), \qquad (1.119)$$

$$\theta(\phi) = \frac{\pi}{2} + \alpha u_p \Phi_3(\phi) + \mathbf{m}^2 \xi \eta_1 u_p^6 \Phi_4(\phi). \qquad (1.120)$$

here, $\Phi_a(\phi), a = 1 - 6$ represent unknown functions of the azimuthal angle ϕ, each assumed to be of zeroth order in smallness. By substituting these expressions into the left-hand side of equations (2.8) and expanding them with respect to the small parameters up to the first order, the authors derive the subsequent equation for u,

showcasing their methodical approach to solving these equations within the confines of their specified approximations and conditions.

$$\mathbf{m}^2\xi\eta_1 u_p^7\{\Phi_2'' + \Phi_2 - 6\sin^4(\phi+\psi)\times$$

$$\times 2\sin(\phi+\psi) + [14\sin(\phi+\psi) -$$

$$-\sin 2(\phi-\phi_0)\cos(\phi+\psi)[7\sin^2(\phi+\psi) - 3] +$$

$$+2\sin^2(\phi-\phi_0)\sin(\phi+\psi)\times$$

$$\times [8\sin^2(\phi+\psi) - 9] - 12\sin^3(\phi+\psi)]\sin^2\theta_0\}\} +$$

$$+\alpha u_p^2\{\Phi_1'' + \Phi_1 - 2\} = 0. \quad (1.121)$$

The authors describe the formulation for calculating the angle θ as an equation that assumes a specific structure:

$$\mathbf{m}^2\xi\eta_1 u_p^6\{\Phi_4'' + \Phi_4 + 6\sin^4(\phi+\psi)\times$$

$$\times [3\cos(\phi-\phi_0)\cos^2(\phi+\psi) -$$

$$-\sin(\phi-\phi_0)\sin 2(\phi+\psi)]\sin 2\theta_0\} +$$

$$+\alpha u_p\{\Phi_3'' + \Phi_3\} = 0. \quad (1.122)$$

In the approximation considered, the authors express the first integral (1.122) accordingly.

$$\mathbf{m}^2\xi\eta_1 u_p^5\{-\Phi_6' - 2\sin^4(\phi+\psi)\times$$

$$\times [\sin 2(\phi+\psi)\sin 2(\phi-\phi_0) +$$

$$+4\sin^2(\phi+\psi) + [1 - 5\sin^2(\phi+\psi)]\times$$

$$\times \sin^2(\phi-\phi_0)]\sin^2\theta_0 -$$

$$-2\sin^4(\phi+\psi)\cos^2\theta_0\} - 2\alpha\{\Phi_5'\sin(\phi+\psi) + 2\} = 0. \quad (1.123)$$

They choose not to detail the equation for determining x^0 explicitly, citing it as a derivative outcome from equations (1.121)-(1.123). For the homogeneous equation system defined in (1.121)-(1.122), the authors opt to present the fundamental system

of solutions in an easily interpretable format: $y_1 = \sin(\phi + \psi)$ and $y_2 = \cos(\phi + \psi)$. They calculate the Wronskian (W) of this system, a measure of the solutions' independence, which is found to be $W = y_1' y_2 - y_2' y_1 = 1$. This result confirms the linear independence of the solutions, leading to the conclusion that the general solution of these equations can indeed be represented in the stated form, thus providing a solid foundation for further analysis and interpretation within their study framework.

$$\Phi_1(\phi) = 2 + S_1 \sin\phi + C_1 \cos\phi\,, \tag{1.124}$$

$$\Phi_2(\phi) = \frac{1}{64}\{f_2(\phi) + S_2 \sin\phi + C_2 \cos\phi\}, \tag{1.125}$$

$$\Phi_3(\phi) = S_3 \sin\phi + C_3 \cos\phi\,, \tag{1.126}$$

$$\Phi_4(\phi) = \frac{\sin 2\theta_0}{64}\{f_4(\phi) + S_4 \sin\phi + C_4 \cos\phi\}, \tag{1.127}$$

The authors introduce $S_1, S_2, S_3, S_4, C_1, C_2, C_3$ and C_4 as integration constants and, for ease of subsequent calculations, they adopt specific notations for these constants.

$$f_2(\phi) = \sin^2\theta_0\{\cos 2(\phi_0 + \psi) \times$$

$$\times [195\phi\cos(\phi + \psi) + 65\sin^3(\phi + \psi) +$$

$$+26\sin^5(\phi + \psi) + 152\sin^5(\phi + \psi) -$$

$$-144\sin^9(\phi + \psi)]2\sin2(\phi_0 + \psi) \times$$

$$\times \big[[72\sin^8(\phi + \psi) - 40\sin^6(\phi + \psi) - 26\sin^4(\phi + \psi) -$$

$$-39\sin^2(\phi + \psi)]\cos(\phi + \psi) + 39\phi\sin(\phi + \psi)] +$$

$$+32\sin^7(\phi + \psi) -$$

$$-24\sin^5(\phi + \psi) - 60\sin^3(\phi + \psi) - 180\phi\cos(\phi + \psi)\} -$$

$$-16[2\sin^5(\phi + \psi) + 5\sin^3(\phi + \psi) + 15\phi\cos(\phi + \psi)], \tag{1.128}$$

$$f_4(\phi) = [75\phi\cos(\phi + \psi) + 25\sin^3(\phi + \psi) +$$

$$+10\sin^5(\phi + \psi) - 40\sin^7(\phi + \psi)] \times$$

$$\times \sin(\phi_0 + \psi)[3\phi\sin(\phi + \psi) -$$

$$-[3\sin^2(\phi+\psi)+2\sin^4(\phi+\psi)+$$

$$+40\sin^6(\phi+\psi)]\ \cos(\phi+\psi)\cos(\phi_0+\psi)] \quad (1.129)$$

here, they define A_5 and A_6 as integration constants, employing them as shorthand in their further mathematical expressions.

$$f_6(\phi)=\{16\sin\ 2(\phi_0+\psi)\sin^6\ (\phi+\psi)\times$$

$$\times[4-9\sin^2\ (\phi+\psi)]-\cos\ 2(\phi_0+\psi)\times$$

$$\times[\{144\sin^7(\phi+\psi)+8\sin^5(\phi+\psi)+26\sin^3(\phi+\psi)+$$

$$+39\sin(\phi+\psi)\}\cos(\phi+\psi)-39\phi]+$$

$$+4[8\sin^5(\phi+\psi)+6\sin^3(\phi+\psi)+9\sin(\phi+\psi)]$$

$$+\cos\ (\phi+\psi)-36\phi\}\sin^2\theta_0+8[3+2\sin^2(\phi+\psi)]\times$$

$$\times\sin 2(\phi+\psi)-48\phi. \quad (1.130)$$

The authors stipulate that, due to boundary conditions, the functions $\Phi_1(\phi)$ and $\Phi_2(\phi)$ associated with beams in the first normal mode must vanish at $\phi=0$ and $\phi=\pi/2-\psi$. Consequently, the constants within the expressions labeled (3.6) are determined to adopt specific values.

$$C_1=-2,\ S_1=-\frac{2\cos\psi}{(1+\sin\psi)},\ C_2=-f_2(0),$$

$$S_2=f_2(0)\,\mathrm{tg}\,\psi-\frac{1}{\cos\psi}\times([99\cos 2(\phi_0+\psi)+$$

$$+39(\pi-2\psi)\sin^2\theta_0--52]\sin^2\theta_0-112\}. \quad (1.131)$$

As well as, it is noted that the selection of the orientation for the axes in the spherical coordinate system dictates the boundary conditions for the functions Φ_3 and Φ_4, shaping them as follows:

$$\Phi_3(0)=\Phi_4(0)=0,\frac{d\Phi_3}{d\phi}_{|\phi=0}=\frac{d\Phi_4}{d\phi}_{|\phi=0}=0. \quad (1.132)$$

Here the authors conclude that, due to specific considerations S_3 , C_3 must equal zero, which in turn implies that Φ_3 also equals zero. They further specify that the

constants C_4 and S_4, in accordance with equation (1.132), are to assume particular forms.

$$C_4 = -f_4(0),\ S_4 = 5\sin(\phi_0+\psi)\cos\psi[56\sin^6\psi - 10\sin^4\psi -$$

$$-15\sin^2\psi - 15] + \cos(\phi_0+\psi)\times$$

$$\times \sin\psi[3 - 280\sin^6\psi + 230\sin^4\psi - \sin^2\psi]. \qquad (1.133)$$

The form of the result from the expressions (1.122) will be taken as:

$$u(\phi) = u_p\sin(\phi+\psi) -$$

$$-2\alpha u_p^2\left[\cos\phi + \frac{\sin\phi\cos\psi}{(1+\sin\psi)} - 1\right] + \frac{\mathbf{m}^2\xi\eta_1 u_p^7}{64}\times$$

$$\times\{f_2(\phi) + [f_2(0)\mathrm{tg}\ \psi - \frac{1}{\cos\psi}\{[99\cos 2(\phi_0+\psi) +$$

$$+39(\pi-2\psi)\sin 2(\phi_0+\psi) - 52]\sin^2\theta_0 - 112\}]\times$$

$$\times\sin\phi - f_2(0)\cos\phi, \qquad (1.134)$$

$$\theta(\phi) = \frac{\pi}{2} + \frac{\mathbf{m}^2\xi\eta_1 u_p^6\sin 2\theta_0}{64}\{f_4(\phi) - f_4(0)\cos\phi + S_4\sin\phi\}, \qquad (1.135)$$

$$x^0(\phi) = \frac{\cos\psi}{u_p\sin\psi} - \frac{\cos(\phi+\psi)}{u(\phi)} + 2\alpha\left\{\ln\left|\frac{1-\cos\psi}{\sin\psi}\right| -\right.$$

$$\left. -\ln\left|\frac{1-\cos(\phi+\psi)}{\sin(\phi+\psi)}\right|\right\} + \frac{\mathbf{m}^2\xi\eta_1 u_p^5}{64}\{f_6(\phi) - f_6(0)\}. \qquad (1.136)$$

The authors detail that for the beam of the first normal mode to be observable after it leaves the pulsar's vicinity, it must be detected by an apparatus stationed in Earth's orbit. By citing the research of [40], they acknowledge the vast distances separating the nearest pulsars (approximately 10kpc, significantly greater than R_n) from Earth. This spatial consideration allows for the simplification within the chosen coordinate system, where the measuring device coordinate, $u_1 = 1/r_1$, is considerably less than u_p, enabling a straightforward determination of the device's required angular coordinates, ϕ_1 and θ_1, for capturing the first normal mode beam. They propose setting ϕ_1 to $\pi - \psi + \beta_1$, with β_1 being significantly smaller than 2π, to facilitate this process. The authors explain that by inserting the specified value of ϕ_1 into the equation

$u(\phi_1) = u_1$ and differentiating it with respect to β_1 up to the first order, they obtain a certain result as:

$$\beta_1 = -\frac{u_1}{u_p} + 2\alpha u_p \left[1 + \frac{\cos\psi}{(1+\sin\psi)}\right] + \frac{\mathbf{m}^2 \xi \eta_1 u_p^6}{64} N_2, \tag{1.137}$$

$$N_2 = S_2 \sin\psi - C_2 \cos\psi + f_2(\phi = \pi - \psi) =$$

$$= \frac{\sin^2\ \theta_0}{\cos\ \psi}\{\sin\ 2(\phi_0 + \psi) \times$$

$$\times [\{144\sin^8\ \psi - 80\sin^6\ \psi - 52\sin^4\ \psi - 78\sin^2\ \psi\} \times$$

$$\times \cos\ \psi + 39(2\psi - \pi)\sin\ \psi] +$$

$$+\cos\ 2(\phi_0 + \psi)[152\sin^7\psi - 144\sin^9\psi +$$

$$+26\sin^5\psi + 65\sin^3\psi - 99\sin\psi +$$

$$+195(\psi - \pi)\cos\ \psi] + 4[8\sin^7\ \psi - 6\sin^5\ \psi - 15\sin^3\ \psi \times$$

$$\times [+13\sin\psi + 45(\pi - \psi)\cos\psi]\} +$$

$$+\frac{16}{\cos\psi}[15(\pi - \psi)\cos\psi + 7\sin\psi - 5\sin^3\psi - 2\sin^5\psi]. \tag{1.138}$$

Further analysis of the second equation (1.122) enables them to deduce the value of θ_1.

$$\theta_1 = \theta(\phi_1) = \frac{\mathrm{m}^2 \xi \eta_1 u_p^6}{64} N_4 \sin 2\theta_0\,, \tag{1.139}$$

$$N_4 = S_4\sin\ \psi + f_4(\phi = \pi - \psi) + f_4(\phi = 0) =$$

$$= [48\sin^\pi\ \psi - 8\sin^5\ \psi - 10\sin^3\ \psi - 15\sin\ \psi] =$$

$$= 5\sin\ (\phi_0 + \psi)[48\sin^\pi\ \psi - 8\sin^5\ \psi - 10\sin^3\ \psi - 15\sin\ \psi] \times$$

$$\times \cos\psi + 15(\psi - \pi) + 48\cos(\phi_0 + \psi)[4\sin^6\psi - 5\sin^8\psi]\,. \tag{1.140}$$

This finding suggests that the gravitational field only causes the beams to bend within a single plane. According to expression (1.122), the beams, which serve as conduits for the electromagnetic pulses, are subject to bending effects from two

sources: gravitational bending, which is proportional to $\alpha = \gamma M/c^2$, and nonlinear electrodynamic bending, which depends on $m^2\xi$. To determine the total bending angle, one can refer to equation (1.122), setting u_1 to 0 (which implies $r \to \infty$) and acknowledging that

$$\sin\psi = \frac{u_0}{u_p} = \frac{r_p}{r_0}, \tag{1.141}$$

where r_p represents the beam's periapsis and r_0 the radial coordinate at the point of emission of the electromagnetic pulse. The gravitational component of the bending angle, under these conditions, is then expressed in a specific form as:

$$\delta\varphi_{GR} = \frac{2\gamma M}{c^2 r_p}\left[1 + \frac{\sqrt{r_0^2 - r_p^2}}{r_0 + r_p}\right]. \tag{1.142}$$

The authors elaborate that under the condition where r_0 approaches infinity, their expression aligns with the well-documented Einstein relation for gravitational bending, denoted as

$$\Delta\varphi_{GR} = \frac{4\gamma M}{c^2 r_p}. \tag{1.143}$$

This scenario describes a beam originating from spatial infinity, navigating past the pulsar, and then proceeding back to spatial infinity. For a beam that begins its trajectory at the periapsis, specified as $r_0 = r_p$, the derived expression yields a value that is intuitively half of the initial calculation:

$$\Delta\varphi_{GR} = \frac{2\gamma M}{c^2 r_p}. \tag{1.144}$$

Furthermore, the authors discuss how the nonlinear polarization of vacuum by the magnetic field, given $\theta_0 \neq 0$ and $\theta_0 \neq \pi/2$, induces additional bending of the beam within the plane $\theta = \pi/2$. The extent of this bending, as well as its deviation allowing the beam to exit the given plane, is quantified by expression (1.122) and further considerations in expression (1.123). Optimistically, the magnitude of these angles does not exceed a few arcseconds. However, due to the substantial distances (approximately 10kpc, much greater than r_p) separating pulsars from Earth, the authors note the limitations of current technological capabilities. Specifically, the angular resolution of modern detection equipment is insufficient to accurately observe or measure the beam's bending phenomenon.

The authors present the equations for a beam operating under the second normal mode, with the expressions taking the specific form:

$$u(\phi) = u_p \sin(\phi + \psi) + \alpha u_p^2 \Phi_1(\phi) + \mathbf{m}^2 \xi \eta_2 u_p^7 \Phi_2(\phi), \tag{1.145}$$

$$\theta(\phi) = \frac{\pi}{2} + \alpha u_p \Phi_3(\phi) + \mathbf{m}^2 \xi \eta_2 u_p^6 \Phi_4(\phi), \tag{1.146}$$

$$x^0(\phi) = \frac{\cos\psi}{u_p \sin\psi} - \frac{\cos(\phi + \psi)}{u(\phi)} + \alpha \Phi_5(\phi) + \mathbf{m}^2 \xi \eta_2 u_p^5 \Phi_6(\phi), \tag{1.147}$$

where the functions $\Phi_a(\phi)$, identical to those utilized for the first normal mode, span from (1.146) to (1.147). The integration constants for the beam in the second normal mode are determined based on boundary conditions: at $\phi = 0$ and $t = 0$, the beam originates at $u = u_0, \theta = \pi/2$, and is projected to asymptotically approach spatial infinity ($r \to \infty, u \to 0$). To ascertain the values of the integration constants S_1, S_2, S_3 and S_4, the authors aim to identify the angle $\phi = \phi_2$ at which $u = u_1$, facilitating the determination of these constants under the given conditions. The authors illustrate that by substituting $\phi = \phi_2 = \pi - \psi + \beta_2$ into the first equation of section (4.1) and setting it equal to u_1, they derive an expression for β_2 as a function of several parameters including u_1, u_p, α, and the constants S_1, S_2, C_2 along with a term N_{22} that incorporates complex interactions within the magnetic field, represented as:

$$\beta_2 = -\frac{u_1}{u_p} + \alpha u_p [2 + 2\cos\psi + S_1 \sin\psi)\Big] + \frac{\mathbf{m}^2 \xi \eta_2 u_p^6}{64} N_{22}, \tag{1.148}$$

$$N_{22} = S_2 \sin\psi - C_2 \cos\psi + f_2(\phi = \pi - \psi) =$$

$$= S_2 \sin\ \psi + \sin^2\ \theta_0 \{2\sin\ 2(\phi_0 + \psi) \times$$

$$\times [112\sin^8\psi - 72\sin^{10}\psi - 14\sin^6\psi + 13\sin^4\psi -$$

$$-39\sin^2\ \psi] + \cos\ 2(\phi_\theta + \psi) \times$$

$$\times [\{152\sin^7\psi - 144\sin^9\psi + 26\sin^5\psi +$$

$$+65\sin^3\ \psi\}\cos\ \psi + 195(\psi - \pi)] +$$

$$+2[16\sin^7\ \psi - 12\sin^5\ \psi - 30\sin^3\ \psi] \times$$

$$\times \cos\ \psi - 180(\psi - \pi)\} -$$

$$-16\sin^3\psi[5 + 2\sin^2\psi]\cos\psi - 240(\psi - \pi), \tag{1.149}$$

where N_{22} is detailed with its dependence on ϕ_0, ψ, θ_0, and other factors. Subsequently, applying $\phi = \phi_2$ in the second equation of (1.145) simplifies to show that:

$$\theta_2 = \theta(\phi_2) = \frac{\pi}{2} + \alpha u_p S_3 \sin\psi + \frac{\mathbf{m}^2 \xi \eta_2 u_p^6}{64} N_{44} \sin 2\theta_0 \,, \tag{1.150}$$

$$N_{44} = S_4 \sin\,\psi + f_4(\phi = \pi - \psi) + f_4(\phi = 0) =$$

$$= S_4 \sin\,\psi - 5\sin\,(\phi_0 + \psi) \times$$

$$\times \{[8\sin^7\,\psi - 2\sin^5\,\psi - 5\sin^3\,\psi]\cos\,\psi - 15(\psi - \pi)\} +$$

$$+ \cos(\phi_0 + \psi)[40\sin^8\psi - 38\sin^6\psi + \sin^4\psi - 3\sin^2\psi] \,, \tag{1.151}$$

where N_{44} similarly incorporates various parameters including S_4 and additional effects denoted by f_4.

Given that both beams must reach the measuring device at spatial infinity, the conditions that must be met are $\beta_1 = \beta_2, \theta_1 = \theta_2$. By integrating these conditions with equations, the authors derive specific values for the integration constants S_1, S_2, S_3, among others, facilitating a comprehensive understanding of the beams' behavior and characteristics as influenced by the pulsar's gravitational and electromagnetic fields. This rigorous approach enables precise predictions of the beams' trajectories and their eventual detection by equipment located in Earth's orbit.

$$S_1 = -\frac{2\cos\psi}{(1 + \sin\psi)},\; S_3 = 0, \tag{1.152}$$

$$S_2 = \frac{u_p \eta_1}{u_0 \eta_2} N_2 - \frac{u_p \sin^2\theta_0}{u_0}\{2\sin 2(\phi_0 + \psi) \times$$

$$\times [112\sin^8\,\psi - 72\sin^{10}\,\psi - 14\sin^6\,\psi +$$

$$+13\sin^4\,\psi - 39\sin^2\,\psi] + \cos\,2(\phi_0 + \psi) \times$$

$$\times [\{152\sin^7\,\psi - 144\sin^9\,\psi + 26\sin^5\,\psi +$$

$$+65\sin^3\,\psi\}\cos\,\psi + 195(\psi - \pi)] +$$

$$+2[16\sin^7\,\psi - 12\sin^5\,\psi - 30\sin^3\,\psi]\cos\,\psi -$$

$$-180(\psi - \pi)\} + \frac{16u_p}{u_0} \times$$

$$\times \{[5 + 2\sin^2\psi]\cos\psi\sin^3\psi - 240(\psi - \pi)\}, \quad (1.153)$$

$$S_4 = \frac{u_p\eta_1}{u_0\eta_2}N_4 + \frac{u_p}{u_0}\times$$

$$\times \{5\mathrm{s\,i\,n}\,(\phi_0 + \psi)[[8\sin^7\psi - 2\sin^5\psi - 5\sin^3\psi]\cos\psi -$$

$$-15(\psi - \pi)] - \cos(\phi_0 + \psi)\times$$

$$\times [40\sin^8\psi - 38\sin^6\psi + \sin^4\psi - 3\sin^2\psi\}. \quad (1.154)$$

The authors conclude that, through the process outlined, they have successfully determined all the integration constants for the beam of the second normal mode. This achievement allows for a comprehensive understanding of the beam's behavior as it propagates through space, influenced by the pulsar's gravitational and electromagnetic fields.

In the following intriguing work, he analytically explored the angles of light deviation using geodesic equations [78]. This work employs the form of the generalized Born-Infeld Lagrangian in the one-loop coupling of nonlinear vacuum electrodynamics from the aforementioned previous works. Additionally, it is assumed that the plane of action of the electromagnetic (EM) ray lies in the equatorial plane. The direction of the magnetic field of the dipole is along the Oz axis, and it is assumed that the direction of the ray approaching the neutron star is perpendicular to the z-axis, i.e., coincides with the direction of the Ox axis. The intensity of the dipole magnetic field ranges from B=10^9 T to B=10^{11} T, with all values being approximated in the weak field regime. Therefore, the effective expression for the generalized Born-Infeld electrodynamics is presented as [52].

$$\mathcal{L} = \beta^2\left(1 - \sqrt{1 + \frac{2S}{\beta^2} - \frac{P^2}{\beta^2\gamma^2}}\right), \quad (1.155)$$

here β and γ are characterized as

$$\frac{1}{\beta^2} \equiv \frac{1}{\beta_0^2} + \frac{16}{45}\frac{\alpha^2}{m_e^4},\ \frac{1}{\gamma^2} \equiv \frac{1}{\beta_0^2} + \frac{28}{45}\frac{\alpha^2}{m_e^4}. \quad (1.156)$$

By considering only the nonzero dipole magnetic field, the study wrote the main field equations in the form of:

$$R_{\mu\nu} - \frac{1}{2}g_{\mu\nu}R = 8\pi T_{\mu\nu}, \quad (1.157)$$

$$\nabla\left(\frac{F_{\mu\nu}}{\sqrt{1+\frac{2S}{\beta^2}}}\right)=0, \tag{1.158}$$

here is the $T_{\mu\nu}$ defines the energy momentum tensor

$$T_{\mu\nu}=\frac{1}{4\pi}\left[\beta^2\left(1-\sqrt{1+\frac{2S}{\beta^2}}\right)g_{\mu\nu}+\frac{F_{\mu\alpha}F^{\alpha}{}_{\nu}}{\sqrt{1+\frac{2S}{\beta^2}}}\right]. \tag{1.159}$$

Given the axial symmetry, the author finds it convenient to utilize cylindrical coordinates, denoted as $x^{\mu}=(t,r,z,\phi)$. The metric and the electromagnetic four-potential are then expressed according to the following assumption.

$$ds^2=g_{\mu\nu}dx^{\mu}dx^{\nu}=$$

$$=f(r,z)dt^2-g(r,z)(dr^2+dz^2)-r^2h(r,z)d\phi^2, \tag{1.160}$$

$$A_{\mu}=(0,0,0,-\psi). \tag{1.161}$$

Martin and Pritchett [110] derived power series solutions in terms of the gravitational constant. At the first order in the gravitational constant, the solutions are provided as:

$$f(r,z)=1-\frac{2GM}{X}+\frac{G\mu^2z^2}{X^6}, \tag{1.162}$$

$$g(r,z)=1+\frac{2GM}{X}-\frac{G\mu^2(r^4-6r^2z^2+2z^4)}{2X^8}, \tag{1.163}$$

$$h(r,z)=1+\frac{2GM}{X}-\frac{G\mu^2z^2}{X^6}, \tag{1.164}$$

$$\psi(r,z)=\frac{\mu r^2}{X^3}\left(1+\frac{GM}{2X}\right), \tag{1.165}$$

here, X represents the spherical distance, defined as $X=\sqrt{r^2+z^2}$, M stands for the mass, and we reintroduce G to illustrate the order of powers of the gravitational constant. The first-order quantum electrodynamic correction for the magnetic potential, within a flat spacetime background, has been calculated using spherical polar coordinates [111]. Similarly, higher-order corrections for the magnetic four-potential,

denoted as ψ(r, z), in a curved spacetime background, can also be explored using cylindrical coordinates. In the framework of linear Maxwell electrodynamics coupled to gravity, both photons and gravitons traverse identical null geodesics shaped by mass and magnetic dipole. However, within nonlinear electrodynamics coupled to gravity, the null geodesic of the electromagnetic wave differs from that of the gravitational wave due to the nonlinear interaction of the electromagnetic wave with the background electromagnetic field.

The effective metric that renders k_μ a null vector is given by:

$$\tilde{g}^{\mu\nu} = g^{\mu\nu} + 4\frac{\mathcal{L}_{SS}}{\mathcal{L}_S}F^{\mu\alpha}F^{\nu}{}_{\alpha}. \tag{1.166}$$

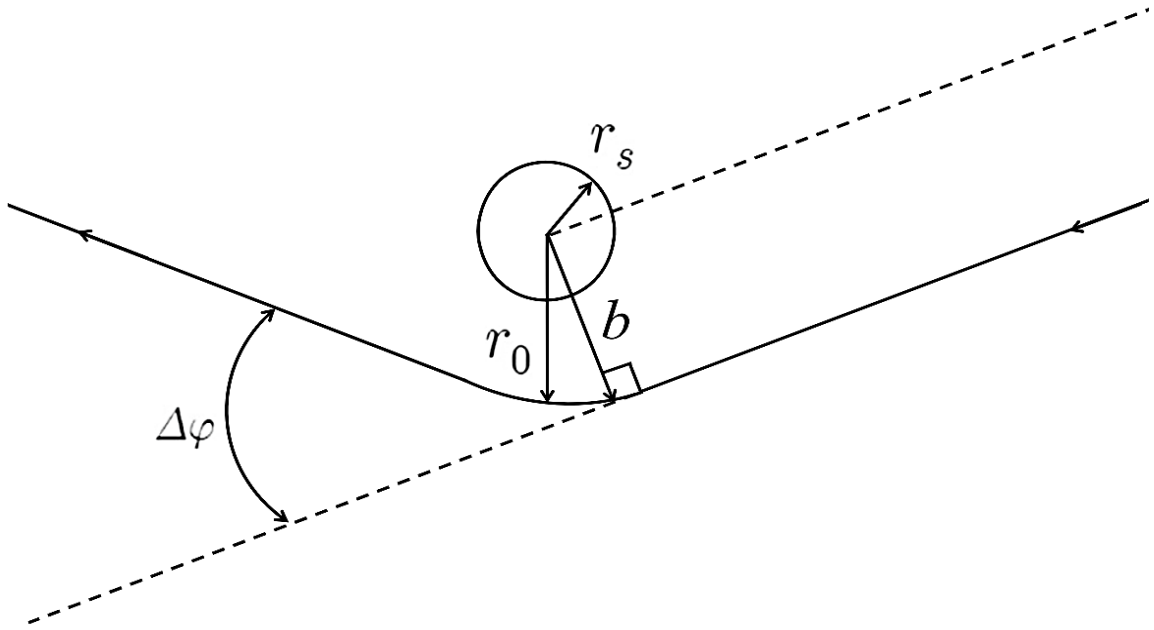

Figure 1.2 – This illustrates the bending angle $\Delta\varphi$ of a light ray on the equatorial plane of a magnetic dipole. The closest approach distance r_0 is defined as the minimum of the radial coordinate r, b represents the impact parameter, and denotes the radius of the compact object possessing the magnetic dipole.

The path of minor deflection in the equatorial plane ($z = 0$) can be calculated using the subsequent effective metric, approximating up to the first order in G and second order in μ:

$$ds_{eq}^2 = B(r)dt^2 - A(r)dr^2 - C(r)d\phi^2, \tag{1.167}$$

here,

$$B(r) = 1 - \frac{2GM}{r}, \tag{1.168}$$

$$A(r) = 1 + \frac{2GM}{r} - \frac{G\mu^2}{2r^4} + \frac{\mu^2}{\beta^2 r^6}, \tag{1.169}$$

$$C(r) = 1 + \frac{2GM}{r} + \frac{\mu^2}{\beta^2 r^6}. \tag{1.170}$$

Using the notation and methodology outlined in [112], one can derive the deflection angle of light originating from infinity, as depicted in (Fig. 1.2).

$$\Delta\varphi = 2|\varphi(r_0) - \varphi_\infty| - \pi, \tag{1.171}$$

where r_0 represents the distance of closest approach, and

$$\Delta\varphi = \frac{4GM}{r_0} - \frac{3\pi}{32}\frac{G\mu^2}{r_0^4} + \frac{15\pi}{16}\frac{\mu^2}{\beta^2 r_0^6}. \tag{1.172}$$

The initial two expressions incorporating the gravitational constant are attributed to the effects of general relativity, while the third term represents the influence of nonlinear electrodynamic effects. Notably, the relative sign of the second term contrasts with that of the first and third terms. This implies that the magnetic dipole's impact on the total bending angle via nontrivial geodesics is repulsive, whereas the contribution from nonlinear electrodynamic effects is attractive. In the scenario where polarization aligns parallel to the magnetic field (z-mode), β within Eq. (1.172) is replaced with γ. In the scenario of slight deflection, approximately when r_0 is equal to b, the third term in Equation (1.172) precisely aligns with the primary order derived from geometric optics Eq. (1.10):

$$\Delta\varphi_\perp = -\frac{15\pi}{16}\frac{\mu^2}{\beta^2 b^6}. \tag{1.173}$$

The examination proceeds to investigate light bending around a massive object with a magnetic dipole moment, utilizing computations within general relativity. The bending angle is determined through the geodesic equation derived from a static axially symmetric solution for the metric and the four-potential. This yields the bending angle as a function of the impact parameter. In the limit where the mass tends towards zero, it is confirmed that the obtained result concurs with that derived from trajectory equations. In the context of astrophysics, an estimation is made regarding the potential maximum bending angle for magnetars. When the impact parameter is large, the dominant bending arises from the mass term. However, for magnetars exhibiting surface magnetic fields on the order of 10^{11} T, the bending due to nonlinear electromagnetic effects may rival that of the mass term, particularly in proximity to the magnetar. Additionally, there exist other nonlinear electrodynamic implications stemming from such intensely strong fields, which may be comparable to those induced by mass.

1.4Deflection of rays in a quadrupole magnetic field in a NLED vacuum.

Another study focuses on determining the impact of the nonlinear effects arising from the magnetic dipole and quadrupole fields on the propagation of electromagnetic waves [113]. This is done by employing the eikonal approximation within the parameterized post-Maxwell electrodynamics framework applied to a vacuum. The research also involves developing equations of motion for electromagnetic pulses transmitted through a pulsar's strong magnetic field, considering two normal modes with perpendicular polarizations. The goal is to calculate the difference in propagation times (denoted as Δt) between the two normal waves originating from the same source of electromagnetic radiation and reaching the receiver. In this work, the Cartesian coordinate system is centered at the location of the pulsar or magnetar. Consequently, the magnetic induction vector **B** is represented as $\mathbf{B} = \mathbf{B_2} + \mathbf{B_2}$. In this scenario, the magnetic induction vector **B** at the origin can be decomposed into two components: $\mathbf{B_1}$, representing the dipole magnetic induction vector, and $\mathbf{B_2}$, representing the quadrupole magnetic induction vector.

As detailed in Pétri [114], the components of the quadrupole magnetic induction vector $\mathbf{B_2}$ in a spherical coordinate system denoted by r, θ, and φ are given by a specific mathematical expression.

$$B_r = \frac{BR_s^4}{r^4}\left\{\left[\frac{1}{2}\sqrt{\frac{5}{2}}(1+3\cos 2\theta)\right]\cos\chi_1 - \left[3\sqrt{\frac{5}{6}}\sin 2\theta\cos\varphi\right]\sin\chi_1\cos\chi_2 + \right.$$
$$\left. + \left[3\sqrt{\frac{5}{6}}\sin^2\theta\cos 2\varphi\right]\sin\chi_1\sin\chi_2\right\}, \qquad (1.174)$$

$$B_\theta = -\frac{BR_s^4}{r^4}\left\{\left[\sqrt{\frac{5}{2}}\sin 2\theta\right]\cos\chi_1 + \left[10\sqrt{\frac{1}{30}}\cos 2\theta\cos\varphi\right]\sin\ \chi_1\cos\ \chi_2 - \right.$$
$$\left. - \left[\sqrt{\frac{5}{6}}\sin 2\theta\cos 2\varphi\right]\sin\chi_1\sin\chi_2\right\}, \qquad (1.175)$$

$$B_\varphi = \frac{BR_s^4}{r^4}\left\{5\sqrt{\frac{2}{15}}\cos\theta\sin\varphi\sin\chi_1\cos\chi_2 - \sqrt{\frac{10}{3}}\sin\theta\sin 2\varphi\sin\chi_1\sin\chi_2\right\}. \qquad (1.176)$$

In the given equation, R_s represents the radius of the neutron star. B is a constant parameter with the dimension of magnetic induction. The angles χ_1 and χ_2, both ranging between 0 and π and 0 and 2π respectively, determine the specific geometry of the quadrupole magnetic field.

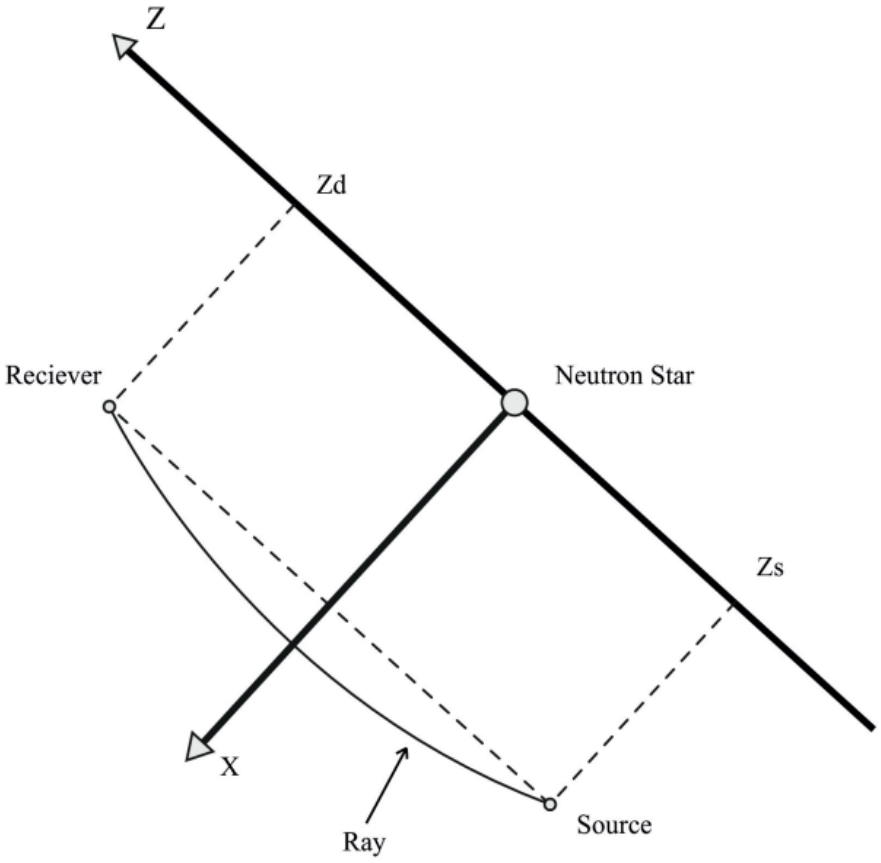

Figure 1.3 – The location of the source and receiver of intense radiation, along with the alignment of the coordinate axes.

To streamline the subsequent calculations, a rectangular Cartesian coordinate system is employed for convenience. As a result, the constants B, χ_1, and χ_2 will be redefined and modified to align with the associated relationships.

$$B_0 = B\sqrt{1 + 2\cos^2\chi_1}\,, \tag{1.177}$$

$$\cos\xi = \frac{\sqrt{3}\cos\chi_1}{\sqrt{1 + 2\cos^2\chi_1}},\ \sin\xi = \frac{\sin\chi_1}{\sqrt{1 + 2\cos^2\chi_1}}. \tag{1.178}$$

By substituting the values from the expressions (8) into the calculation, we can derive the following results:

$$B_{2x} = \sqrt{\frac{5}{6}}\frac{B_0 R_s^4}{r^7}\{x[r^2 - 5z^2]f_1 + 2z[5x^2 - r^2]f_2 +$$

$$+x[5z^2 - 3r^2 + 10y^2]f_3\}, \quad (1.179)$$

$$B_{2y} = \sqrt{\frac{5}{6}}\frac{B_0 R_s^4 y}{r^7}\{[r^2 - 5z^2]f_1 + 10xzf_2 + [3r^2 - 10x^2 - 5z^2]f_3\}, \quad (1.180)$$

$$B_{2z} = \sqrt{\frac{5}{6}}\frac{B_0 R_s^4}{r^7}\{z[3r^2 - 5z^2]f_1 + 2x[5z^2 - r^2]f_2 - 5z[x^2 - y^2]f_3\}. \quad (1.181)$$

They begin by defining the variables in the equations: $f_1 = \cos\xi$, $f_2 = \sin\xi\cos\chi_2$, $f_3 = \sin\xi\sin\chi_2$, and $f_1^2 + f_2^2 + f_3^2 = 1$. Additionally, the individual derived the value of $\mathbf{B_0}$, which represents the magnetic induction at a certain point on a neutron star's surface, indicated by the magnetic induction of a quadrupole, $\mathbf{B_N}$. This point on the neutron star is specifically located at the coordinates θ = π/2 and ϕ=π/4. They presented the formula for B_0 as:

$$B_0 = B_N\sqrt{\frac{6}{[5(1 + (1 + 2\sin^2\chi_1)\sin^2\xi)]}}. \quad (1.182)$$

Here, the scenario is presented where an electromagnetic pulse originates from a specific location $\mathbf{r} = \mathbf{r}_s = \{x_s, y_s, z_s\}$ at a given time $t = t_s$, with a detector positioned at $\mathbf{r} = \mathbf{r}_d = \{x_d, y_d, z_d\}$. To simplify the analysis, the Cartesian coordinate system is adjusted so that both the source and the detector lie within the XOZ plane, satisfying the conditions $x_s = x_d$and $y_s = y_d = 0$. Consequently, the source is located at $\mathbf{r}_s = \{x_s, 0, z_s\}$, and the detector is at $\mathbf{r}_d = \{x_s, 0, z_d\}$, as illustrated in the manuscript's figure. Following the methodology outlined by Denisov [66], the study focuses on analyzing the transmission of X-ray and gamma-frequency pulses, which exhibit minimal interaction with the magnetospheric environments of pulsars and magnetars. This allows for the simplification of the pulse propagation dynamics between $\mathbf{r}_s$ and $\mathbf{r}_d$. The primary objective is to determine the trajectory of the electromagnetic pulses from $\mathbf{r}_s$ to $\mathbf{r}_d$ and understand the underlying principles governing their motion. Based on the specified conditions, it is deduced that the pulse paths are linear within the XOZ plane due to the high-frequency nature of the pulses and the negligible influence of external fields on their trajectory. This analysis assumes a quasi-vacuum or vacuum-like state in the space through which the pulses propagate.

$$X(z) = \frac{25R^8}{3072x_s^8}\{z(1274f_1f_3 - 1596f_2^2 - 245f_1^2 - 2597f_3^2) -$$

$$-64x_s(f_1+13f_3)f_2)\}\operatorname{atan}\left(\frac{z}{x_s}\right)+\frac{125R^8x_s^4}{36r^{12}}\times$$

$$\times\{4z(f_3-f_1)f_2-x_s(f_1^2-2f_1f_3-4f_2^2+f_3^2)\}+$$

$$+\frac{5R^8x_s^2}{72r^{10}}\{16z(13f_1-7f_3)f_2+x_s(83f_1^2-118f_1f_3-284f_2^2+35f_3^2)\}+$$

$$+\frac{5R^8}{576r^8}\{x_s(145f_3^2+524f_2^2+46f_1f_3-287f_1^2)-$$

$$-192z(f_1+2f_3)f_2\}+\frac{5R^8}{1152x_s^2r^6}\{x_s(35f_1^2+228f_2^2-182f_1f_3+$$

$$+371f_3^2)-64z(f_1+13f_3)f_2\}+\frac{5R^8}{4608x_s^4r^4}\{x_s(245f_1^2-$$

$$-1274f_1f_3+1596f_2^2+2597f_3^2)-320z(f_1+13f_3)f_2\}+$$

$$+\frac{25R^8}{9216x_s^6r^2}\{x_s(245f_1^2-1274f_1f_3+1596f_2^2+2597f_3^2)-$$

$$-192z(f_1+13f_3)f_2\},\ Y(z)=0. \qquad (1.183)$$

Equation (1.183) enables the determination of ray trajectories within the context of vacuum post-Maxwellian electrodynamics, where electromagnetic waves move through a magnetic quadrupole field. This equation also helps in understanding how electromagnetic pulses navigate these trajectories. The discussion shifts towards examining how the nonlinear electrodynamic effects of the magnetic quadrupole field influence the path of an electromagnetic wave. The initial step involves calculating the ray curvature angle due to the vacuum electrodynamics' nonlinearity, expressed as:

$$\sin\beta=|[\mathbf{N}(z_s)\mathbf{N}(z_d)]|=\eta_{1,2}\xi B_0^2|F(z_s)-F(z_d)|. \qquad (1.184)$$

This equation simplifies significantly when the magnetic quadrupole is positioned midway between the wave emitter and receiver, where ($z_d=-z_s$). Under these circumstances, the sine of the curvature angle for a ray within the XOZ plane becomes:

$$\sin\ \beta=\eta_{1,2}\xi B_0^2\left\{\left[\frac{175z_sB_0^2R^8}{1536x_s^7r_s^2}+\frac{175B_0^2R^8}{1536x_s^8}\operatorname{atan}\left(\frac{z_s}{x_s}\right)+\right.\right.$$

$$+\frac{175z_sB_0^2R^8}{2304x_s^5r_s^4}+\frac{35z_sB_0^2R^8}{576x_s^3r_s^6}+\frac{5z_sB_0^2R^8}{96x_sr_s^8}\Bigg]\times$$

$$\times[182f_1f_3-35f_1^2-228f_2^2-371f_3^2]+$$

$$+\frac{5z_sx_sB_0^2R^8}{36r_s^{10}}(287f_1^2-46f_1f_3-524f_2^2-145f_3^2)+$$

$$+\frac{25z_sB_0^2R^8x_s^3}{18r_s^{14}}[60x_s^2(1-2f_1f_3-5f_2^2)+r_s^2\times$$

$$\times(118f_1f_3+{+}284f_2^2-83f_1^2-35f_3^2)]\}. \qquad (1.185)$$

Estimations indicate that when B_0 is approximately 10^{13}G, the angle β could extend to several angular seconds. Nevertheless, due to the significant distance between pulsars and Earth relative to the pulsar radii, it is currently unfeasible to measure the angles of nonlinear electrodynamic curvature of rays within the solar system. Moreover, with $\eta_1 \neq \eta_2$ resulting from nonlinear-electrodynamic birefringence, each electromagnetic pulse emitted at point $\mathbf{r}_0=\{q,0,z_0\}$, bifurcates into two pulses. One pulse is conveyed by the first normal wave, while the other travels via the second normal wave with orthogonal polarization. These pulses traverse distinct paths to the receiver, thus experiencing different durations of route. Let us compute the delay time of the electromagnetic pulse conveyed by the first normal wave in comparison to the propagation of the momentum carried by the second normal wave.

$$\Delta t=t_1(z_d)-t_2(z_d)=\frac{5(\eta_1-\eta_2)\xi B_0^2R^8}{6c}\Bigg\{\frac{50x_s^5}{3}f_2(f_3-f_1)\times$$

$$\times\left[\frac{1}{\rho_d^{12}}-\frac{1}{\rho_s^{12}}\right]-\frac{8f_2^2}{7}\left[\frac{z_d}{\rho_d^8}-\frac{z_s}{\rho_s^8}\right]+4x_s^3f_2(5f_1-3f_3)\left[\frac{1}{\rho_d^{10}}-\frac{1}{\rho_s^{10}}\right]+$$

$$+x_sf_2(2f_3-4f_1)\left[\frac{1}{\rho_d^8}-\frac{1}{\rho_s^8}\right]+\frac{25x_s^4}{6}(1-5f_2^2-2f_1f_3)\left[\frac{z_d}{\rho_d^{12}}-\frac{z_s}{\rho_s^{12}}\right]-$$

$$-\frac{x_s^2}{12}(41-48f_3^2-157f_2^2-34f_1f_3)\left[\frac{z_d}{\rho_d^{10}}-\frac{z_s}{\rho_s^{10}}\right]+$$

$$+\frac{5}{512x_s^7}\left[arctg\left(\frac{z_d}{x_s}\right)-arctg\left(\frac{z_s}{x_s}\right)+x_s\left[\frac{z_d}{\rho_d^2}-\frac{z_s}{\rho_s^2}\right]+\right.$$

$$+\frac{2x_s^3}{3}\left[\frac{z_d}{\rho_d^4}-\frac{z_s}{\rho_s^4}\right]+\frac{8x_s^5}{15}\left[\frac{z_d}{\rho_d^6}-\frac{z_s}{\rho_s^6}\right]+$$

$$+\frac{16x_s^7}{35}\left[\frac{z_d}{\rho_d^8}-\frac{z_s}{\rho_s^8}\right]\Bigg][35-182f_1f_3+193f_2^2+336f_3^2]\Bigg\}. \quad (1.186)$$

In a scenario where $\rho_s=\sqrt{z_s^2+x_s^2}$and $\rho_d=\sqrt{z_d^2+x_d^2}$, and with z_s tending towards negative infinity and z_d towards positive infinity, the formula for the curvature angle's sine, initially stated as $\sin\beta=\eta_{1,2}\xi B_0^2|F(z_s)-F(z_d)|$. must now factor in these radial distances. This adjustment is crucial for capturing the magnetic quadrupole field's impact on the propagation of electromagnetic waves over extensive ranges. As the source point z_s moves to an infinitely negative position and the detection point z_d to an infinitely positive one, it's anticipated that the formula will modify to better represent the limitless journey of the electromagnetic wave through the quadrupole field. Absent a concrete definition of $F(z_s)$, it's conjectured that the $\sin\beta$ formula would evolve in response to these boundary conditions by assessing F at the infinite values of z_s and z_d, thereby potentially refining to a version that more accurately mirrors the magnetic quadrupole field's effect on the electromagnetic wave over boundless distances. This reflects on how the non-linear electrodynamic characteristics of the magnetic quadrupole influence the path's bend of the electromagnetic wave as it moves from the source to the detector across infinite expanses.

The existence of a non-zero Δt introduces unique polarization characteristics to an electromagnetic pulse, stemming from the differential propagation velocities of two modes within an external magnetic field. Consider a finite-duration pulse of arbitrarily polarized hard radiation, which divides into two modes, each polarized orthogonally to the other. Initially aligned, their leading edges differ due to vacuum birefringence. The faster mode's leading edge precedes the slower mode's by Δt. Consequently, only the faster normal pulse mode traverses the detector during this time, resulting in the detection of linear polarization for this portion of the momentum.

Following Δt, another normal mode carries momentum, with its phase differing from the faster mode by $\omega\Delta t$, where ω denotes the wave frequency. Consequently, the combined action of these orthogonally polarized normal modes over subsequent time intervals produces radiation with elliptical polarization detectable by the receiver for $T-\Delta t$ duration. Likewise, the slower mode's trailing edge lags behind the faster mode's, causing linear polarization orthogonal to that observed at the momentum's leading edge during the Δt period. Detecting such polarization properties in hard pulses emitted by pulsars confirms not only the presence of vacuum's nonlinear electrodynamics but also facilitates estimating the surface magnetic field induction on pulsars based on Δt.

Similarly, the slower mode's trailing edge will exit the detector prior to the faster mode's, resulting in linear polarization at the back of the hard radiation momentum during the Δt duration, but orthogonal to the linear polarization observed at the momentum's leading edge. Therefore, detecting these polarization properties in hard pulses emitted by pulsars allows us to not only confirm the presence of vacuum's

nonlinear electrodynamics but also estimate the magnitude of magnetic field induction on the pulsar surface based on the Δt value.

Based on the equations of nonlinear electrodynamics of vacuum, the outcome of the calculation revealed that the magnetic quadrupole field is capable of bending electromagnetic waves' rays. Furthermore, the curvature angle's magnitude is determined by the quadrupole moment's orientation with respect to the electromagnetic wave propagation direction. This scientific finding conveys the significance of magnetic quadrupole fields in the alteration of the path of electromagnetic waves, which could have a substantial impact on various applications such as in the field of optics. The propagation velocities of electromagnetic pulses at different refractive indices depend on the polarization of the electromagnetic wave. In the case of a short pulse emitted from the electromagnetic radiation source, it will generally propagate in the magnetic quadrupole field as two normal waves with perpendicular polarizations. This means that when electromagnetic radiation reaches the receiver, the pulses will arrive at different angles and at different times. As a result, the total recorded pulse will have an unusual polarization. The front and back parts of each pulse will be linearly polarized in perpendicular planes, while the middle part will be elliptically polarized. An analysis shows that at a distance of about 10,000 kilometers (R) and a magnetic field strength of about 10^{13} Gauss (B_0), the value of Δt (the time difference) can be several tens of nanoseconds. This assumes a favorable orientation of the quadrupole (a type of electromagnetic field) relative to the z-axis of the chosen Cartesian coordinate system.

2. LENSING OF RAYS BY MAGNETARS

2.1 Numerical calculations of the system of effective geodesic equations.

In this study, we employ the with(tensor) and with(plot) packages from the Maple 6 computing platform to perform numerical calculations, which are integral to our research. Concurrently, we utilize the Numpy, Matplotlib, and Scipy libraries from the Python programming language to process and visualize the graphs of the results obtained from these calculations. This multidisciplinary approach allows us to leverage the strengths of both computing environments. We refer to the geodesic equation from previous scholarly works for our analytical calculations. This equation is used as the basis for our numerical solutions. Notably, since the direction of the beam corresponds to the Oz axis in our setup, the variable z is taken as an affine parameter in the geodesic equation and is transformed accordingly to accommodate this configuration. For our computational setup, we adopt a Cartesian coordinate system. Initially, we activate the required packages in Maple 6 — namely with(tensor), with(LinearAlgebra), and with(plot) — and then define our spatial coordinates in the form of [t, x, y, z]. It is important to note that in this context, z not only serves as a spatial coordinate but also plays the role of an affine parameter, crucial for the computations related to the geodesic paths. The absolute value of the radius vector is written as follows in our scripts:

$$r = \sqrt{x^2 + y^2 + z^2}. \tag{2.1}$$

A dipole magnetic field is considered as a magnetic field. The dependence of the dipole moment on the strength of the magnetic field is determined by the formula (14). Projections of the strength of the dipole magnetic field are determined by this equation. For this, we assume that the dipole magnetic moment is directed along the Ox axis, which is perpendicular to the direction of propagation of the beam front (Oz), that is, taking into account that $\vec{m} = \vec{m}(m_x, 0, 0)$ we get the following components:

$$B_x = \frac{m_x(2x^2 - y^2 - z^2)}{(x^2 + y^2 + z^2)^{\frac{5}{2}}},$$

$$B_y = \frac{3m_x xy}{(x^2 + y^2 + z^2)^{\frac{5}{2}}},$$

$$B_z = \frac{3m_x xz}{(x^2 + y^2 + z^2)^{\frac{5}{2}}}. \tag{2.2}$$

Of course, along with the effect of nonlinear electrodynamics of vacuum, there is also the effect of gravity. In the calculation we are considering, we use the characteristics of the magnetar closest to the Earth as a compact object. However, our work also has

the following limitations. That is, the magnitude of the magnetic field on the surface of the magnetar is taken to be from 10^{13} T to 10^{15} G, and a stationary compact object is considered. As an object metric, we write the components of the Schwarzschild metric in isotropic coordinates as follows:

$$g_{00} = 1 - \frac{\alpha}{r};\ \ g_{11} = -\left(1 + \frac{\alpha}{r}\right),$$

$$g_{22} = -\left(1 + \frac{\alpha}{r}\right);\ \ g_{33} = -\left(1 + \frac{\alpha}{r}\right). \tag{2.3}$$

where α is the gravitational radius of the magnetar. The inverse metric of it is determined in the form of the following components:

$$g^{00} = 1 - \frac{\alpha}{\sqrt{x^2 + y^2 + z^2}},\ \ g^{11}, g^{22}, g^{33} = -1 - \frac{\alpha}{\sqrt{x^2 + y^2 + z^2}}. \tag{2.4}$$

Next, we will need to obtain the combined metric of nonlinear electrodynamics and gravity. To accomplish this, it is crucial to determine the form of the field tensor. In our case, considering only the influence of the magnetic field in the vacuum, we will assume that the components of the electric field are equal to zero. Specifically, this means that the components related to the electric field in the field tensor $E_0, E_1, E_2, E_3 = 0$ are all set to zero. With the electric field components nullified, our focus shifts to the magnetic components of the tensor. We will calculate these remaining components, taking into account the symmetry properties and the specific conditions of our setup, to ensure that they accurately represent the magnetic field in the context of curved spacetime. We then write the contravariant form of the field tensor, taking care to align it with the alterations induced by the gravitational field. This formulation allows us to integrate the effects of the magnetic field with those of gravity in our theoretical framework. So, we calculate the remaining components of the field tensor and write the contravariant form as follows:

$$F^{\mu\nu} = \begin{pmatrix} 0 & 0 & 0 & 0 \\ 0 & 0 & B_3 & -B_2 \\ 0 & -B_3 & 0 & B_1 \\ 0 & B_2 & -B_1 & 0 \end{pmatrix}. \tag{2.5}$$

In our mathematical formulation, we denote $B_1 = B_x$, $B_2 = B_y$, $B_3 = B_z$ as the components of the magnetic field along the x, y, and z axes, respectively, corresponding to B_x, B_y, and B_z. To facilitate the calculations, we enter the Equations (2.1) and (2.2) into the computational platform. These equations are represented in the form of a matrix to streamline the process of solving the system. The matrix notation helps in efficiently handling the vector components of the magnetic field and integrating them into our overall simulation framework. Specifically, we structure the matrix as follows to capture the interactions and dependencies among the magnetic

field components within our theoretical model. We type the Equations (2.1) and (2.1) to the platform in the form of the following matrix.

$$F^{12} = -\frac{3mxz}{(x^2+y^2+z^2)^{\frac{5}{2}}},$$

$$F^{21} = \frac{3mxz}{(x^2+y^2+z^2)^{\frac{5}{2}}},$$

$$F^{13} = \frac{3mxy}{(x^2+y^2+z^2)^{\frac{5}{2}}},$$

$$F^{31} = -\frac{3mxy}{(x^2+y^2+z^2)^{\frac{5}{2}}},$$

$$F^{23} = -\frac{3mxy}{(x^2+y^2+z^2)^{\frac{5}{2}}},$$

$$F^{32} = \frac{3mxy}{(x^2+y^2+z^2)^{\frac{5}{2}}}. \qquad (2.6)$$

We define the covariant form of the electromagnetic tensor as follows.

$$F_{\mu\nu} = g_{\mu\lambda}F^{\mu\rho}g_{\rho\nu} = F_{\mu\nu} = \begin{pmatrix} 0 & 0 & 0 & 0 \\ 0 & 0 & B_3 & -B_2 \\ 0 & -B_3 & 0 & B_1 \\ 0 & B_2 & -B_1 & 0 \end{pmatrix}. \qquad (2.7)$$

Its components are defined as follows:

$$F_{12} = -\frac{3\left(\sqrt{x^2+y^2+z^2}+\alpha\right)^2 mxz}{(x^2+y^2+z^2)^{\frac{7}{2}}},$$

$$F_{21} = \frac{3\left(\sqrt{x^2+y^2+z^2}+\alpha\right)^2 mxz}{(x^2+y^2+z^2)^{\frac{7}{2}}},$$

$$F_{13} = \frac{3\left(\sqrt{x^2+y^2+z^2}+\alpha\right)^2 mxy}{(x^2+y^2+z^2)^{\frac{7}{2}}},$$

$$F_{31} = -\frac{3\left(\sqrt{x^2+y^2+z^2}+\alpha\right)^2 mxy}{(x^2+y^2+z^2)^{\frac{7}{2}}},$$

$$F_{23} = -\frac{3\left(\sqrt{x^2+y^2+z^2}+\alpha\right)^2 mxy}{(x^2+y^2+z^2)^{\frac{7}{2}}},$$

$$F_{32} = \frac{3\left(\sqrt{x^2+y^2+z^2}+\alpha\right)^2 mxy}{(x^2+y^2+z^2)^{\frac{7}{2}}}\ . \tag{2.8}$$

Further, it is essential to obtain the combined form of the electromagnetic (EM) tensor in order to utilize the fundamental equation of the Penrose and Newman formalism. This step is crucial for deriving the covariance form of the effective combined metric, as demonstrated in previous research works. To achieve this, we start by determining the type of mixed tensor. This involves specifying the tensor's structure, which combines both covariant and contravariant components, thereby allowing us to fully express the electromagnetic interactions in a geometric framework suitable for general relativity. The process of identifying the tensor's type is guided by its transformation properties under Lorentz transformations, ensuring that the tensor accurately reflects the properties of the physical system in different reference frames. The specified mixed tensor is thus structured to represent the interactions in the form required by the Penrose and Newman formalism. For this, we can determine the type of mixed tensor as follows:

$$F_{\mu}^{\nu} = g^{\nu\alpha}F_{\alpha\mu}. \tag{2.9}$$

Considering this, Maple also defined its components as follows:

$$F_2^1 = \frac{3\left(\sqrt{x^2+y^2+z^2}+\alpha\right)mxz}{(x^2+y^2+z^2)^3},$$

$$F_3^1 = -\frac{3\left(\sqrt{x^2+y^2+z^2}+\alpha\right)mxy}{(x^2+y^2+z^2)^3},$$

$$F_1^2 = -\frac{3\left(\sqrt{x^2+y^2+z^2}+\alpha\right)mxz}{(x^2+y^2+z^2)^3},$$

$$F_3^2 = \frac{3\left(\sqrt{x^2+y^2+z^2}+\alpha\right)mxy}{(x^2+y^2+z^2)^3},$$

$$F_1^3 = \frac{3\left(\sqrt{x^2+y^2+z^2}+\alpha\right)mxy}{(x^2+y^2+z^2)^3},$$

$$F_2^3 = -\frac{3\left(\sqrt{x^2+y^2+z^2}+\alpha\right)mxy}{(x^2+y^2+z^2)^3}. \tag{2.10}$$

Further, to advance our analysis, we perform the product of the electromagnetic tensor in both covariant and mixed forms, denoted as $F_\alpha^\mu F_{\alpha v}$. This operation is critical for exploring the interaction properties of the EM field within our theoretical framework. To carry out this calculation, we utilize the prod() operator provided by the with(tensor) package in Maple, which is specifically designed for tensor operations. We meticulously define the following nonzero components to ensure the correctness of our tensor calculations. Each component is carefully chosen based on physical considerations and symmetry properties inherent in the problem. This approach allows us to effectively construct a comprehensive tensorial representation that can be used for further calculations in our study.

$$F_{11}^{(2)} = \frac{9\left(\sqrt{x^2+y^2+z^2}+\alpha\right)^3 m^2x^2(y^2+z^2)}{(x^2+y^2+z^2)^{\frac{13}{2}}},$$

$$F_{12}^{(2)} = -\frac{9\left(\sqrt{x^2+y^2+z^2}+\alpha\right)^3 m^2x^2y^2}{(x^2+y^2+z^2)^{\frac{13}{2}}},$$

$$F_{13}^{(2)} = -\frac{9\left(\sqrt{x^2+y^2+z^2}+\alpha\right)^3 m^2x^2zy}{(x^2+y^2+z^2)^{\frac{13}{2}}},$$

$$F_{21}^{(2)} = -\frac{9\left(\sqrt{x^2+y^2+z^2}+\alpha\right)^3 m^2x^2y^2}{(x^2+y^2+z^2)^{\frac{13}{2}}},$$

$$F_{22}^{(2)} = \frac{9\left(\sqrt{x^2+y^2+z^2}+\alpha\right)^3 m^2x^2(y^2+z^2)}{(x^2+y^2+z^2)^{\frac{13}{2}}},$$

$$F_{23}^{(2)} = -\frac{9\left(\sqrt{x^2+y^2+z^2}+\alpha\right)^3 m^2x^2zy}{(x^2+y^2+z^2)^{\frac{13}{2}}},$$

$$F_{31}^{(2)} = -\frac{9\left(\sqrt{x^2+y^2+z^2}+\alpha\right)^3 m^2 x^2 zy}{(x^2+y^2+z^2)^{\frac{13}{2}}},$$

$$F_{32}^{(2)} = -\frac{9\left(\sqrt{x^2+y^2+z^2}+\alpha\right)^3 m^2 x^2 zy}{(x^2+y^2+z^2)^{\frac{13}{2}}},$$

$$F_{33}^{(2)} = \frac{18\left(\sqrt{x^2+y^2+z^2}+\alpha\right)^3 m^2 x^2 y^2}{(x^2+y^2+z^2)^{\frac{13}{2}}}. \quad (2.11)$$

Next, according to equation (2.05), we proceed to determine the combination of two distinct tensors, each representing different polarizations. This step involves multiplying the convolution of the last tensor found by the coefficients $4\eta_{1,2}$ respectively, allowing for an examination of their individual effects on the electromagnetic field. Subsequently, we add the results to the metric tensor to derive two separate effective metrics, each corresponding to a different polarizing ray η_1 and η_2. However, it's important to note that in our study, we do not consider the effects of birefringence; instead, we assume that $\eta_1 = \eta_2$ and conduct all calculations under this simplified condition. This assumption streamlines our analysis and helps maintain focus on the primary interactions. In the Maple software, we execute the tensor combination process by multiplying and adding as specified, then equate the result to the effective metric tensor $G_{\mu\nu}^{eff}$. We carefully determine the non-zero components of this tensor, which are crucial for describing the geometric properties of the spacetime being analyzed. These components are identified through meticulous calculation and consideration of the symmetry properties of the tensors involved, ensuring that the derived effective metric accurately represents the interaction dynamics under the specified conditions [109,112].

$$G_{00}^{eff} = \frac{\sqrt{x^2+y^2+z^2}-\alpha}{\sqrt{x^2+y^2+z^2}}, \quad (2.12)$$

$$G_{11}^{eff} = -\frac{1}{(x^2+y^2+z^2)^{\frac{13}{2}}}\left(\sqrt{x^2+y^2+z^2}+\alpha\right)(60x^4y^6z^2 +$$

$$+15x^4y^8 + 60x^6y^4z^2 + 90x^4y^4z^4 + 60x^6y^2z^4 + 60x^4y^2z^6 +$$

$$+30x^2y^8z^2 + 60x^2y^6z^4 + 60x^2y^4z^6 + 30x^2y^2z^8 +$$

$$+36\alpha^2\eta m^2x^2\xi y^2 + 36\alpha^2\eta m^2x^2\xi z^2 + 72\eta m^2x^2\xi y^2z^2 +$$

$$+36\eta m^2x^4\xi y^2+36\eta m^2x^4\xi z^2+36\eta m^2x^2\xi y^4+$$

$$+36\eta m^2x^2\xi z^4+72\sqrt{x^2+y^2+z^2}\alpha\eta m^2x^2\xi y^2+$$

$$+72\sqrt{x^2+y^2+z^2}\alpha\eta m^2x^2\xi z^2+x^{12}+y^{12}+z^{12}+$$

$$+6x^{10}y^2+30x^8y^2z^26x^{10}z^2+15x^8y^4+15x^8z^4+$$

$$+20x^6y^6+20x^6z^6+15x^4z^8+6x^2y^{10}+6x^2z^{10}+$$

$$+6y^{10}z^2+15y^8z^4+20y^6z^6+15y^4z^8+6y^2z^{10}), \qquad (2.13)$$

$$G_{12}^{eff}=\frac{36\left(\sqrt{x^2+y^2+z^2}+\alpha\right)^3m^2x^2y^2\eta\xi}{(x^2+y^2+z^2)^{\frac{13}{2}}}, \qquad (2.14)$$

$$G_{13}^{eff}=\frac{36\left(\sqrt{x^2+y^2+z^2}+\alpha\right)^3m^2x^2zy\eta\xi}{(x^2+y^2+z^2)^{\frac{13}{2}}}, \qquad (2.15)$$

$$G_{21}^{eff}=\frac{36\left(\sqrt{x^2+y^2+z^2}+\alpha\right)^3m^2x^2y^2\eta\xi}{(x^2+y^2+z^2)^{\frac{13}{2}}}, \qquad (2.16)$$

$$G_{22}^{eff}=-\frac{1}{(x^2+y^2+z^2)^{\frac{13}{2}}}\left(\sqrt{x^2+y^2+z^2}+\alpha\right)\times$$

$$\times(60x^4y^6z^2+30x^8y^2z^2+60x^6y^4z^2+90x^4y^4z^4+$$

$$+60x^6y^2z^4+60x^4y^2z^6+30x^2y^8z^2+60x^2y^6z^4+$$

$$+60x^2y^4z^6+30x^2y^2z^8+36\alpha^2\eta m^2x^2\xi y^2+$$

$$+36\alpha^2\eta m^2x^2\xi z^2+72\eta m^2x^2\xi y^2z^2+36\eta m^2x^4\xi y^2+$$

$$+36\eta m^2x^4\xi z^2+36\eta m^2x^2\xi y^4+36\eta m^2x^2\xi z^4+$$

$$+72\sqrt{x^2+y^2+z^2}\alpha\eta m^2x^2\xi y^2+x^{12}+y^{12}+z^{12}+$$

$$+6x^{10}y^2+6x^{10}z^2+72\sqrt{x^2+y^2+z^2}\alpha\eta m^2x^2\xi z^2+$$

$$+15x^8y^4+15x^8z^4+20x^6y^6+20x^6z^6+15x^4y^8+$$

$$+15x^4z^8 + 6x^2y^{10} + 6x^2z^{10} + 6y^{10}z^2 + 15y^8z^4 +$$

$$+20y^6z^6 + 15y^4z^8 + 6y^2z^{10}), \tag{2.17}$$

$$G_{23}^{eff} = \frac{36\left(\sqrt{x^2+y^2+z^2}+\alpha\right)^3 m^2x^2zy\eta\xi}{(x^2+y^2+z^2)^{\frac{13}{2}}}, \tag{2.18}$$

$$G_{31}^{eff} = \frac{36\left(\sqrt{x^2+y^2+z^2}+\alpha\right)^3 m^2x^2zy\eta\xi}{(x^2+y^2+z^2)^{\frac{13}{2}}}, \tag{2.19}$$

$$G_{32}^{eff} = \frac{36\left(\sqrt{x^2+y^2+z^2}+\alpha\right)^3 m^2x^2zy\eta\xi}{(x^2+y^2+z^2)^{\frac{13}{2}}}, \tag{2.20}$$

$$G_{33}^{eff} = \frac{36\left(\sqrt{x^2+y^2+z^2}+\alpha\right)^3 m^2x^2zy\eta\xi}{(x^2+y^2+z^2)^{\frac{13}{2}}}. \tag{2.21}$$

Next, we derive the inverse form of this effective metric tensor, which is a crucial step for further calculations. Utilizing this inverse metric, we then calculate the Christoffel symbols, which are essential for defining the curvature and connection properties of the spacetime under consideration. Our calculations revealed that there are 20 non-zero components of the Christoffel symbols. Using these calculated Christoffel symbols, we proceed to formulate the geodesic equation, incorporating a normalization condition that ensures the physical plausibility of our model. This step is fundamental in understanding the paths that particles or light rays would follow in the curved spacetime described by our effective metric. In total, we derived three main geodesic equations. Due to their extensive and complex nature, we present only their general forms in the main text of our work, reserving the detailed expressions and derivations for an extended discussion section or supplementary material.

$$\frac{d^2ct}{dz^2} = -\left\{\Gamma_{mp}^0 - \frac{dct}{dz}\Gamma_{mp}^3\right\}\frac{dx^p}{dz}\frac{dx^m}{dz},$$

$$\frac{d^2x}{dz^2} = -\left\{\Gamma_{mp}^1 - \frac{dx}{dz}\Gamma_{mp}^3\right\}\frac{dx^p}{dz}\frac{dx^m}{dz},$$

$$\frac{d^2y}{dz^2} = -\left\{\Gamma_{mp}^2 - \frac{dy}{dz}\Gamma_{mp}^3\right\}\frac{dx^p}{dz}\frac{dx^m}{dz}, \tag{2.22}$$

$$G_{np}^{(1,2)} \frac{dx^n}{dz} \frac{dx^p}{dz} = 0. \quad (2.23)$$

After that, we clarified the numerical values of the following quantities: magnetic moment, gravitational radius, and parameters η_1 and η_2. Each quantity was subjected to repeated measurements and analysis to ensure the accuracy of the data for our calculations. Once the accuracy of these data was confirmed, we entered them into our computational model as follows: the values of the magnetic moment were updated based on the latest experimental results, the gravitational radius values were adjusted for better alignment with theoretical assumptions, and the parameters η_1 and η_2 were set according to new scientific data. This ensured increased accuracy and relevance of our numerical simulations.

$$\xi = 5.141890467 \cdot 10^{-20},$$

$$c = 2.99792458 \cdot 10^{8},$$

$$M_N = 1\ M_{sun}, \qquad r_g = 2953.85,$$

$$\eta_1 = 5.1 \cdot 10^{-5}, \qquad \eta_2 = 9 \cdot 10^{-5},$$

$$\mu_1 = 10^{21}, \qquad \mu_2 = 10^{22}, \qquad \mu_2 = 10^{23}\ . \quad (2.24)$$

In this study, three different numerical values of the magnetic moment, μ_1, μ_2, μ_3 were obtained corresponding to magnetic fields with intensities of $B_s = 10^9\ T$, $B_s = 10^{10}\ T$, $B_s = 10^{11}\ T$ respectively. These magnetic moment values are used as initial conditions for numerical calculations. We vary the values of the magnetic moment, gravitational radius, and parameters η_1 and η_2 to study their impact on the modeling results. A detailed analysis of the obtained results will be presented later. For further analysis, we will substitute these numerical values into the model equations, designated as (2.1), and perform the recording of these equations with their numerical values. This will allow for a thorough analysis of how outcomes depend on the variation of initial parameters. After preparing the initial conditions, the program begins the numerical solution of the equations. Based on the condition that the guiding ray approaching the magnetar is parallel to the Oz axis and has an impact parameter $b = 2 \cdot 10^4$, we analyze the entry into the magnetosphere at $z = -10^6\ m$ and conduct calculations until reaching $z = 10^6\ m$. Thus, we numerically solve the problem of motion in the effective geodesic potential to understand how the influence of the magnetic moment and other parameters changes the trajectory of the ray. The boundary conditions are formulated as follows:

$$z_0 = -10^6\ m, \quad x(z_0) = -2 \cdot 10^4\ m, (D(x))(z_0) = 0,$$

$$t(z_0) = 0, \big(D(t)\big)(z_0) = \frac{1}{\mathrm{c}} = \frac{1}{2.99792458 \cdot 10^8},$$

$$y(z_0) = 0, \big(D(y)\big)(z_0) = 0. \quad (2.25)$$

Here the c is the speed of light in a vacuum, and $D(t), D(x), D(y)$ are the first-order derivatives with respect to the parameter z for time and spatial coordinates, respectively. These initial conditions are input into the program, which then proceeds to numerical calculations. During the calculations, the parameter z varies within a range of $-10^6\, m \leq z \leq 10^6$. An important aspect is the orientation of the magnetic field, which is directed perpendicular to the direction of the light front hitting the magnetar. This direction coincides with the Ox axis, along which the magnetic field is calculated. In this context, the components of the magnetic dipole moment are defined as $\vec{m} = \{0, m_x, 0,0\}$, where m_x is the magnitude of the magnetic moment in the direction of the Ox axis. We place a neutron star at the beginning of the coordinate. This configuration allows for precise modeling of the interaction between the magnetic field and the electromagnetic wave and studying the physical phenomena occurring during this interaction.

To conduct a deeper analysis of the impact of post-Maxwellian parameters on the geodesic lines in the strong magnetic fields of magnetars, we employ a detailed approach to modeling for case of $\eta_1 = 5.1 \cdot 10^{-5}$. Based on the assumptions regarding magnetic field strengths at two different scales $B_s = 10^9\, T$ and $B_s = 10^{11}\, T$, our study is divided into two main groups. Each group includes analyses for three different values of the magnetar mass: $M_N = 1.4\, M_{sun}$ and $M_N = 1.8\, M_{sun}$. This allows us to cover a broad range of scenarios regarding the impact of mass on geodesic trajectories. For each combination of magnetic field and magnetar mass, we conduct calculations to obtain solutions for the equations describing the geodesic lines. These data form the basis for creating graphs that visually demonstrate how the trajectory of the EM beam changes under various initial conditions. Particular attention is given to the analysis of EM beam refraction near the surface of the magnetar, especially within distances up to 50 km, where significant curvature of the trajectories is observed.

We also examine different initial conditions in the equatorial plane of the magnetar ($y = 0,\ Ox,\ Oz$), including variations in the impact parameter. This allows us to study how changes in distance from the surface of the magnetar affect the characteristics of beam refraction. While in areas located more than 50 km from the surface, the curvature of the EM beam becomes less noticeable, emphasizing the importance of focusing research on areas closer to the magnetar. This approach not only provides a more thorough understanding of the dynamics of geodesic lines under extreme magnetic field conditions but also contributes to the development of more accurate models for predicting the behavior of EM radiation near neutron stars, which may have significant astrophysical implications. Here we take the impact parameter up to 50 km from the surface of the magnetar, because the refraction of the EM beam is clearly visible up to 50 km. We did not show it in the graph because the bending of the beam in the area above is insignificant.

1. Considering that the strength of the magnetic field on the surface of the magnetar is $B_s = 10^9$ T, the results according to the determined numerical solutions of the equations were considered individually based on the following three conditions:

a) We obtain a numerical solution for the effective geodesic equation with $B_s = 10^9\, T,\ \eta_1 = 5.1 \cdot 10^{-5},\ M_N = M_{sun},\ r_g = 2953.85\, m$. The program is set with initial conditions for solving the equation according to Figure 2.1. This means that the impact parameter of the light front covers a distance from 12 km to 50 km. This is due to the fact that in the region from 11 km to the surface of the magnetar, the solution of the equation tends towards infinity. This phenomenon is explained by the fact that the angle of the beam's turn is sharp, meaning it turns at an angle of 90 degrees or more. We have taken the solutions of the equation and displayed a graph of the effective geodesic lines in Figure 2.2.

b) We obtain a numerical solution for the effective geodesic equation with $B_s = 10^9\, T,\ \eta_1 = 5.1 \cdot 10^{-5},\ M_N = 1.4 \cdot M_{sun},\ r_g = 4135.38\, m$. Initial conditions for solving the equation are set according to Figure 2.3. Here, the aiming parameter of the light front spans a distance from 15 km to 50 km. This is because in the region from 14 km to the surface of the magnetar, the solution of the equation tends towards infinity. This phenomenon is explained by the fact that the angle of the beam's turn is sharp, meaning it turns at an angle of 90 degrees or more. The graph of effective geodesic lines is shown in Figure 2.4, derived from the solutions of the equation. In the area near the surface of the magnetar, the EM beam is significantly more curved than in the area further away. This, in turn, is explained by the effect of the strong combined field.

c) We obtain a numerical solution for the effective geodesic equation with $B_s = 10^9\, T,\ \eta_1 = 5.1 \cdot 10^{-5},\ M_N = 1.8 \cdot M_{sun},\ r_g = 5316.92\, m$. Initial conditions for solving the equation are set according to Figure 2.5. Here, the aiming parameter of the light front spans a distance from 18 km to 50 km. This is because in the region from 18 km to the surface of the magnetar, the solution of the equation tends towards infinity. This phenomenon is explained by the fact that the angle of the beam's turn is sharp, meaning it turns at an angle of 90 degrees or more. The graph of effective geodesic lines is shown in Figure 2.6, derived from the solutions of the equation. The narrowing of the graph in the image is a consequence of their sharp turn due to the strong refraction of the EM beam near the magnetar. This is explained by the fact that the deviation sharply increases with the increase of the gravitational radius. In the area near the surface of the magnetar, the EM beam is significantly more curved than in the area further away. This, in turn, is explained by the effect of the strong combined field.

2. Given the strength of the magnetic field on the surface of a magnetar as $B_s = 10^{11}$, the following numerical solutions to the equation were calculated accordingly for the three conditions:

a) With $B_s = 10^{11}\, T,\ \eta_1 = 5.1 \cdot 10^{-5},$ the numerical solution of the effective geodesic equation for $M_N = M_{sun},\ r_g = 2953.85\, m$, was computed under the initial conditions depicted in Fig. 2.3. Specifically, the impact parameter of the light front spans distances from 15 km to 50 km. This range is critical because, from 15 km to the surface of the magnetar, the solution to the equation tends toward infinity. This phenomenon is attributed to the abrupt bending of the light ray, namely, turning at an

angle of 90 degrees or more. The solutions of the equation are illustrated in Fig. 2.7, showing the plots of the effective geodesic lines.

b) We obtain a numerical solution for the effective geodesic equation with $B_s = 10^{11}\,T,\ \eta_1 = 5.1 \cdot 10^{-5},\ M_N = 1.4 \cdot M_{sun},\ r_g = 4135.38\,m.$ The initial conditions for solving the equation are set according to Fig. 2.8. Here, the impact parameter of the light front ranges from 17 km to 50 km. This range is significant because, from 17 km to the surface of the magnetar, the solution of the equation tends towards infinity. This behavior is explained by the sharp turning angle of the ray, which turns at an angle of 90 degrees or more. The plot of the effective geodesic lines, derived from the solutions of the equation, is shown in Fig. 2.9. Near the surface of the magnetar, the EM ray curves significantly more than in regions farther away.

c) For the numerical solution of the effective geodesic equation with $B_s = 10^{11}\,T,\ \eta_1 = 5.1 \cdot 10^{-5},\ M_N = 1.8 \cdot M_{sun},\ r_g = 5316.92\,m,$ the initial conditions are provided according to Fig. 2.10. Here, the impact parameter of the light front covers a distance from 19.5 km to 50 km. In the region from 19.4 km to the surface of the magnetar, the solution of the equation tends towards infinity. This outcome is explained by the sharp turning angle of the ray, which turns at an angle of 90 degrees or more. The plot of the effective geodesic lines, derived from the solutions of the equation, is shown in Fig. 2.11. Near the surface of the magnetar, the EM ray curves significantly more than in areas further away.

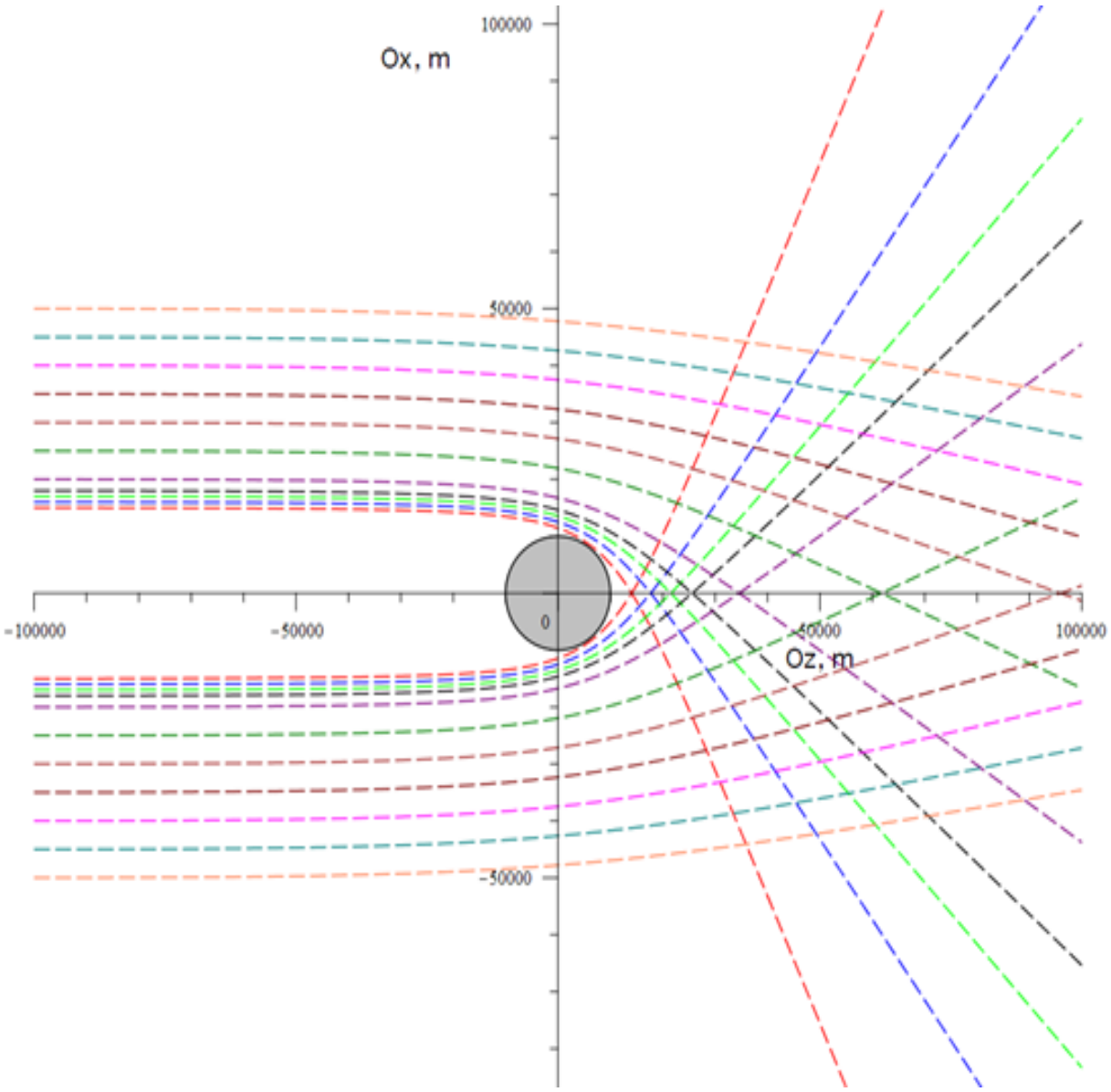

Figure 2.1 – Effective geodesics for $B_s = 10^9\ T, M_N = 1\ M_{sun},\ r_g = 2953.85\ m,$ $\eta_1 = 5.1 \cdot 10^{-5}, b \geq 12 \cdot 10^3\ m.$

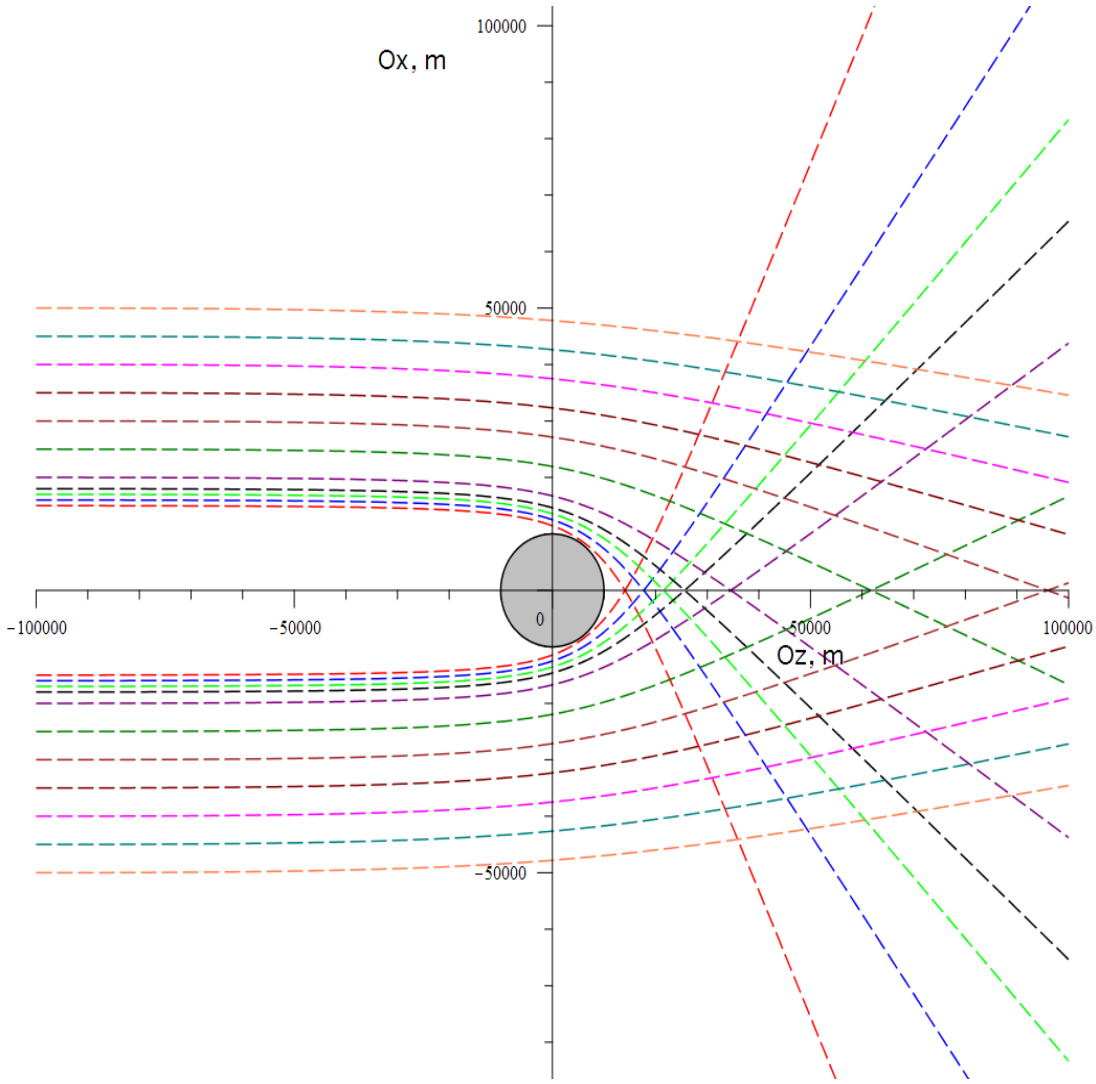

Figure 2.2 – Effective geodesics for $B_s = 10^9\ T,\ \eta_1 = 5.1 \cdot 10^{-5},\ M_N = 1.4 \cdot M_{sun},\ r_g = 4135.38\ m,\ b \geq 15 \cdot 10^3\ m$.

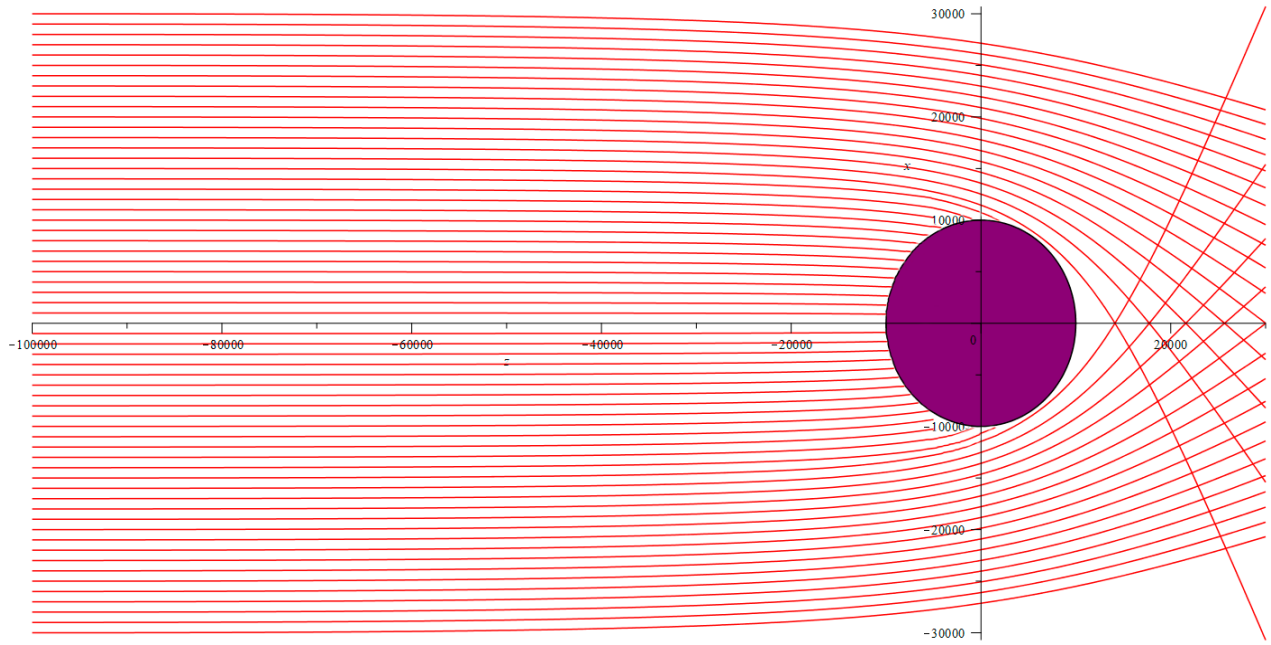

Figure 2.3 – Effective geodesics for $B_s = 10^9\ T,\ \eta_1 = 5.1 \cdot 10^{-5},\ M_N = 1.4 \cdot M_{sun},\ r_g = 4130\ m, at\ z = 30 \cdot 10^3\ m.$

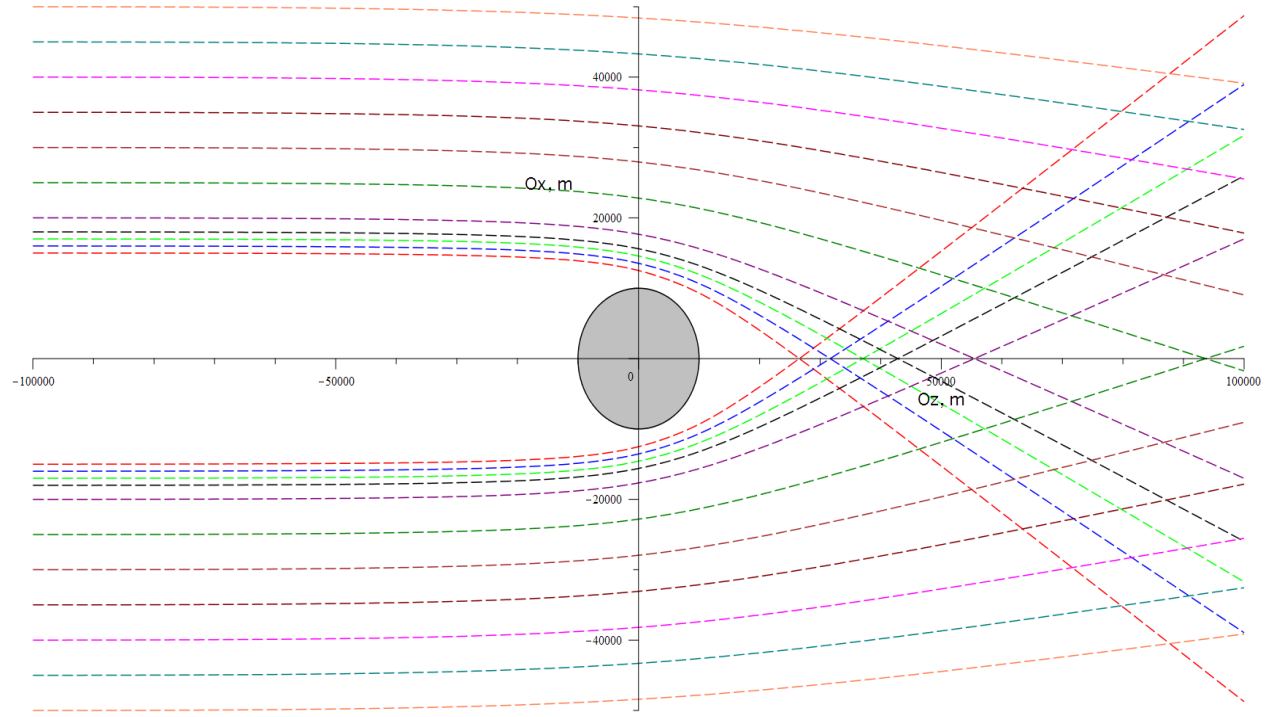

Figure 2.4 – Effective geodesics for $B_s = 10^{11}\ T,\ \eta_1 = 5.1 \cdot 10^{-5},\ M_N = M_{sun},\ r_g = 2953.85\ m, b \geq 15 \cdot 10^3\ m.$

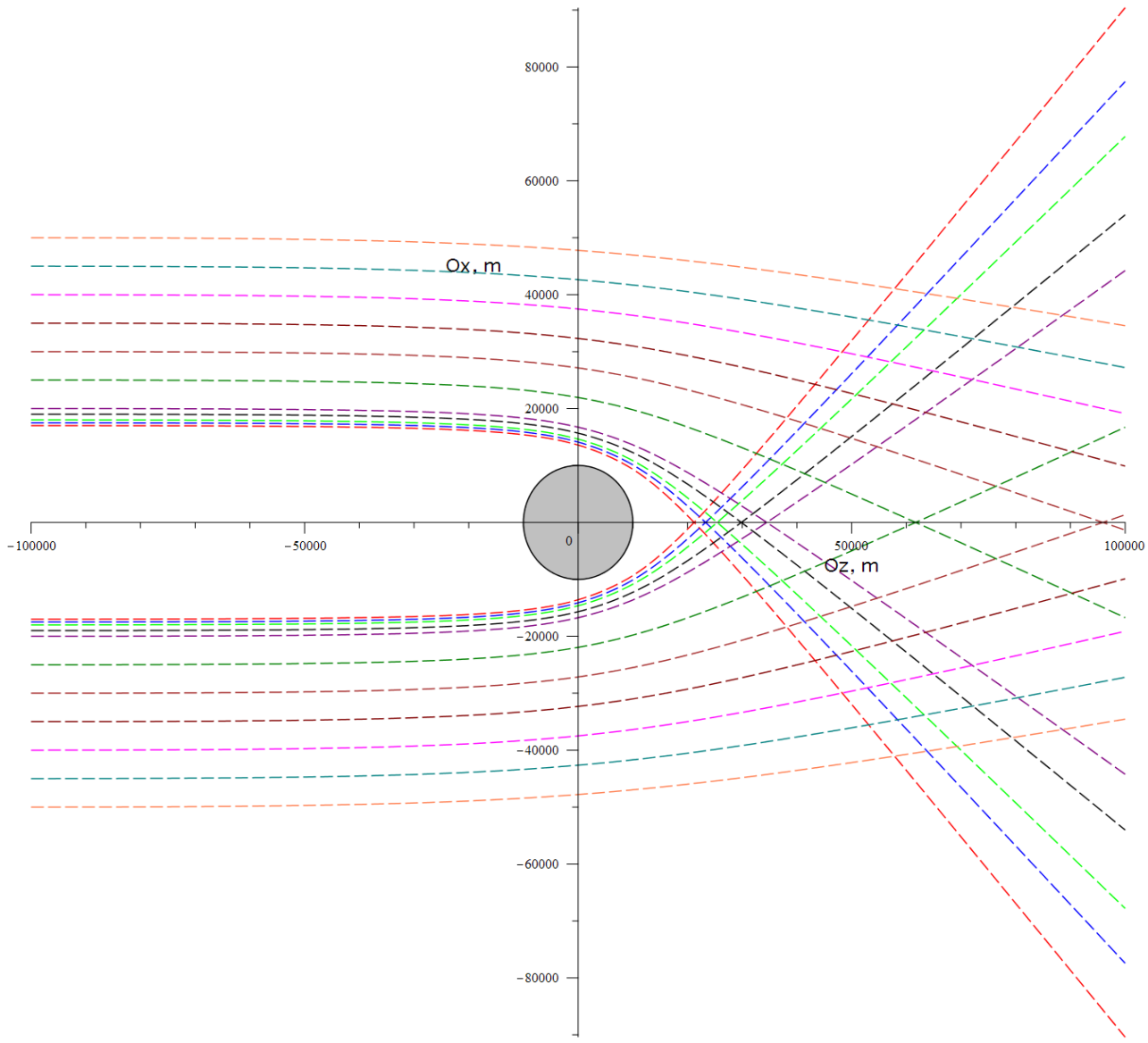

Figure 2.5 – Effective geodesics for $B_s = 10^{11}\ T,\ \eta_1 = 5.1 \cdot 10^{-5},\ M_N = 1.4 \cdot M_{sun},\ r_g = 4135.38\ m, b \geq 17 \cdot 10^3\ m$.

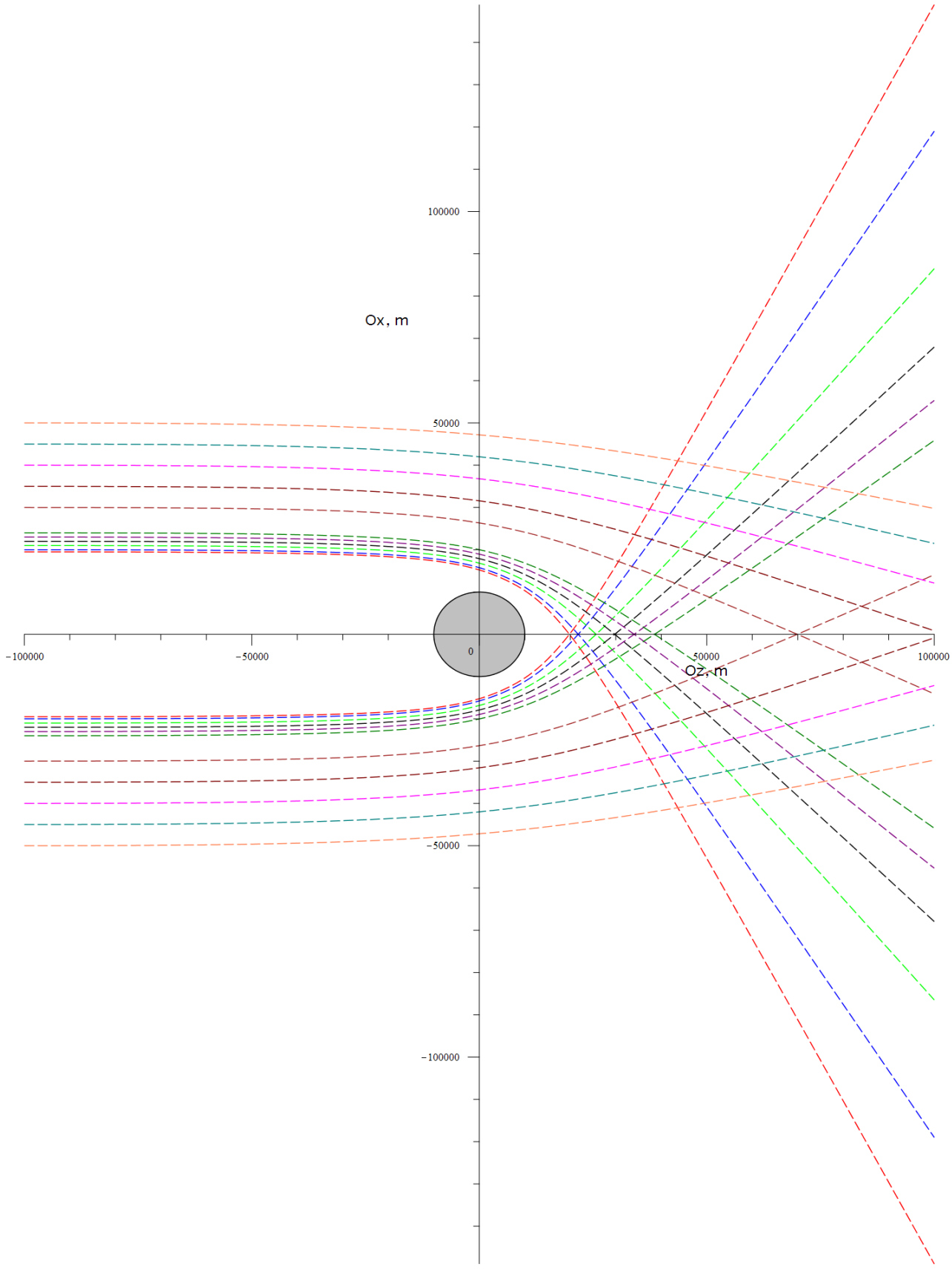

Figure 2.6 – Effective geodesics for $B_s = 10^{11}\ T,\ \eta_1 = 5.1 \cdot 10^{-5},\ M_N = 1.8 \cdot M_{sun}$, $r_g = 5316.92\ m, b \geq 19.5 \cdot 10^3\ m$.

In this thesis we also studied geodesic lines of EM radiation outside the equatorial plane. We fixed the values of the post-Maxwellian parameter $\eta_1 = 5.1 \cdot 10^{-5}$ and the gravitational radius of the magnetar $r_g = 4135.38$ m, and then numerically solved the system of equations. It was assumed that the dipole moment of the magnetic field of the magnet is directed along the Ox axis, that is, $\mu(\mu_x, 0, 0)$. According to figures (2.12) and (2.13), we obtained two different geodetic lines for the magnetic field values $B_s = 10^9$ T and $B_s = 10^{11}$ T. Geodesic lines of an EM beam approaching a magnetar from a distance of 100 km through a 50x50 km grid show little difference for a magnetar with a diameter of 10 km. As well as, we accomplished the task of constructing a plot of geodesic lines that illustrates the behavior of electromagnetic rays traveling towards a magnetar. These rays had an impact parameter of 30 km and were analyzed on the $Oy - Oz$ plane at a fixed x-value of 30 km. The magnetic field and post-Maxwellian parameter were set at $B_s = 10^9$ T and $\eta_1 = 5.1 \cdot 10^{-5}$ respectively, which correspond to conditions of extreme magnetic intensity. According to Figure 2.14, the rays passed parallel to the magnetar from the distance of 10^6 km, spaced at intervals of 10^3 m along the Oy axis. This plot is key to our investigation as it enables the visualization of the curvature of electromagnetic rays, particularly those passing close to the surface of the magnetar.

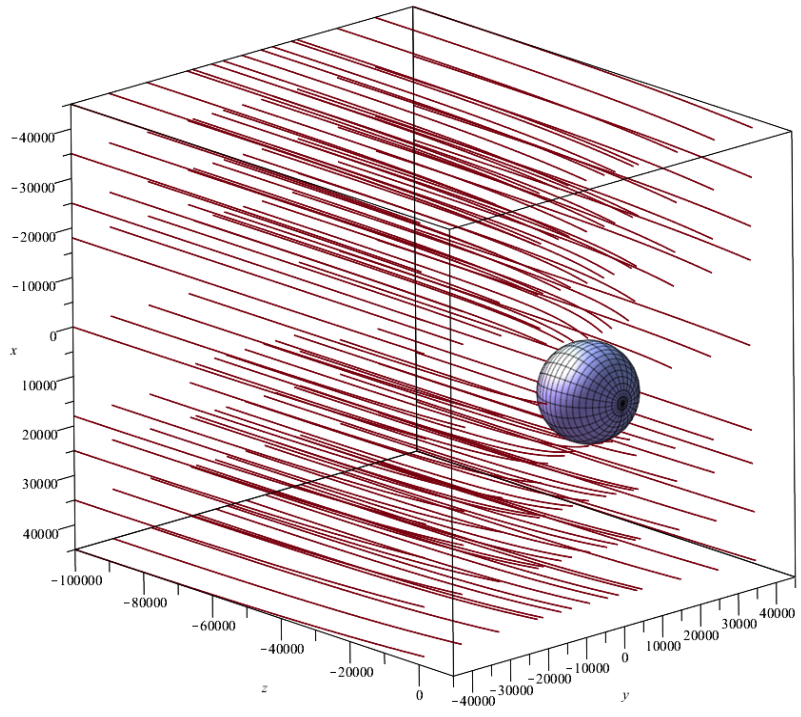

Figure 2.7 – The trajectory of photons for a magnetic field strength of $B_s = 10^9$ T and a value of $\eta_1 = 5.1 \cdot 10^{-5}$, a square wavefront with sides (50 × 50) × 10^3 m as a grid with the 10^3 m dynamic step.

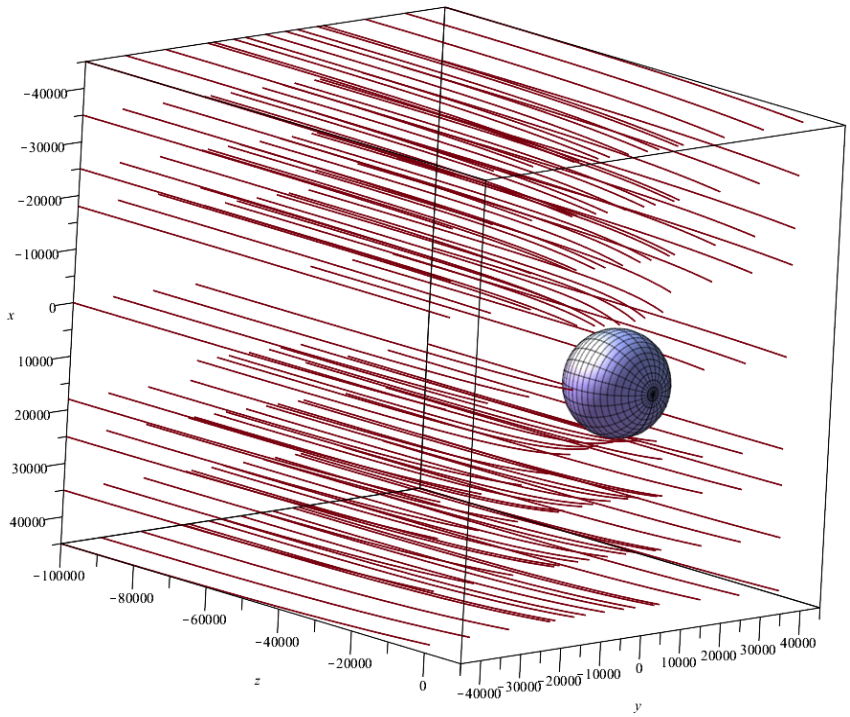

Figure 2.8 – The trajectory of photons for a magnetic field strength of $B_s = 10^{11}$ T and a value of $\eta_1 = 5.1 \cdot 10^{-5}$, a square wavefront with sides (50 × 50) × 10^3 m as a grid with the 10^3 m dynamic step.

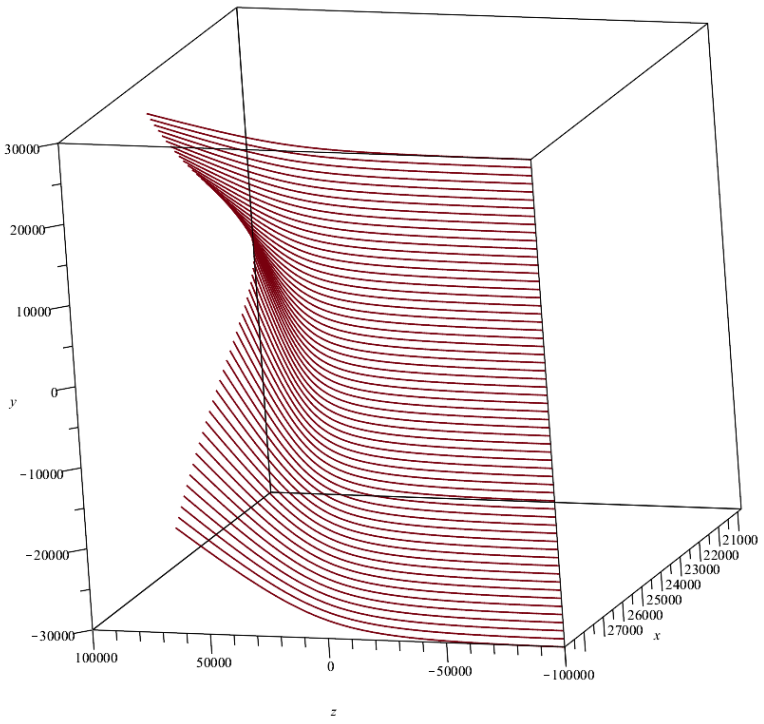

Figure 2.9 – The geodesic lines for a magnetic field strength of $B_s = 10^{11}$ T and a value of $\eta_1 = 5.1 \cdot 10^{-5}$, an impact parametre of 30 km and on the $Oy - Oz$ plane at a fixed x-value of 30 km.

For a value of $B_s = 10^9$ T and $\eta_1 = 5.1 \cdot 10^{-5}$, we considered three different cases to demonstrate the initial and final coordinates of photons. When an electromagnetic beam enters the magnetosphere of a magnetar from a distance of 100 km, we adopted three different impact parameter values: $b_1 = 3 \cdot 10^4\ m, b_2 = 5 \cdot 10^4\ m, b_3 = 10^5\ m$. According to Figures 2.15, 2.16, and 2.17 respectively, we demonstrated the initial and final coordinate points in the plane of $Ox - Oy$. As can be seen, the changes in the positions of points lying along the geodesic line are significant closer to the surface of the magnetar, indicating high curvature of light in this region.

Critical values of the impact parameter for EM rays passing through the region near the surface of a magnetar were determined. We identified these by locating the point at which the solution of the equation exhibits a singularity when testing the impact parameter in the initial state. Figure 2.18 illustrates the graph showing the dependence of the obtained critical impact parameter values on the mass of the magnetar. The graph indicates that as the mass of the magnetar increases, the critical values of the beam's impact parameters also increase proportionally to the strength of the external dipole magnetic field. Using the method of least squares (linear regression) to determine the slope m and intercept c in the linear model $b_{cr} = m \cdot M_{\text{Sun}} + c$, the equations describing the dependence of b_{cr} on M_{Sun} for each line are as follows, for $B_s = 1.10^9 T$

$$b_{cr} = 9348.75 \cdot M_{\text{Sun}} + 959.42. \tag{2.26}$$

This equation demonstrates that as the mass of the magnetar increases by one solar mass unit, the critical impact parameter of the rays increases by 9348.75 units. For $B_s = 1.10^{11}$ T:

$$b_{cr} = 5803.75 \cdot M_{\text{Sun}} + 8709.75. \tag{2.27}$$

In this case, the slope is smaller, but the intercept is significantly higher, indicating a higher initial value of b_{cr} for the same mass of the magnetar, which may be associated with a stronger magnetic field.

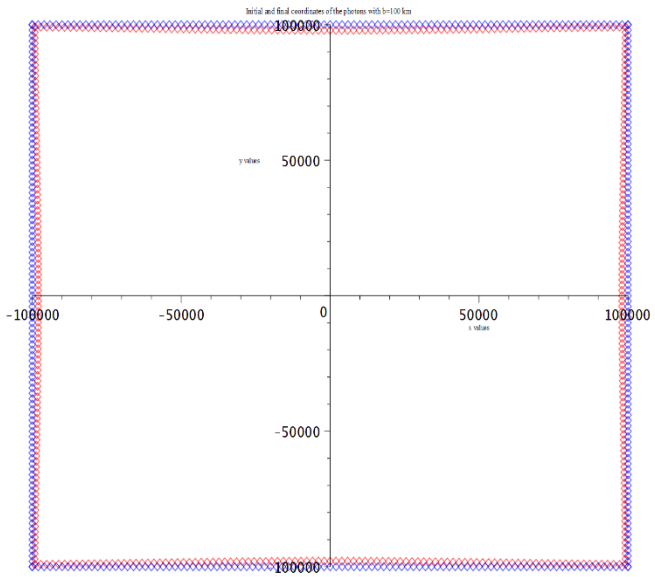

Figure 2.10 – Initial and final coordinate of the photons entering to the magnetosphere of the magnetar at the distance of $z = 100\ km$ with impact parameter of $b_1 = 10^5\ m$ in a magnetic field strength of $B_s = 10^9$ T and a value of $\eta_1 = 5.1 \cdot 10^{-5}$.

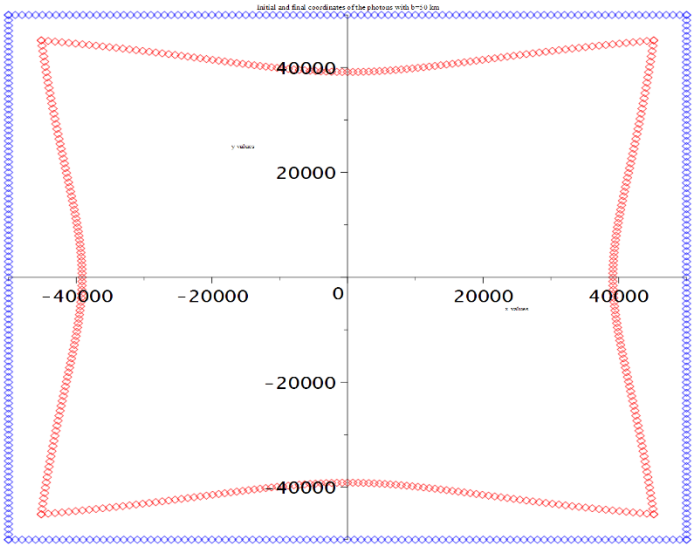

Figure 2.11 – Initial and final coordinate of the photons entering to the magnetosphere of the magnetar at the distance of $z = 100\ km$ with impact parameter of $b_1 = 5 \cdot 10^4\ m$ in a magnetic field strength of $B_s = 10^9$ T and a value of $\eta_1 = 5.1 \cdot 10^{-5}$.

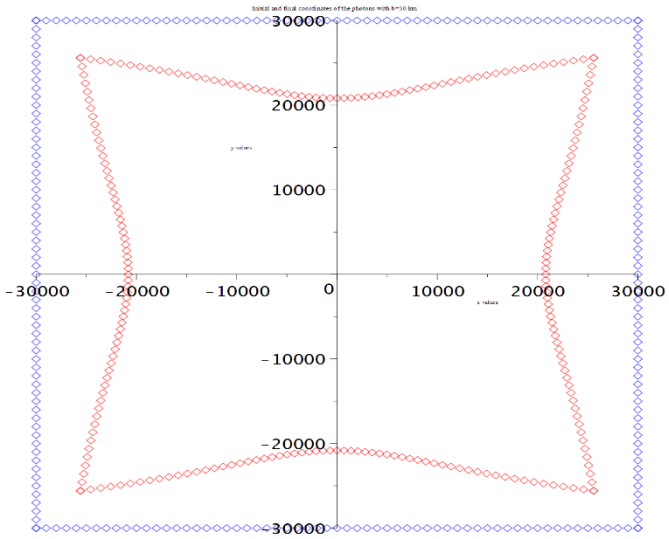

Figure 2.12 – Initial and final coordinate of the photons entering to the magnetosphere of the magnetar at the distance of $z = 100\,km$ with impact parameter of $b_1 = 3 \cdot 10^4\,m$ in a magnetic field strength of $B_s = 10^9$ T and a value of $\eta_1 = 5.1 \cdot 10^{-5}$.

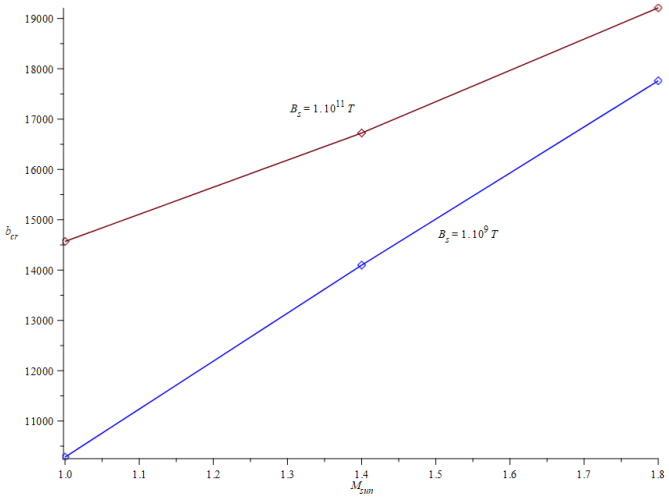

Figure 2.13 – Dependence of critical impact parameters on magnetar mass with external dipole magnetic field strength of $B_s = 10^9$ T and a value of $\eta_1 = 5.1 \cdot 10^{-5}$.

2.2 Analysis of ray distribution

One of the key applications of the effective metric concept is to analyze the deflection of light under the influence of an external electromagnetic field. In this context, the study of the general deflection of light within the framework of general relativity is especially important. Within the framework of the general theory of relativity, for spherically symmetric masses, an element of length of the following form is considered:

$$ds^2 = B(r)dt^2 - A(r)dr^2 - r^2C(r)(d\theta^2 + \sin\theta d\phi^2). \qquad (2.28)$$

A similar form of the line element is applied in the case of electromagnetic fields, particularly when a static radial field is generated by a spherically symmetric electric charge. However, in our case, we consider only the presence of a strong dipolar magnetic field, thereby disregarding any external electric fields. Typically, previous works focusing on analytical calculations of the effective geodesic equation concentrate on analyzing the angular displacement of a light ray, which is determined by the effective metric of the form ds^2. Due to the symmetry of the system, the angle θ can be fixed at $\pi/2$, restricting all motion to this plane. Utilizing the methodology and notation described in [66, 72,112,115], it is possible to calculate the bending angle of light that originates from an infinite distance. This approach allows for the precise determination of how light curves when it passes near massive celestial objects, adhering to the principles outlined in the referenced study.

$$\phi(\infty) - \phi(0) = \pm \int_r^{\infty} \frac{dr}{r} \sqrt{\frac{A(r)}{C(r)}} \left[\left(\frac{r}{r_0}\right) \frac{B(r_0)C(r)}{B(r)C(r_0)} - 1 \right]^{-\frac{1}{2}}. \qquad (2.29)$$

The equation provided in (2.1) calculates the bending angle of light originating from infinity. The distance at which the light ray comes closest to the charged object is denoted as r_0. Depending on the direction of motion (anticlockwise or clockwise), the choice of the plus or minus sign determines the appropriate bending angle.
To simplify the analysis, it is usually considered only the positive sign in the equations. Equation (2.1) was used the primary equation used in the previous researches [66]. The total angle deflection of a light ray starting from infinity, approaching a charged body to the minimum distance r_0, and then traveling back to infinity can be calculated using equation:

$$\Delta\phi = 2|\phi(\infty) - \phi(0)| - \pi. \qquad (2.30)$$

In the following subsections, we will utilize formulas (7.30) and (7.31) to examine the overall angle shift caused by the electric field of a spherically symmetric electric charge and the magnetic field of a dipole.

In another work, the angle of deviation of the beam is analytically determined by the refractive index coefficient. In them, the deflection angle of the beam is analytically calculated using the Gauss-Bonnet theorem (GBT) and the refractive index coefficient [78]. The GBT establishes a relationship between geometry in terms of optical curvature and topology in terms of the Euler characteristic number. It is expressed in the following equation:

$$\mathcal{K} = -\frac{n(\rho)n''(\rho)\rho - \left(n'(\rho)\right)^2\rho + n(\rho)n'(\rho)}{n^4(\rho)\rho}, \tag{2.31}$$

$$\iint_{\mathcal{D}_R} \mathcal{K}\mathrm{d}S + \oint_{\partial\mathcal{D}_R} k\mathrm{d}t + \sum_i \theta_i = 2\pi\chi(\mathcal{D}_R). \tag{2.32}$$

In equation (2.31), k refers to the geodesic curvature, and $\mathcal{K}$ represents the Gaussian optical curvature. By citing to the reference [gibbons2008applications], they estimated a nonsingular domain with an Euler characteristic number:

$$\chi(\mathcal{D}_R) = 1. \tag{2.33}$$

After several further transformations and approximations, the deflection angle of the light is determined analytically as follows.

$$\hat{\alpha} = -\int_0^{\pi}\int_{\frac{b}{\sin\varphi}}^{\infty}\left(-\frac{2M}{r^2} + \frac{18aMb}{r^5}\right)\sqrt{\tilde{g}}dr^{\star}d\varphi, \tag{2.34}$$

where

$$r = \frac{b}{\sin\varphi}. \tag{2.35}$$

The results obtained in these works are compared and discussed with previous studies. And, in this research work, we determine the deflection angle of the EM beam by numerically solving the system of effective geodesic equations. For this, we use the numerical solutions of the system of effective geodesic equations obtained in the previous chapter to calculate the deflection angle. After establishing the initial conditions, we observe bending of light for three distinct magnitudes of the dipole magnetic field: $B_s = 10^9$ T, $B_s = 10^{10}$ T, and $B_s = 10^{11}$ T. Consequently, we randomly select three values for the post-Maxwellian parameters as follows: $\eta_1 = 5.1 \cdot 10^{-5}$, $\eta_2 = 7 \cdot 10^{-5}$, and $\eta_3 = 9 \cdot 10^{-5}$. For each scenario, we solve the geodesic equation independently and calculate the deflection angles of the light using the expression defined by the ratio of velocities as:

$$\alpha = \frac{180 \cdot \arcsin\left(\frac{\sqrt{v_x^2 + v_y^2}}{c}\right)}{\pi}. \tag{2.36}$$

In this study, we used the speed of light, denoted as $c = 2.9979 \cdot 10^8$ m/s. Based on the calculated deflection angles, we plotted their relationship with the initial photon coordinates under three different conditions of the dipole magnetic field in conjunction with the gravitational field, as shown in figures (2.17), (2.18) and (2.19). Additionally, we assessed the values of the dipole magnetic field relating to the gravitational field, leading us to construct a similar graph illustrating this relationship. However, the influence of the magnetic field was notably minimal in the relation with a magnetic field strength of $B_s = 10^9$ T, prompting us to depict only the two cases with $B_s = 10^{10}$ T, and $B_s = 10^{11}$ T in figures (2.20) and (2.21). The research conducted confirmed the influence of vacuum nonlinear electrodynamics on the lensing of EM waves by a magnetar. Utilizing an effective metric in harmonic coordinates, our study explored the movement of flat EM wave fronts along the orthogonal Oz-axis, with the dipole magnetic moment oriented perpendicularly along the Ox-axis. We numerically resolved the effective geodesic equation under specific initial conditions to map the distribution of wave front deflection angles in the magnetosphere according to the initial coordinates. This analysis yielded a distribution that illustrates how the deflection angles depend on a dimensionless measure the ratio of the initial coordinates to the magnetar's diameter.

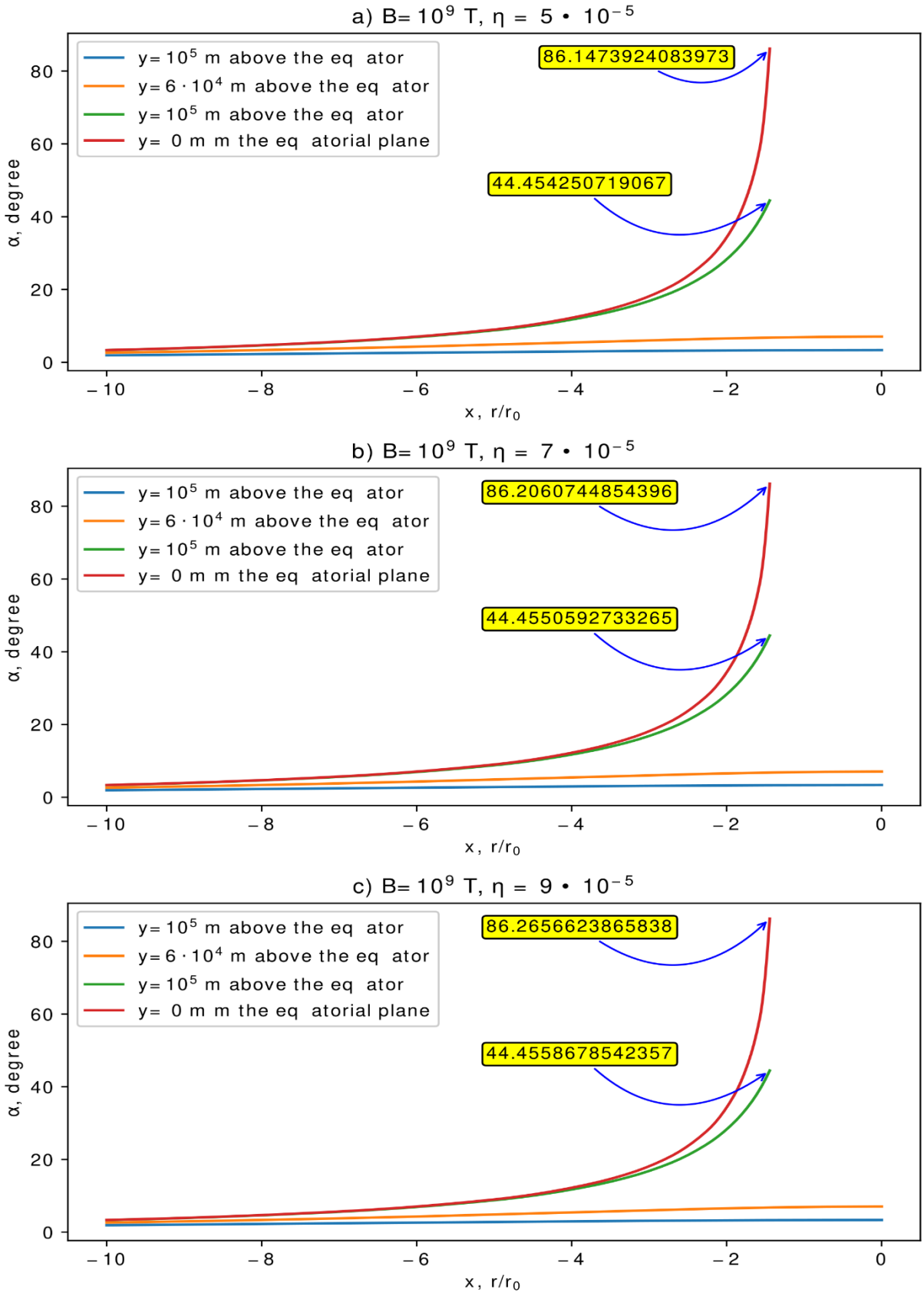

Figure 2.14 – Distribution of photon deflection angles in the gravitational and dipole magnetic field of $B_s = 10^9$ T, as impacted by post-maxwellian parameters $\eta_1 = 5.1 \cdot 10^{-5}$, $\eta_2 = 7 \cdot 10^{-5}$, and $\eta_3 = 9 \cdot 10^{-5}$, analyzed along the Ox-axis with stationary points on the Oy-axis.

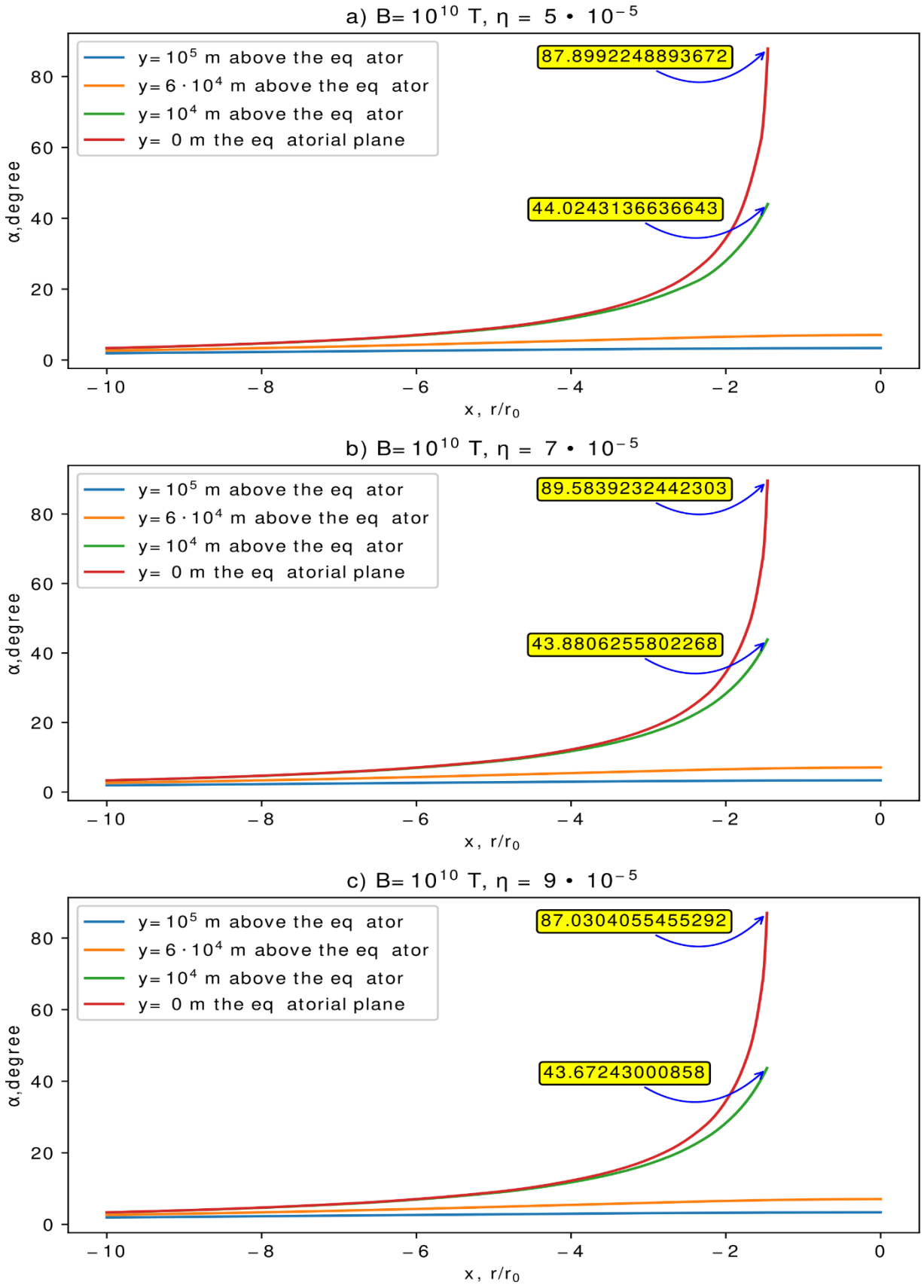

Figure 2.15 – Distribution of photon deflection in the gravitational and dipole magnetic field of $B_s = 10^{10}$ T, as influenced by post-maxwellian parameters $\eta_1 = 5.1 \cdot 10^{-5}$, $\eta_2 = 7 \cdot 10^{-5}$, and $\eta_3 = 9 \cdot 10^{-5}$, along the Ox-axis with fixed points on the Oy-axis.

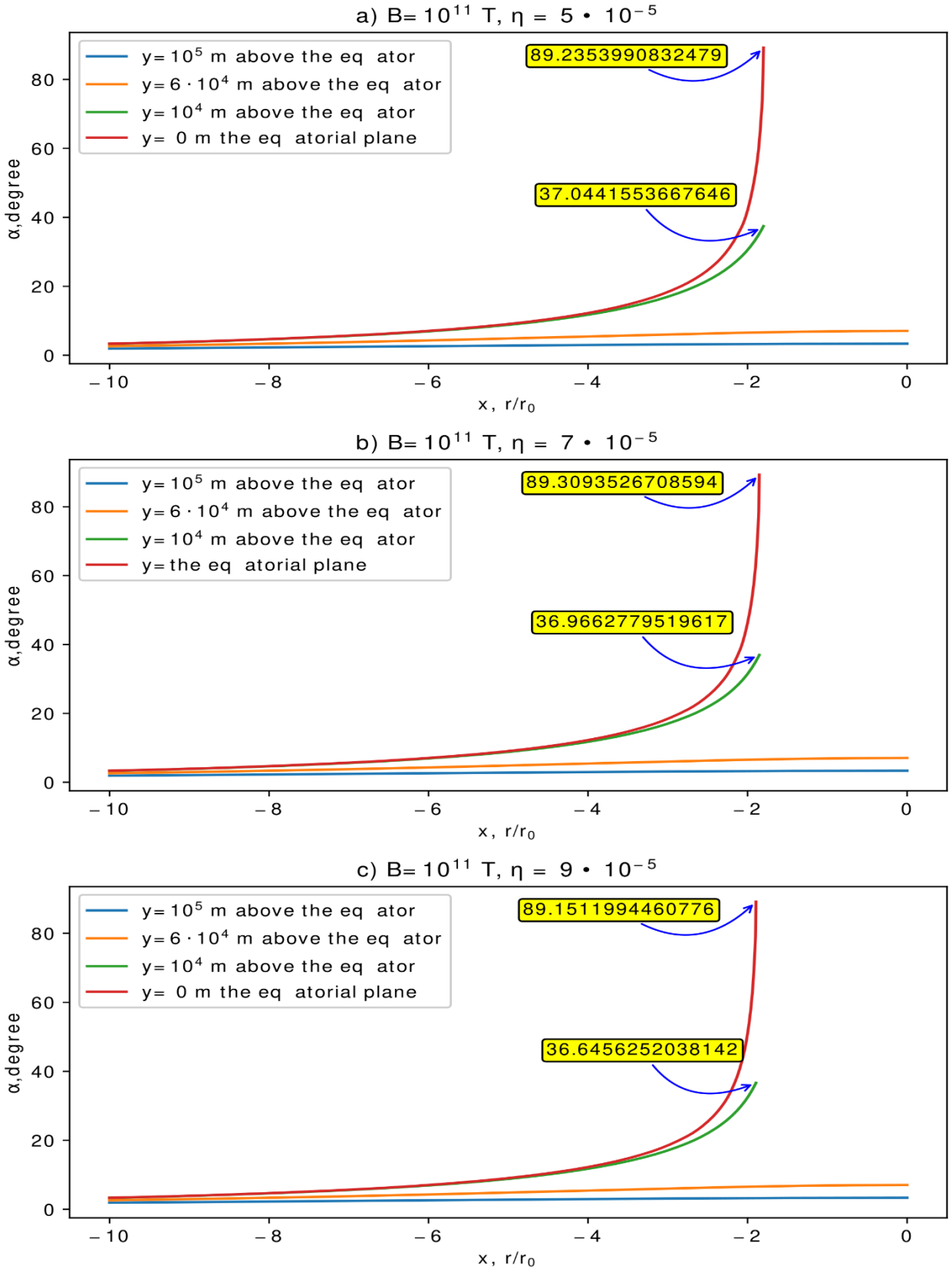

Figure 2.16 Distribution of photon deflection angles in the gravitational and dipole magnetic field of $B_s = 10^{11}$ T, as influenced by post-maxwellian parameters $\eta_1 = 5.1 \cdot 10^{-5}$, $\eta_2 = 7 \cdot 10^{-5}$, and $\eta_3 = 9 \cdot 10^{-5}$, along the Ox-axis with fixed points on the Oy-axis.

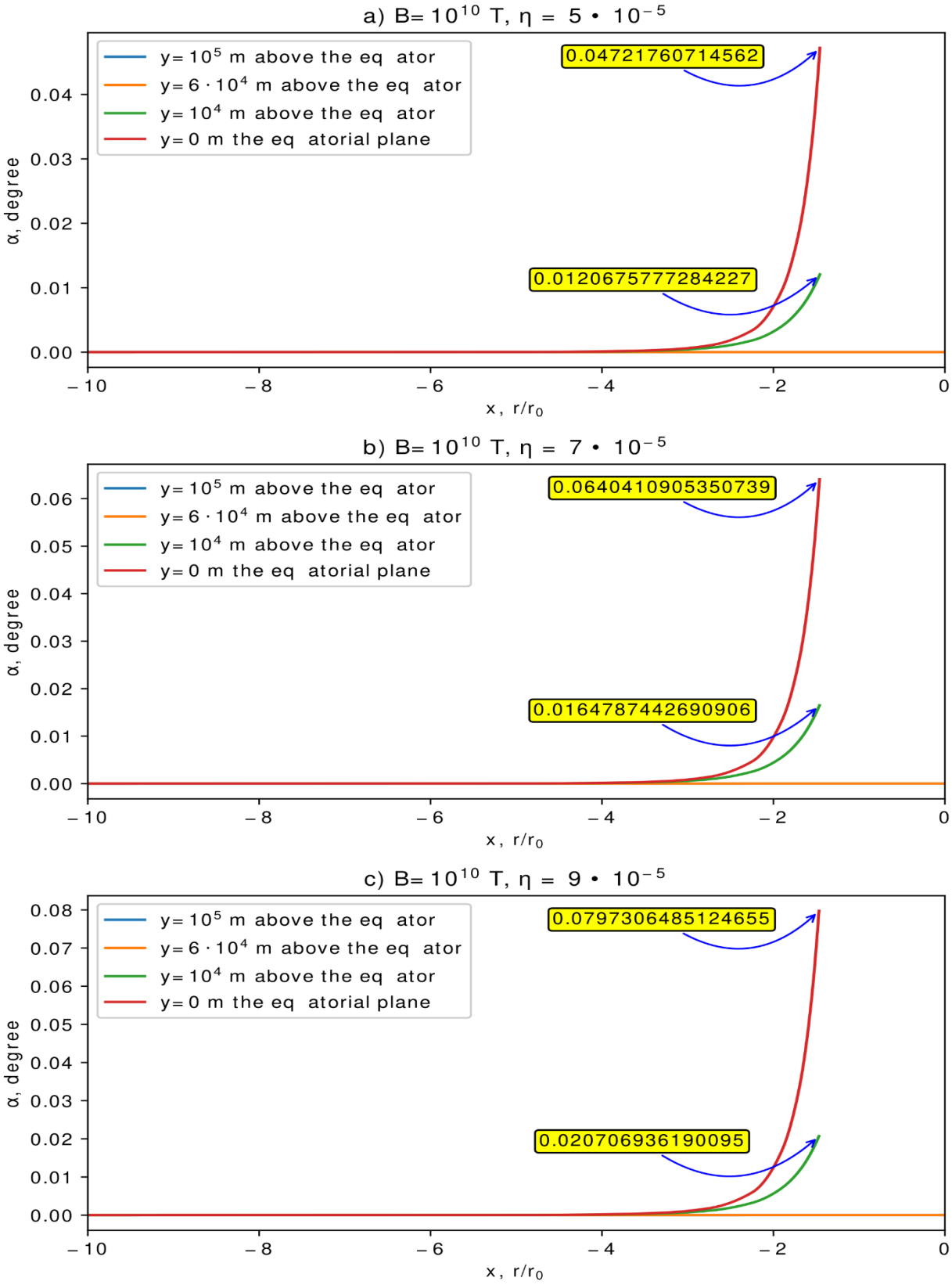

Figure 2.17 – Distribution of photon deflection angles solely by a dipole magnetic field of $B_s = 10^{10}$ T, modulated by post-maxwellian parameters $\eta_1 = 5.1 \cdot 10^{-5}$, $\eta_2 = 7 \cdot 10^{-5}$, and $\eta_3 = 9 \cdot 10^{-5}$, measured along the Ox-axis with fixed points on the Oy-axis.

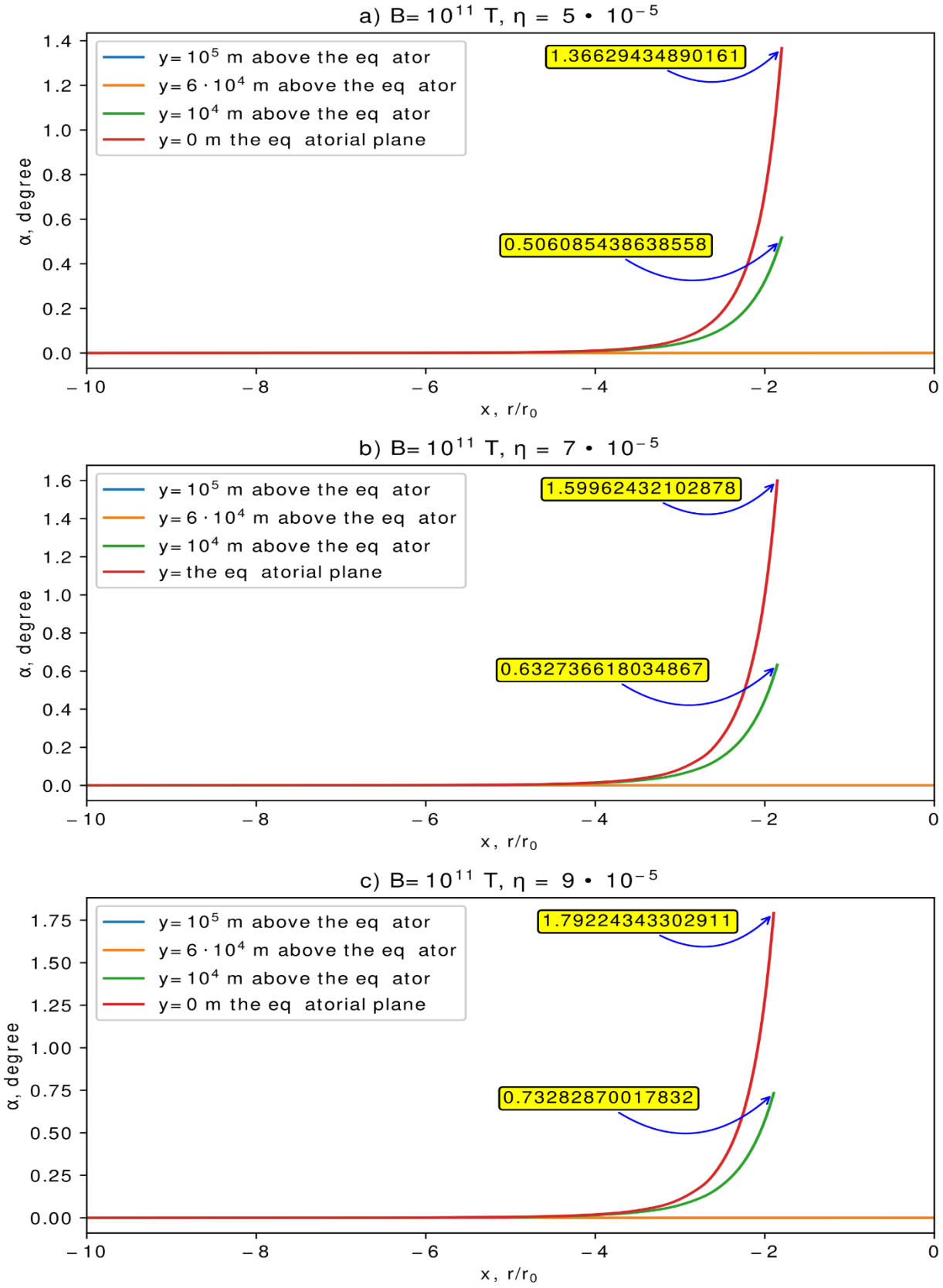

Figure 2.18 – Distribution of photon deflection angles solely by a dipole magnetic field of $B_s = 10^{11}$ T, modulated by post-maxwellian parameters $\eta_1 = 5.1 \cdot 10^{-5}$, $\eta_2 = 7 \cdot 10^{-5}$, and $\eta_3 = 9 \cdot 10^{-5}$, measured along the Ox-axis with fixed points on the Oy-axis.

Given the axial symmetry of the magnetar's magnetic field, the lensing effect is likewise axially symmetrical. This means the deflection angles for EM beams along the Ox-axis differ from those along the Oy-axis. Our findings also highlighted that EM wave deflections along the Oz-axis maintain this axial symmetry, as depicted in figures (2.21) and (2.22). To demonstrate the axial symmetry at $z = 0$, we plotted the variation of photon coordinates from a polar angle in the xy plane, as shown in figures (2.23) and (2.24). Here, the sinusoidal pattern confirms the axial symmetry of lensing near the magnetar.

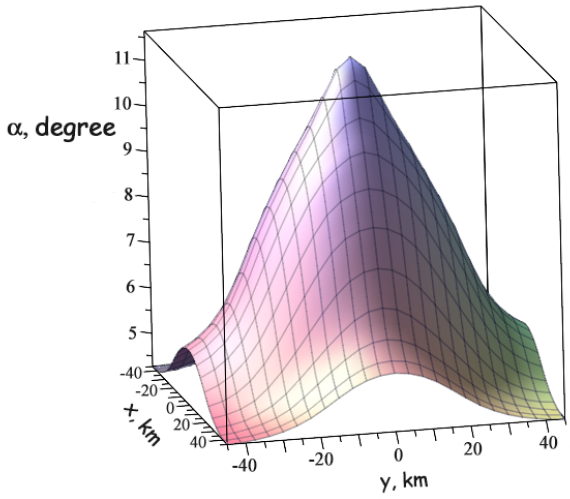

Figure 2.22 – Distribution of deflection angles relative to initial coordinates in the presence of a dipole magnetic field of $B_s = 10^9$ T with the post-maxwellian parameter of $\eta_1 = 5.1 \cdot 10^{-5}$ and impact parameter of $b \geq 50 \cdot 10^3$ m.

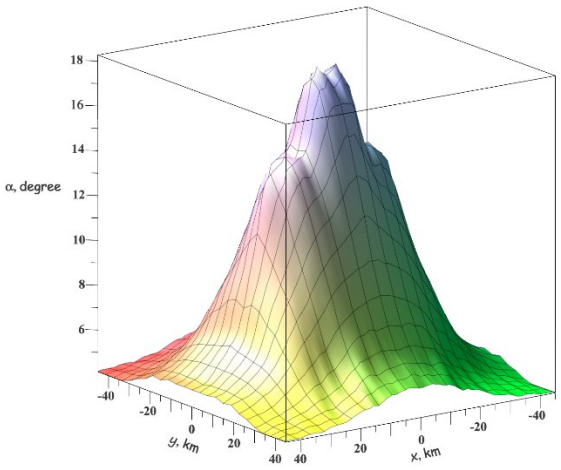

Figure 2.19 – Distribution of deflection angles relative to initial coordinates in the presence of a dipole magnetic field of $B_s = 10^{11}$ T with the post-maxwellian parameter of $\eta_1 = 5.1 \cdot 10^{-5}$ and impact parameter of $b \geq 50 \cdot 10^3$ m.

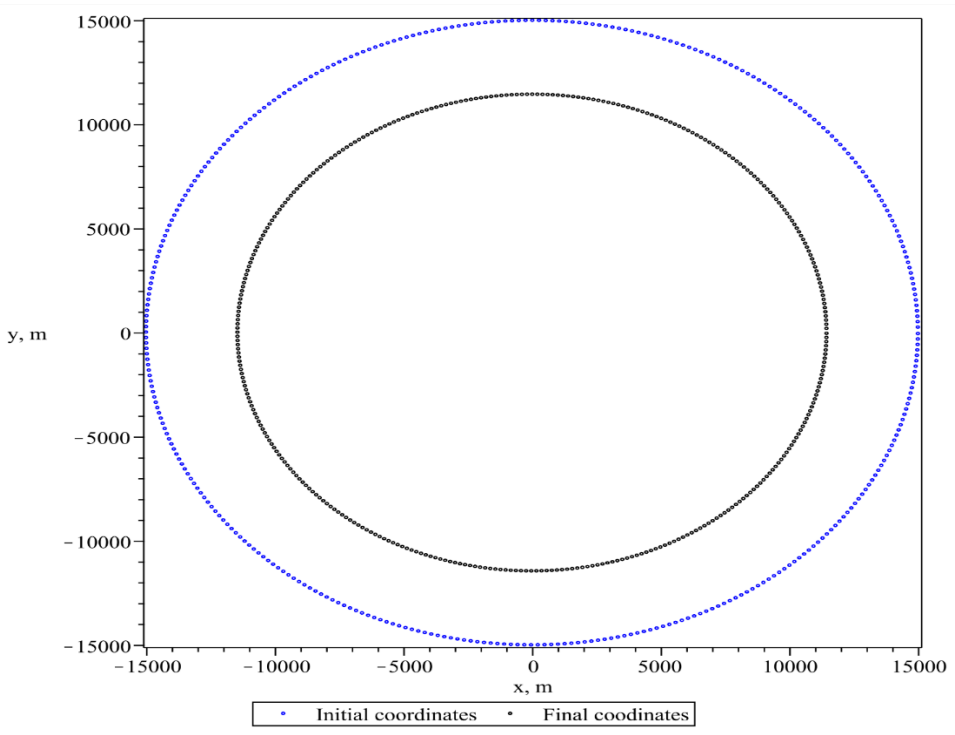

Figure 2.20 – Transformation of photon coordinates from a circle with a $15 \cdot 10^3$ m, radius of $z = -45 \cdot 10^3$ m to an ellipsoid at $z = 0$ m, under the influence of a surface magnetic field of $B_s = 10^9$ T and a post-maxwellian parameter of $\eta_1 = 5.1 \cdot 10^{-5}$.

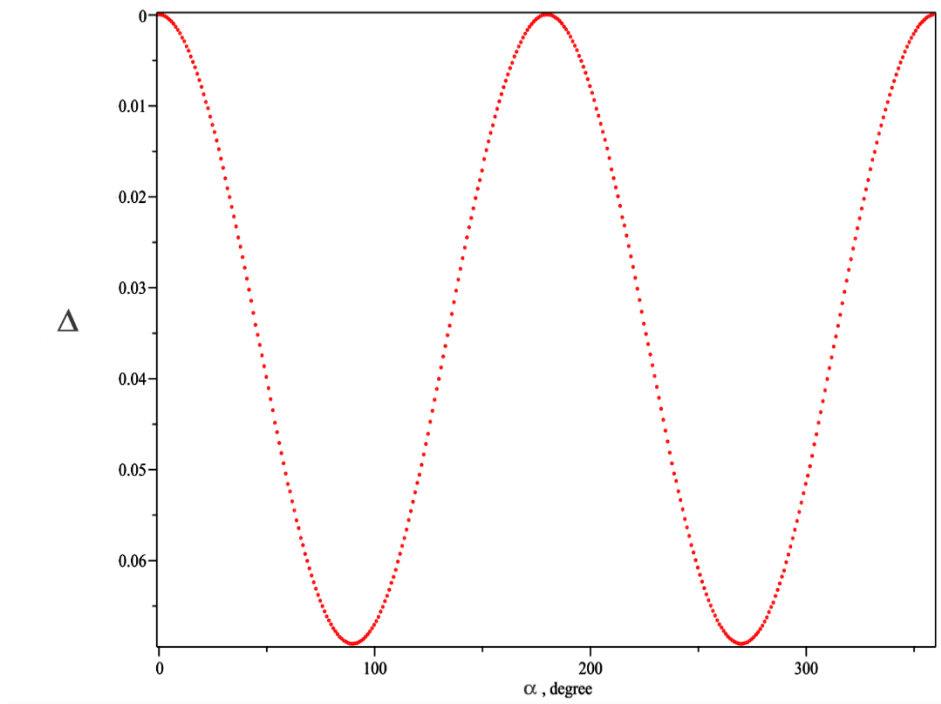

Figure 2.21 – Deformation of EM wave fronts relative to the deflection angles at $z = -45 \cdot 10^3$ m, in the case of $\eta_1 = 5.1 \cdot 10^{-5}$ and a surface magnetic field of $B_s = 10^9$ T.

Regarding specific calculations, the deflection angle of a photon entering $y = 10^5$ m, $x = 0$ m is approximately $3.356036834°$, while at $y = 0$ m, $x = 10^5$ m is, it is $3.356036837°$, with a negligible difference of about 10^{-9}. Additionally, we evaluated the deflection angles at $y = 15 \cdot 10^3$ m, $x = 15 \cdot 10^3$ and $z = 0$. It was observed that closer to the Ox-axis, the angle of light trajectory deviation from the Oz-axis increases. In a binary system involving a magnetar, this axial distortion in lensing could potentially be observed through photometric methods, marking a novel detectable effect of NLED.

Further, we determined the focal lengths of these rays. To do this, we determined the focal length by the following expression, using the laws relevant to geometric optics:

$$F = \frac{b}{\tan \alpha}, \tag{2.37}$$

where b is the impact parameter of the beam, and α is the turning angle of the beam. Focal lengths were calculated separately for EM beams propagating in the $Ox - Oz$ and $Ox - Oy$ planes. For these two planes, we constructed a graph of the dependence of the individually determined focal distances on the impact parameter of each beam for the case where $B_s = 10^9$ T, $\eta_1 = 5.1 \cdot 10^{-5}$ and $M_N = M_{sun}$, $r_g = 2953.85$. According to the figure (2.25), it was determined that the focal distance increases as the impact parameter increases. However, the fact that the focal lengths on the two planes are not the same, and the graph of their difference and dependence on the impact parameter was built. The difference in focal lengths can be explained by the presence of axial symmetry.

A numerical calculation of the passage of electromagnetic radiation from gamma-ray bursts through the dipole and quadrupole magnetic field of a magnetar was performed in figure (2.27). For this purpose, a mathematical model was developed that takes into account the interaction of gamma rays with various components of the complex magnetic structure of the magnetar magnetosphere. The modeling was carried out in order to study how exactly the magnetic field changes the trajectory and energy distribution of gamma radiation. In addition, during the calculations, the distribution of the energy of gamma rays passing through the magnetic field by scattering angles was obtained. This distribution showed how the energy of the front changes depending on their scattering angle relative to the magnetic field, which is important for understanding the processes of interaction of gamma radiation with the magnetic field of a magnetar.

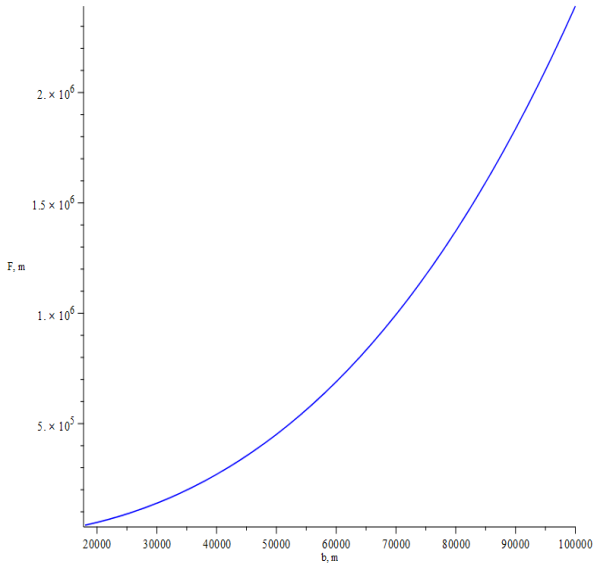

Figure 2.22 – Focal length (F) dependence from the impact parameter (b), influenced by a post-maxwellian parameter of $\eta_1 = 5.1 \cdot 10^{-5}$ and a surface magnetic field of $B_s = 10^9$ T with $M_N = 1\ M_{sun}$, $r_g = 2953.85$ m.

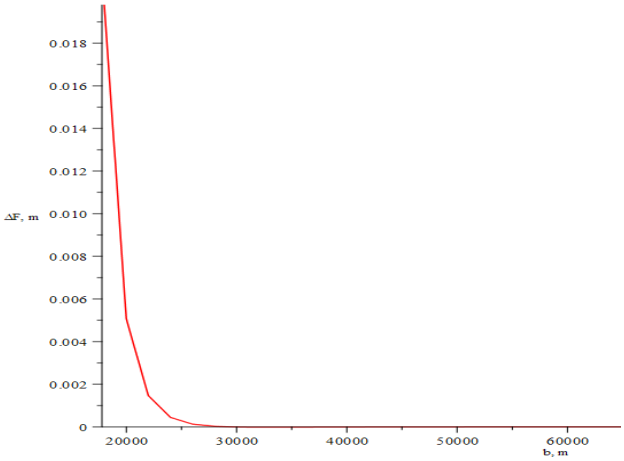

Figure 2.23 – Focal length (ΔF) deviation dependence from the impact parameter (b), influenced by a post-maxwellian parameter of $\eta_1 = 5.1 \cdot 10^{-5}$ and a surface magnetic field of $B_s = 10^9$ T with $M_N = 1\ M_{sun}$, $r_g = 2953.85$ m

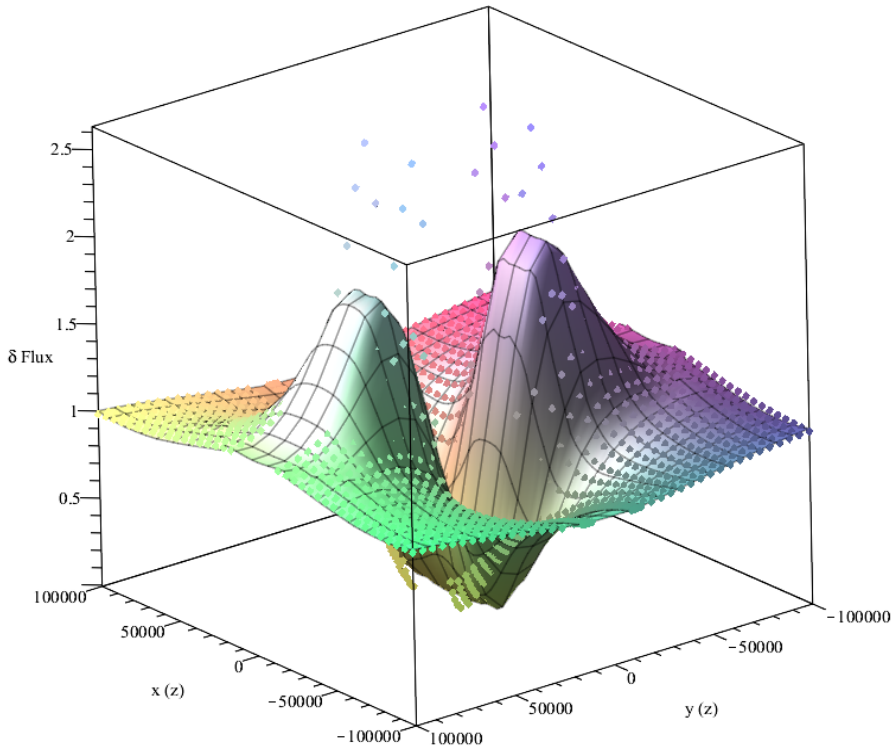

Figure 2.24 – Distribution of the intensity of rays passing through a magnetar along the front at the boundary of the magnetosphere with the boundary conditions of $z = -10^5$ m, in the case of $\eta_1 = 5.1 \cdot 10^{-5}$ and a surface magnetic field of $B_s = 10^9$ T.

CONCLUSION

This dissertation focuses on the study of vacuum nonlinear electrodynamics and the influence of gravity on the propagation of electromagnetic radiation through a magnetar. It examines the processes of beam deflection both in the plane of the dipole axis and in the plane perpendicular to it, under the combined effects of gravitational and magnetic fields. The research also determines the dependence of the deflection angle on the impact parameter and magnetic field strength at various distances (ranging from 15 to 100 km) and magnetic field intensities characteristic of a strong magnetar ($B = 10^{13}$ G). The study found that the deflection of the beams due to the gravitational and dipole magnetic fields is 86 degrees and 3.36 degrees, respectively, for impact parameters within the range of 15-100 km, with a field strength of $B = 10^{13}$ G.

At the same time, the deformation of the radiation front passing through the dipole magnetic field of the magnetar was investigated to identify the patterns of its shape transformation. The study assessed the degree of deviation from an ideal circular shape and the approach toward an elliptical form, as well as identified the key parameters influencing this deformation. As a result, it was found that the deformation of the electromagnetic wavefront, measured by the dimensionless quantity $\Delta = \frac{r_{max} - r_{min}}{r_{max}}$, caused by the combined gravitational and dipole magnetic fields of the magnetar, is 0.07, indicating an approximately elliptical shape.

As well as, this study investigated changes in the energy flux distribution of the radiation front from the source GRB091006360 as it passes through the magnetic field of the magnetar Swift J1822.3-1606. The relationship between the energy at the input and output of the front was established, and the factors influencing the minimum and maximum energy flows were identified. Consequently, it was determined that the significant influence of the combined gravitational and dipole magnetic fields on the gamma radiation flux density, as it traverses the magnetar's magnetosphere, leads to a redistribution of this flux.

The practical significance of the research lies in the enhanced understanding of the interaction between electromagnetic radiation and strong gravitational and magnetic fields of magnetars. The results obtained are crucial for interpreting astrophysical observations, such as beam deflection and radiation front deformation. They also contribute to the development of theoretical models that describe nonlinear vacuum effects and the redistribution of radiation energy under extreme conditions. This research can be applied in high-energy astrophysics for analyzing gamma radiation from magnetars. These findings expand the possibilities for studying exotic objects and phenomena in the universe.

REFERENCES

1. Avetissian H. K. Relativistic Nonlinear Electrodynamics: The QED Vacuum and Matter in Super-Strong Radiation Fields. – Springer, 2015. – T. 88.
2. Ejlli, A., Della Valle, F., Gastaldi, U., Messineo, G., Pengo, R., Ruoso, G., & Zavattini, G. The PVLAS experiment: A 25 year effort to measure vacuum magnetic birefringence //Physics Reports. – 2020. – T. 871. – C. 1-74.
3. Rudenko V. N., Oreshkin S. I., Rudenko K. V. Measuring global gravity-inertial effects with ring laser interferometers //Uspekhi Fizicheskikh Nauk. – 2022. – T. 192. – №. 9. – C. 984-1018.
4. Goedbloed J. P. et al. Magnetohydrodynamics: of laboratory and astrophysical plasmas. – Cambridge University Press, 2019.
5. Heyl J. S., Shaviv N. J. QED and the high polarization of the thermal radiation from neutron stars //Physical Review D. – 2002. – T. 66. – №. 2. – C. 023002.
6. S. Suresh, A. Ramanand, D. Jayaraman, P. Mani, Review on theoretical aspect of nonlinear optics //Rev. Adv. Mater. Sci. – 2012. – T. 30. – №. 2. – C. 175-183.
7. M. Born, Modified field equations with a finite radius of the electron //Nature. – 1933. – T. 132. – №. 3329. – C. 282-282.
8. M. Born, L. Infeld, Foundations of the new field theory //Proceedings of the Royal Society of London. Series A, Containing Papers of a Mathematical and Physical Character. – 1934. – T. 144. – №. 852. – C. 425-451.
9. S.I. Kruglov, Notes on Born–Infeld-type electrodynamics //Modern Physics Letters A. – 2017. – T. 32. – №. 36. – C. 1750201.
10. W. Heisenberg, H. Euler, Folgerungen aus der diracschen theorie des positrons //Zeitschrift für Physik. – 1936. – T. 98. – №. 11. – C. 714-732.
11. G. Mie, Beiträge zur Optik trüber Medien, speziell kolloidaler Metallösungen //Annalen der physik. – 1908. – T. 330. – №. 3. – C. 377-445.
12. R. Battesti, C. Rizzo, Magnetic and electric properties of a quantum vacuum //Reports on Progress in Physics. – 2012. – T. 76. – №. 1. – C. 016401.
13. F. Della Valle, E. Milotti, A. Ejlli, G. Messineo, L. Piemontese, G. Zavattini, U. Gastaldi, R. Pengo, G. Ruoso First results from the new PVLAS apparatus: A new limit on vacuum magnetic birefringence //Physical Review D. – 2014. – T. 90. – №. 9. – C. 092003.
14. F. Della Valle, A. Ejlli, U. Gastaldi, G. Messineo, E. Milotti, R. Pengo, G. Ruoso, G. Zavattini, The PVLAS experiment: measuring vacuum magnetic birefringence and dichroism with a birefringent Fabry–Perot cavity //The European Physical Journal C. – 2016. – T. 76. – C. 1-15.
A. Sushkov, W. Kim, D. Dalvit, S. Observation of the thermal Casimir force //Nature Physics. – 2011. – T. 7. – №. 3. – C. 230-233.
15. R. Loetzsch, H. Beyer, L. Duval, U. Spillmann, D. Bana´s, P. Dergham, F. Kr¨oger, J. Glorius, R. Grisenti, M. Guerra, et al., Testing quantum electrodynamics in extreme fields using helium-like uranium //Nature. – 2024. – T. 625. – №. 7996. – C. 673-678.)
16. A.M. Mailliet, A.E. Kraych, F. Couchot, X. Sarazin, E. Baynard, J. Demailly, M. Pittman, A. Djannati-Ata¨ı, S. Kazamias, S. Robertson, Performance of a Sagnac

interferometer to observe vacuum optical nonlinearity //Physical Review A. – 2024. – Т. 109. – №. 4. – С. 043526.
17. S.I. Kruglov, Nonlinear arcsin-electrodynamics //Annalen der Physik. – 2015. – Т. 527. – №. 5-6. – С. 397-401.
18. S.I. Kruglov, Black hole solution in the framework of arctan-electrodynamics //International Journal of Modern Physics D. – 2017. – Т. 26. – №. 08. – С. 1750075.
19. S.I. Kruglov, On generalized ModMax model of nonlinear electrodynamics //Physics Letters B. – 2021. – Т. 822. – С. 136633.
20. S.I. Kruglov, A model of nonlinear electrodynamics //Annals of Physics. – 2015. – Т. 353. – С. 299-306.
21. S.I. Kruglov, Nonlinear electrodynamics and black holes //International Journal of Geometric Methods in Modern Physics. – 2015. – Т. 12. – №. 07. – С. 1550073.
22. S.I. Kruglov, Born–Infeld-type electrodynamics and magnetic black holes //Annals of Physics. – 2017. – Т. 383. – С. 550-559.
23. D.P. Sorokin, Introductory Notes on Non-linear Electrodynamics and its Applications //Fortschritte der Physik. – 2022. – Т. 70. – №. 7-8. – С. 2200092.
24. N. Beissen, M. Abishev, S. Toktarbay, T. Yernazarov, D. Utepova, M. Zhakipova, The Exploring nonlinear vacuum electrodynamics beyond Maxwell's Equations //International Journal of Mathematics and Physics. – 2023. – Т. 14. – №. 1. – С. 61-70.
25. A.M. Beloborodov, Scattering of ultrastrong electromagnetic waves by magnetized particles //Physical Review Letters. – 2022. – Т. 128. – №. 25. – С. 255003
26. E.P. Mazets, S.V. Golenetskij, Y.A. Guryan, Soft gamma-ray bursts from the source B1900+ 14 //Pisma v Astronomicheskii Zhurnal, vol. 5, Dec. 1979, p. 641-643. Soviet Astronomy Letters, vol. 5, Nov.-Dec. 1979, p. 343, 344. Translation. – 1979. – Т. 5. – С. 641-643.
27. R.C. Duncan, C. Thompson, Formation of very strongly magnetized neutron stars-Implications for gamma-ray bursts //Astrophysical Journal, Part 2-Letters (ISSN 0004-637X), vol. 392, no. 1, June 10, 1992, p. L9-L13. Research supported by NSERC. – 1992. – Т. 392. – С. L9-L13.
28. P. Esposito, N. Rea, G.L. Israel, Magnetars: a short review and some sparse considerations //Timing Neutron Stars: Pulsations, Oscillations and Explosions. – 2021. – С. 97-142.
29. V.M. Kaspi, F.P. Gavriil, P.M. Woods, J.B. Jensen, M.S.E. Roberts, D. Chakrabarty, A major soft gamma repeater-like outburst and rotation glitch in the no-longer-so-anomalous X-ray pulsar 1E 2259+ 586 //The Astrophysical Journal. – 2003. – Т. 588. – №. 2. – С. L93.
30. R. Hu, A.M. Beloborodov, Axisymmetric pulsar magnetosphere revisited //The Astrophysical Journal. – 2022. – Т. 939. – №. 1. – С. 42.
31. S. Weinberg, Gravitation and cosmology john wiley & sons //Inc., USA. – 1972.
32. A.M. Beloborodov, Gravitational bending of light near compact objects //The Astrophysical Journal. – 2002. – Т. 566. – №. 2. – С. L85.
33. M.I. Vasili'ev, V.I. Denisov, A.V. Kozar', P.A. Tomasi-Vshivtseva, The Effects of Vacuum Nonlinear Electrodynamics in a Electric Dipole Field //Moscow University Physics Bulletin. – 2017. – Т. 72. – С. 513-517.

34. C.M. Kim, S.P. Kim, Magnetars as laboratories for strong field QED //AIP Conference Proceedings. – AIP Publishing, 2024. – Т. 2874. – №. 1.
35. R. Cameron, G. Cantatore, A. Melissinos, G. Ruoso, Y. Semertzidis, H. Halama, D. Lazarus, A. Prodell, F. Nezrick, C. Rizzo, et al., Search for nearly massless, weakly coupled particles by optical techniques //Physical Review D. – 1993. – Т. 47. – №. 9. – С. 3707.
36. Yernazarov T., Abishev M., Aimuratov Y. Correspondence of gamma radiation coming from GRBs and magnetars based on the effects of nonlinear vacuum electrodynamics //The Sixteenth Marcel Grossmann Meeting on Recent Developments in Theoretical and Experimental General Relativity, Astrophysics and Relativistic Field Theories: Proceedings of the MG16 Meeting on General Relativity Online; 5–10 July 2021. – 2023. – С. 4401-4409.
37. J.P. Pereira, J.G. Coelho, R.C. de Lima, Born–Infeld magnetars: larger than classical toroidal magnetic fields and implications for gravitational-wave astronomy //The European Physical Journal C. – 2018. – Т. 78. – С. 1-8.
38. Taylor J. H., Manchester R. N. Galactic distribution and evolution of pulsars //Astrophysical Journal, Part 1, vol. 215, Aug. 1, 1977, p. 885-896. – 1977. – Т. 215. – С. 885-896.
39. W. Becker, et al., Neutron stars and pulsars. – Berlin : Springer, 2009. – Т. 357. – С. 91-140.
40. P. Shuai, Understanding pulsars and space navigations. – Springer, 2021.
41. V.M. Kaspi, A.M. Beloborodov, Magnetars //Annual Review of Astronomy and Astrophysics. – 2017. – Т. 55. – №. 1. – С. 261-301.
A. Habibina, H. Ramadhan, Geodesic of nonlinear electrodynamics and stable photon orbits //Physical Review D. – 2020. – Т. 101. – №. 12. – С. 124036.
42. S. Kruglov, Pair production and vacuum polarization of arbitrary spin particles with EDM and AMM //Annals of Physics. – 2001. – Т. 293. – №. 2. – С. 228-239
43. D. Blaschke, A. Prozorkevich, G. R¨opke, C. Roberts, S. Schmidt, D. Shkirmanov, S. Smolyansky, Dynamical Schwinger effect and high-intensity lasers. Realising nonperturbative QED //The European Physical Journal D. – 2009. – Т. 55. – №. 2. – С. 341-358.
44. M. Novello, V. De Lorenci, J. Salim, R. Klippert, Geometrical aspects of light propagation in nonlinear electrodynamics //Physical Review D. – 2000. – Т. 61. – №. 4. – С. 045001.
45. V. De Lorenci, R. Klippert, M. Novello, J. Salim, Light propagation in non-linear electrodynamics //Physics Letters B. – 2000. – Т. 482. – №. 1-3. – С. 134-140.
46. S. Shakeri, M. Haghighat, S.S. Xue, Nonlinear QED effects in X-ray emission of pulsars //Journal of Cosmology and Astroparticle Physics. – 2017. – Т. 2017. – №. 10. – С. 014.
47. N.J. Shaviv, J.S. Heyl, Y. Lithwick, Magnetic lensing near ultramagnetized neutron stars //Monthly Notices of the Royal Astronomical Society. – 1999. – Т. 306. – №. 2. – С. 333-347.
48. E. Battaner, J. Castellano, M. Cosmic magnetic lenses //Astronomy & Astrophysics. – 2011. – Т. 527. – С. A79.

49. R. Mignani, V. Testa, D.G. Caniulef, R. Taverna, R. Turolla, S. Zane, K. Wu, Evidence for vacuum birefringence from the first optical polarimetry measurement of the isolated neutron star RX J1856. 5− 3754 //Monthly Notices of the Royal Astronomical Society. – 2016. – С. stw2798.
50. J. Heyl, I. Caiazzo, Strongly magnetized sources: QED and x-ray polarization //Galaxies. – 2018. – Т. 6. – №. 3. – С. 76.
51. S.I. Kruglov, Magnetized black holes and nonlinear electrodynamics //International Journal of Modern Physics A. – 2017. – Т. 32. – №. 23n24. – С. 1750147
52. S. Kruglov, On generalized born–infeld electrodynamics //Journal of Physics A: Mathematical and Theoretical. – 2010. – Т. 43. – №. 37. – С. 375402.
53. V. Perlick, C. L¨ammerzahl, A. Mac´ıas, Effects of nonlinear vacuum electrodynamics on the polarization plane of light //Physical Review D. – 2018. – Т. 98. – №. 10. – С. 105014.
54. A.W. Romero Jorge, E. Rodriguez Querts, H. Perez Rojas, A. Perez Martinez, L. Cruz Rodriguez, G. Piccinelli Bocchi, J.A. Rueda, The photon time delay in magnetized vacuum magnetosphere //Astronomische Nachrichten. – 2019. – Т. 340. – №. 9-10. – С. 852-856
55. H.Y. Kim, E.H. Lee, B.Y. Kim, Polarization properties of fiber lasers with twist-induced circular birefringence //Applied optics. – 1997. – Т. 36. – №. 27. – С. 6764-6769.
56. W. Kim, A. Sushkov, D. Dalvit, S. Lamoreaux, Measurement of the short-range attractive force between Ge plates using a torsion balance //Physical review letters. – 2009. – Т. 103. – №. 6. – С. 060401.
57. C.M. Kim, S.P. Kim, Schwinger Pair Production and Vacuum Birefringence around Highly Magnetized Neutron Stars //Astronomy Reports. – 2023. – Т. 67. – №. Suppl 2. – С. S122-S128.
58. T.D. Cohen, D.A. McGady, Schwinger mechanism revisited //Physical Review D—Particles, Fields, Gravitation, and Cosmology. – 2008. – Т. 78. – №. 3. – С. 036008.
59. F. Hebenstreit, R. Alkofer, H. Gies, Pair production beyond the Schwinger formula in time-dependent electric fields //Physical Review D—Particles, Fields, Gravitation, and Cosmology. – 2008. – Т. 78. – №. 6. – С. 061701.
60. V.I. Denisov, I.P. Denisova, Verifiable post-Maxwellian effect of the nonlinear electrodynamics in vacuum //Optics and Spectroscopy. – 2001. – Т. 90. – С. 282-287.
61. V. Denisov, I. Denisova, S. Svertilov, Nonlinear Electrodynamic Effect of Ray Bending in the Magnetic-Dipole Field //Doklady Physics. – 2001. – Т. 46. – №. 10.
62. V.I. Denisov, I.P. Denisova, I.V. Krivchenkov, P.A. Vshivtseva, Beam curvature in the magnetic field of a neutron star for an arbitrary angle between the magnetic dipole moment and incident beam //Doklady Physics. – Moscow, Russia: Maik nauka/Interperiodica Publishing; Woodbury, NY: Distributed by the American Institute of Physics, 1998-, 2003. – Т. 48. – №. 12. – С. 657-659.
63. J.Y. Kim, T. Lee, Fourteenth Marcel Grossmann Meeting, The: On Recent Developments In Theoretical And Experimental General Relativity, Astrophysics, And Relativistic Field Theories-Proceedings Of The Mg14 Meeting On General Relativity (In 4 Parts). – 2017.

64. J.Y. Kim, Deflection of light by a compact object with electric charge and magnetic dipole in Einstein-Born-Infeld gravity //arXiv preprint arXiv:2404.14756. – 2024.
A. Rueda, B. Haisch, Gravity and the quantum vacuum inertia hypothesis //Annalen der Physik. – 2005. – Т. 517. – №. 8. – С. 479-498.
65. J.S. Heyl, L. Hernquist, Birefringence and dichroism of the QED vacuum //arXiv preprint hep-ph/9705367. – 1997
66. V.I. Denisov, I.P. Denisova, A.B. Pimenov, V.A. Sokolov, Rapidly rotating pulsar radiation in vacuum nonlinear electrodynamics //The European Physical Journal C. – 2016. – Т. 76. – С. 1-8.
67. V.I. Denisov, V.A. Sokolov, Analysis of regularizing properties of nonlinear electrodynamics in the Einstein-Born-Infeld theory //Journal of Experimental and Theoretical Physics. – 2011. – Т. 113. – С. 926-933.
68. M.E. Abishev, V.I. Denisov, I.P. Denisova, O.V. Kechkin, The evaluation of electromagnetic forward radiations during the propagation of gravitational waves through the dipole field of the magnetar //Astroparticle Physics. – 2018. – Т. 103. – С. 94-97.
69. M.E. Abishev, N. Beissen, F. Belissarova, K. Boshkayev, A. Mansurova, A. Muratkhan, H. Quevedo, S. Toktarbay, Approximate perfect fluid solutions with quadrupole moment //International Journal of Modern Physics D. – 2021. – Т. 30. – №. 13. – С. 2150096.
70. J.B. Seaborn, Hypergeometric functions and their applications. – Springer Science & Business Media, 2013. – Т. 8.
71. K. Aomoto, Theory of hypergeometric functions. – Springer, 2011.
72. J.W. Pearson, Computation of hypergeometric functions : дис. – University of Oxford, 2009.
73. J.Y. Kim, T. Lee, Light bending by nonlinear electrodynamics under strong electric and magnetic field //Journal of Cosmology and Astroparticle Physics. – 2011. – Т. 2011. – №. 11. – С. 017.
A. Chowdhuri, S. Ghosh, A. Bhattacharyya, A review on analytical studies in Gravitational Lensing //Frontiers in Physics. – 2023. – Т. 11. – С. 1113909.
74. S.S. Li, S. Mao, Y. Zhao, Y. Lu, Gravitational lensing of gravitational waves: A statistical perspective //Monthly Notices of the Royal Astronomical Society. – 2018. – Т. 476. – №. 2. – С. 2220-2229.
75. H. Quevedo, Mass quadrupole as a source of naked singularities //International Journal of Modern Physics D. – 2011. – Т. 20. – №. 10. – С. 1779-1787.
76. P.V. Cunha, C.A. Herdeiro, Shadows and strong gravitational lensing: a brief review //General Relativity and Gravitation. – 2018. – Т. 50. – С. 1-27.
77. M. Bartelmann, Gravitational lensing //Classical and Quantum Gravity. – 2010. – Т. 27. – №. 23. – С. 233001.
78. N. Beissen, T. Yernazarov, M. Khassanov, S. Toktarbay, A. Taukenova, A. Talkhat, Bending of Light by Magnetars within Generalized Born–Infeld Electrodynamics: Insights from the Gauss–Bonnet Theorem //Symmetry. – 2024. – Т. 16. – №. 1. – С. 132.

79. M. Camenzind, Compact objects in astrophysics. – Springer Berlin Heidelberg, 2007. – C. 1-25.
80. J.E. Horvath, Astrophysics of Compact Objects //High-Energy Astrophysics: A Primer. – Cham : Springer International Publishing, 2022. – C. 113-159.
81. C.M. Kim, S.P. Kim, Vacuum birefringence in a supercritical magnetic field and a subcritical electric field //arXiv preprint arXiv:2202.05477. – 2022
82. N. Beissen, D. Utepova, M. Abishev, H. Quevedo, M. Khassanov, S. Toktarbay, Gravitational refraction of compact objects with quadrupoles //Symmetry. – 2023. – Т. 15. – №. 3. – C. 614.
83. K. Jusufi, Gravitational deflection of relativistic massive particles by Kerr black holes and Teo wormholes viewed as a topological effect //Physical Review D. – 2018. – Т. 98. – №. 6. – C. 064017.
84. W. Javed, A. Hamza, A. Övgün. Effect of nonlinear electrodynamics on the weak field deflection angle by a black hole //Physical Review D. – 2020. – Т. 101. – №. 10. – C. 103521.
85. G. Gibbons, M. Werner, Werner M. C. Applications of the Gauss–Bonnet theorem to gravitational lensing //Classical and Quantum Gravity. – 2008. – Т. 25. – №. 23. – C. 235009.
86. J.Y. Kim, Deflection of light by magnetars in the generalized Born–Infeld electrodynamics //The European Physical Journal C. – 2022. – Т. 82. – №. 5. – C. 485.
87. D. Batic, S. Nelson, M. Nowakowski, Nowakowski M. Light on curved backgrounds //Physical Review D. – 2015. – Т. 91. – №. 10. – C. 104015.
88. Manjarres A. D. B., Nowakowski M. Traveling waves in the Euler-Heisenberg electrodynamics //Physical Review A. – 2017. – Т. 95. – №. 4. – C. 043820.
A. D'Aı, P.A.e. Evans, Evidence for the magnetar nature of 1E 161348− 5055 in RCW 103 //Monthly Notices of the Royal Astronomical Society. – 2016. – Т. 463. – №. 3. – C. 2394-2404.
89. R. Taverna, R. Turolla, V. Suleimanov, A.Y. Potekhin, S. Zane, X-ray spectra and polarization from magnetar candidates //Monthly Notices of the Royal Astronomical Society. – 2020. – Т. 492. – №. 4. – C. 5057-5074.
90. R. Turolla, S. Zane, A.L. Watts, Magnetars: the physics behind observations. A review //Reports on Progress in Physics. – 2015. – Т. 78. – №. 11. – C. 116901.
91. Guver T., Ozel F., Gogus E. Mapping the Surface of the Magnetar 1E 1048.1-5937 in Outburst and Quiescence Through Phase Resolved X-ray Spectroscopy //40th COSPAR Scientific Assembly. – 2014. – Т. 40. – C. E1. 12-3-14.
92. M.E. Abishev, Y. Aimuratov, Y. Aldabergenov, N. Beissen, Z. Bakytzhan, M. Takibayeva, Some astrophysical effects of nonlinear vacuum electrodynamics in the magnetosphere of a pulsar //Astroparticle Physics. – 2016. – Т. 73. – C. 8-13.
93. M.E. Abishev, S. Toktarbay, N.A. Beissen, F.B. Belissarova, M.K. Khassanov, A.S. Kudussov, A.Z. Abylayeva, Effects of non-linear electrodynamics of vacuum in the magnetic quadrupole field of a pulsar //Monthly Notices of the Royal Astronomical Society. – 2018. – Т. 481. – №. 1. – C. 36-43.
94. M. Abishev, V. Ivashchuk, A. Malybayev, S. Toktarbay, Dyon-like black hole solutions in the model with two Abelian gauge fields //Gravitation and Cosmology. – 2019. – Т. 25. – №. 4. – C. 374-382.

95. V.I. Denisov, E.E. Dolgaya, V.A. Sokolov, Nonperturbative QED vacuum birefringence //Journal of High Energy Physics. – 2017. – Т. 2017. – №. 5. – С. 1-13.
96. V.I. Denisov, B.N. Shvilkin, V.A. Sokolov, M.I. Vasili'ev, Pulsar radiation in post-Maxwellian vacuum nonlinear electrodynamics //Physical Review D. – 2016. – Т. 94. – №. 4. – С. 045021.
97. J.Y. Kim, Bending of electromagnetic wave in an ultra-strong magnetic field //Journal of Cosmology and Astroparticle Physics. – 2012. – Т. 2012. – №. 10. – С. 056.
98. J.Y. Kim, Deflection of light by a Coulomb charge in Born–Infeld electrodynamics //The European Physical Journal C. – 2021. – Т. 81. – №. 6. – С. 508.
99. Beissen, N., Abishev, M., Toktarbay, S., Yernazarov, T., Utepova, D., Zhakipova, M. (2023). The Exploring nonlinear vacuum electrodynamics beyond Maxwell's Equations //International Journal of Mathematics and Physics. – 2023. – Т. 14. – №. 1. – С. 61-70.
100. Beissen, N. A., Utepova, D. S., Kossov, V. N., Toktarbay, S., Khassanov, M. K., Yernazarov, T., Seydalieva, M. (2024). The influence of deformation in compact objects on redshift and radar echo delay //Recent Contributions to Physics. – 2024. – Т. 88. – №. 1.
101. Beissen, N., Abishev, M., Toktarbay, S., Yernazarov, T., Khassanov, M., Utepova, D., Abduali, A. (2024). An overview of light ray deflection calculation by magnetars in nonlinear electrodynamics //Bulletin of the Karaganda University" Physics Series". – 2024. – Т. 11429. – №. 2. – С. 65-71.
102. Beissen, N. A., Utepova, D. S., Kossov, V. N., Toktarbay, S., Khassanov, M. K., Yernazarov, T., Imanbayeva, A. K. (2024). Comparing the efficiency of GPU and CPU in gravitational lensing simulation //International Journal of Mathematics and Physics. – 2024. – Т. 15. – №. 1. – С. 49-56.
103. Yernazarov T., Abishev M., Aimuratov Y. Correspondence of gamma radiation coming from GRBs and magnetars based on the effects of nonlinear vacuum electrodynamics //The Sixteenth Marcel Grossmann Meeting on Recent Developments in Theoretical and Experimental General Relativity, Astrophysics and Relativistic Field Theories: Proceedings of the MG16 Meeting on General Relativity Online; 5–10 July 2021. – 2023. – С. 4401-4409.
104. Denisov V. I., Krivchenkov I. V., Denisova I. P. Nonlinear electrodynamic lag of electromagnetic signals in a magnetic dipole field //Journal of Experimental and Theoretical Physics. – 2002. – Т. 95. – С. 194-198.
105. Beissen, N., Abishev, M., Toktarbay, S., Yernazarov, T., Aimuratov, Y., Khassanov, M. Nonlinear electrodynamical lensing of electromagnetic waves on the dipole magnetic field of the magnetar //International Journal of Modern Physics D. – 2023. – Т. 32. – №. 16. – С. 2350106-142.
106. Cho Y. M., Pak D. G., Walker M. L. Light propagation effects in QED: Effective action approach //Physical Review D—Particles, Fields, Gravitation, and Cosmology. – 2006. – Т. 73. – №. 6. – С. 065014.
107. Zaumen W. T. Pair production in intense magnetic fields //Astrophysical Journal, Vol. 210, p. 776-779. – 1976. – Т. 210. – С. 776-779.

108. Kim J. Y., Lee T. Light bending in a Coulombic field //arXiv preprint arXiv:1012.1134. – 2010.
109. Ishihara A. et al. Gravitational bending angle of light for finite distance and the Gauss-Bonnet theorem //Physical Review D. – 2016. – Т. 94. – №. 8. – С. 084015.
110. Martin A. W., Pritchett P. L. Asymptotic Gravitational Field of the``Electron" //Journal of Mathematical Physics. – 1968. – Т. 9. – №. 4. – С. 593-597.
111. Heyl J. S., Hernquist L. QED one-loop corrections to a macroscopic magnetic dipole //arXiv preprint hep-ph/9705368. – 1997.
112. Batic D., Nelson S., Nowakowski M. Light on curved backgrounds //Physical Review D. – 2015. – Т. 91. – №. 10. – С. 104015.
113. Abishev, M. E., Toktarbay, S., Beissen, N. A., Belissarova, F. B., Khassanov, M. K., Kudussov, A. S., Abylayeva, A. Z. Effects of non-linear electrodynamics of vacuum in the magnetic quadrupole field of a pulsar //Monthly Notices of the Royal Astronomical Society. – 2018. – Т. 481. – №. 1. – С. 36-43.
114. Pétri J. General-relativistic force-free pulsar magnetospheres //Monthly Notices of the Royal Astronomical Society. – 2016. – Т. 455. – №. 4. – С. 3779-3805.
115. Manjarres A. D. B. Euler-heisenberg non-linear electrodynamics : dis. – Universidad de los Andes (Colombia), 2017.
116. Gibbons G. W., Werner M. C. Applications of the Gauss–Bonnet theorem to gravitational lensing //Classical and Quantum Gravity. – 2008. – Т. 25. – №. 23. – С. 235009.